UNIVERSITY OF CALIFORNIA, SAN DIEGO

Diffusive Growth and Noisy Replication: Models at the Interface of Statistical Physics and Biological Evolution

A dissertation submitted in partial satisfaction of the
requirements for the degree
Doctor of Philosophy

in

Physics

by

Christopher Scott Wylie

Committee in charge:

Professor Herbert Levine, Chair
Professor Russell Doolittle
Professor Terence Hwa
Professor Massimiliano Di Ventra
Professor Hans Wenzl

2009

The dissertation of Christopher Scott Wylie is approved, and it is acceptable in quality and form for publication on microfilm and electronically:

_____

_____

_____

_____

_____
Chair

University of California, San Diego

2009

TABLE OF CONTENTS

LIST OF FIGURES

LIST OF TABLES

ACKNOWLEDGEMENTS

As I complete my Ph.D I am overwhelmed with gratitude to those who made this accomplishment possible.

Any honest accounting of thanks must begin with my mother, for the many sacrifices she has made on my behalf, and for her unwavering love and support. We've never talked much about academic things, but she plays an essential role in any success I achieve in academia or elsewhere. My father and my siblings are also unwavering in their support and continually enrich my perspectives.

I'm also deeply grateful to my lifelong friend Gwen Dawson, who profoundly shaped my intellectual and personal development during formative years. I'm certain that I would not be where I am without her influence. Jenny, Eitan, and Todd are priceless friends who have made San Diego that much more enjoyable. I thank Anat Burger for so many things– listening to my nonsense, sharing highs and lows, and providing uncannily good advice. David Erickson and Barrett Deris, aka Little Larry Sellers, have provided many laughs and answered my random biology questions.

Terry Hwa teaches excellent, original classes and showes us that real contact between physics and biology is possible. He expects too much, but I have learned a lot from his criticism. Pat Diamond also gives you more than your money's worth in a class and has provided tough, valuable criticism. Lin Chao has given me encouragement, stimulating conversations, and an extremely valuable biological perspective.

My collaborators, or course, have been tremendously helpful. David Kessler supplies humor, creativity, and expertise in applied math. In the context of chapter three he taught me, better than any textbook could, the equivalence between solving a Fokker-Planck equation and doing a path integral. Aaron Trout is a talented and versatile intellectual who made significant contributions in chapter four, particularly in designing efficient and conceptually enlightening computer simulations. Last but certainly not least, Herbie Levine has been a fantastic advisor and collaborator. He has shown me some mathematical techniques but, far more importantly, he has illustrated that real understanding entails synergistically melding mathematics and intuition.

The NSF funded Center for Theoretical Biological Physics (CTBP) fosters interaction between grad students, postdocs, and professors doing exciting work on different

related topics. Those members who proactively organize and interact with one another make the CTBP a truly unique and enriching community. Chief among these are the directors Herbie Levine and José Onuchic, whose service and vision make the CTBP possible.

The text and data of chapter two, in full, has been published in “C. S. Wylie, D. A. Kessler, and H. Levine, “Fluctuation-induced instabilities in front propagation up a comoving reaction gradient in two dimensions”, *Physical Review E*, 74, 2006. The dissertation author was the lead investigator and author of this article.

The text and data of chapter three, in full, has been published in C. S. Wylie, C. Ghim, D.A. Kessler, and H. Levine “The fixation probability of rare mutators in finite asexual populations”, *Genetics*, 181, 2009. The dissertation author was the lead investigator and author of this article.

Text and data in chapter four is being prepared for publication. The dissertation author is the primary investigator and author of the prepared manuscript. Aaron Trout, David Kessler, and Herbert Levine are co-authors of the prepared manuscript.

VITA

2000	B. A. in Physics, Philosophy. Rice University. Houston, Texas
2003-2004	Graduate Teaching Assistant. University of California, San Diego
2008	Summer Graduate Teaching Fellow. University of California, San Diego
2009	Ph. D. in Physics. University of California, San Diego

PUBLICATIONS

C. S. Wylie, D. A. Kessler, and H. Levine, "Fluctuation-induced instabilities in front propagation up a comoving reaction gradient in two dimensions", *Physical Review E*, 74, 2006

C. S. Wylie, C. Ghim, D.A. Kessler, and H. Levine "The fixation probability of rare mutators in finite asexual populations", *Genetics*, 181, 2009

ABSTRACT OF THE DISSERTATION

Diffusive Growth and Noisy Replication: Models at the Interface of Statistical Physics and Biological Evolution

by

Christopher Scott Wylie

Doctor of Philosophy in Physics

University of California, San Diego, 2009

Professor Herbert Levine, Chair

The bulk of this dissertation consists of three separate research projects. Each of them involves models of multi-locus evolution in the context of finite population size, genetic linkage, and both beneficial and deleterious mutations. Each project employs stochastic computer simulations and numerical solutions to equations which approximate a full stochastic model.

The first project, presented in chapter two, was conceived as a problem in the field of non-equilibrium statistical physics known as "front propagation" and was published in *Physical Review E*. The connection to biological evolution is due to my advisor, Herbert Levine, and his colleagues who pointed out an analogy between diffusive fronts propagating through physical space and a mutating population evolving through fitness space.

The second project, presented in chapter three and published in *Genetics*, is more biologically oriented than the first project. It concerns the evolutionary pressures acting on the rate at which organisms produce spontaneous mutation. Our results agree with experimental data and also make testable predictions. The mathematical methods used

are familiar from non-equilibrium statistical physics, but are quite distinct from those used in the first project.

The third project, presented in chapter four, is currently being prepared for publication. It concerns the evolutionary advantage of "competence" for genetic transformation in bacteria, which is conceptually similar to sex. Thus, issues related to the evolution of sex have bearing on this project, and vice versa. A puzzling feature of competence in many species is that normal, vegetatively growing cells stochastically switch in and out of the competence phenotype. We believe that this project provides a novel explanation for this puzzling "mixed strategy."

A common theme in this dissertation is the drastic effect of having a finite population size N. In each project, the system behaves *qualitatively* differently in the $N \to \infty$ limit than for any finite N. Thus, although "mean field theory" provides helpful approximations in many areas of physics and stochastic processes, it should be used cautiously in evolutionary problems or those with a similar mathematical structure.

1 Introduction

1.1 General features of evolutionary models

From the outset, it may be unclear how one could quantitatively model evolution. The term "evolution" might conjure thoughts of one species transforming into another or of organisms' beautiful physiological and behavioral adaptations to their environment. The worthwhile and fascinating study of evolution on that scale is called "macroevolution." This dissertation has, at most, only a vague conceptual bearing on macroevolution.

By contrast, "microevolution" focuses on the frequency trajectories of genetic variants in a population. These trajectories are governed by the (stochastic) processes of birth, death, mutation, and, in most species, recombination. Abstract mathematical models of these processes were pioneered in the 1930's by R.A. Fisher, J.B.S. Haldane, and S.G. Wright, thus spawning the field called "population genetics." Population genetic models have the following core features:

- *Representation of the genome*– The model genome often consists of of many "sites." In some studies these are interpreted as base pairs or codon triplets, in which case the model sequences can be directly compared to real sequences. In many other studies, including those in this dissertation, each site is interpreted abstractly, as a more or less fit variant. In chapter three, the whole of each organism is reduced to its genome, thus neglecting the specific features of its physiology or behavior. In chapter four, cells also express one of two epigenetically determined phenotypes.

- *Fitness function*– Each genome is assigned a fitness which is manifested in its

birth and/or death rate. A time dependent fitness function could be used to model a changing environment, although this is not done in this dissertation.

- *Mutation model*– Genomes may change due to mutation. In real systems, these include point mutations, small and large insertions/deletions, translocations, inversions, etc. As is common in population genetics, only point mutations are explicitly modeled in this dissertation.

- *Recombination model*– Genomes may also change due to "recombination," where genomic fragments are somehow exchanged between different members of the population. Chapters two and three concern strictly asexual evolution, in which there is no recombination. Chapter four concerns bacterial transformation, which is a form of recombination. Details of the model can be found in 4.3.4.

- *Birth death process*– Cells replicate themselves and can also be removed from the population by death. Chapter three of this dissertation employs Moran's overlapping generations model, whereas chapter four, for reasons discussed there, uses a density dependent "logistic" model. Birth-death models are described in more detail below.

Many population genetics models also include migration, but this effect is not investigated in this dissertation.

Once these choices are made, the "cells" in the population are allowed to replicate, mutate, die, etc. Often, the mean fitness of the cells will increase and the cells become better adapted insofar as they increase the chosen fitness function. However, it is also possible for the mean fitness to *decrease*. In particular, if the population is sufficiently small and fitness increasing mutations (i.e. "beneficial mutations") are sufficiently rare compared to fitness decreasing mutations (i.e. "deleterious mutations"), then mean fitness will actually decrease. This phenomenon is called "Muller's ratchet." As is common (although not universal) in population genetics, I will refer to both the fitness increasing and fitness decreasing cases as "evolution" since they each emerge from the same mechanistic process. The example of Muller's ratchet emphasizes the crucial point that *evolution is distinct from, and sometimes even opposed to, adaptation.* Adaptation (i.e. fitness maximization) is merely one very important consequence of evolution.

1.2 Genome, mutation, and fitness model

Throughout this dissertation, genomes are represented by a string of L bits $\{\sigma_i\}$. In chapters two and three, each bit should be interpreted as a non-conserved nucleotide that (ignoring transversions) can be in either a favored (one) or disfavored (zero) configuration. $1 \to 0$ and $0 \to 1$ mutations each occur with rate μ_o per cell replication. The fraction of mutations that are beneficial (deleterious) is thus determined entirely by how many zeros (ones) are in the genome.

In the setting of chapter four, it is more appropriate to interpret each bit σ_i as a fairly long ($\sim 10^4$, see 4.3.4), contiguous set of nucleotides. In this case, mutation is more likely to damage the fragment than to improve it. This fact is incorporated by setting the transition rate from $0 \to 1$ much lower than that from $1 \to 0$ in chapter four.

In general, fitness is determined by both birth and death rates. For the bulk of this dissertation, we assume a simple additive form for the fitness function: $fitness = \frac{1}{L}\sum_{i=1}^{L}\sigma_i$. There are several implicit assumptions in this fitness function, including:

- Each bit contributes independently to fitness. In biological parlance, we assume that there is no epistasis. In real cells, many genes obviously interact with one another (e.g. in the same metabolic pathway) and thus probably have non-additive fitness effects. These interactions are often incorporated in a simplistic way by introducing curvature into the fitness function: Deleterious fitness effects of pairs of mutants can be either greater than ("synergistic epistasis") or less than ("antagonistic epistasis") their individual effects. Experimental data suggests that these cases occur more or less equally often [Ric02]. In a more realistic but intractable model, fitness would depend on the *entire* genomic configuration $\{\sigma_i\}$ rather than simply on the number of ones.

- The fitness of a genome is independent of its frequency in the population. For complex ecological situations (e.g. mimicry, division of labor, etc.), this approximation is certainly not true. However, it may be true more often in simple microbial populations, although there are exceptions, e.g. [Kas02].

1.3 Birth-death models

Without birth and death, the genetic composition of populations would be determined mainly by the random processes of mutation and recombination. Differential birth and death decrease the genetic diversity and increases the genetic order in populations. The stochastic fluctuations in these processes give rise to "random genetic drift," which is perhaps unfortunate nomenclature since it is a *diffusion* term in the corresponding Fokker-Planck equation. This section discusses the simple birth-death models used throughout this dissertation.

1.3.1 Moran's model

Each cell carries a birth rate r_i determined by its genome. Birth and death are strictly coupled. The following sequence of actions occurs every discrete timestep:

1. A randomly selected cell is chosen as a potential parent.

2. The selected cell gives birth with probability proportional to r_i. All selection occurs here, and thus r_i reflects the fitness of the cell. If it does not give birth, the simulation advances to the next timestep.

3. A randomly chosen cell, other than the baby, is killed. Since this step follows the birth of another cell, it forms a sort of implicit interaction between cells.

4. The baby undergoes a deleterious (beneficial) mutation with probability equal to its deleterious (beneficial) mutation rate.

1.3.2 Logistic model

Each cell carries both a raw birth rate r_i that is determined by the genome, as well as a death rate δ_i. This setup allows these processes to be decoupled. Total population size is controlled by scaling all birth rates by the density dependent logistic factor $\mathscr{L} = 1 - N/\kappa$. Since the replication of one cell decreases $\mathscr{L}$ for all others, it represents the implicit interaction between cells in this model. κ is called the "carrying capacity" which is imagined to be set by the availability of space and/or nutrients.

1. A random waiting time is chosen according to an exponential distribution with rate parameter R equal to the total sum of all birth ($B = \mathscr{L}\sum r_i$) and death ($\Delta = \sum \delta_i$) rates throughout the population.

2. A second random number is generated, this time uniformly distributed between zero and R. If this number is less than B, birth occurs. Otherwise death occurs.

3. If birth was chosen in step two, a particular cell is now chosen with probability r_i in a procedure similar to step two of Moran's model.

4. Upon birth, mutation may occur, exactly as in Moran's model.

5. If death was chosen in step two, a particular cell is now picked with probability δ_i and removed from the population.

Since each cell carries both a birth and death rate, the concept of fitness is more subtle here than in Moran's model. As discussed in chapter four, the coexistence condition for two cell types is $r_i/\delta_i = r_j/\delta_j$. In this sense, fitness is captured by the ratio r/δ. On the other hand, if we imagine the overall growth of the population as it expands to fill the carrying capacity, each of two types will grow exponentially. In that case $r - \delta$ captures fitness. These and many other issues relating to this model are discussed in references [PQ07a, PQ07b, PQP08].

1.4 Mean-field theory

A full description of the population entails the number of cells with each possible sequence: $n_{\{\sigma\}}(t)$. The deterministic description (mean-field theory) of $n_{\{\sigma\}}(t)$ is called "quasispecies theory," pioneered by Eigen[Eig71]. In the context of the Moran birth-death model, the quasispecies equation simply keeps track of birth, death, and mutations

$$\frac{d}{dt}n_{\{\sigma\}} = (r_{\{\sigma\}} - \bar{r})n_{\{\sigma\}} + \sum_{\{\sigma'\}} M_{\{\sigma'\},\{\sigma\}} r_{\{\sigma'\}} n_{\{\sigma'\}} \tag{1.1}$$

$M_{\{\sigma'\},\{\sigma\}}$ is the mutation rate from sequence $\{\sigma'\}$ to $\{\sigma\}$, which depends on the number of mutations separating them. $\bar{r}$ is the average birth rate which always equals the average death rate in Moran's model. Although useful in some contexts, a limitation of Eq.1.1 is

that it neglects fluctuations. This might not be essential if the number of sequences $n_{\{\sigma\}}$ is large compared to its fluctuations $\sim \sqrt{n_{\{\sigma\}}}$, i.e. $\sqrt{n_{\{\sigma\}}} \gg 1$. However, there are 2^L possible sequences and only N cells to occupy them. Therefore, unless $N \sim 2^L$, Eq.1.1 will not apply in sparsely populated regions of sequence space.

One way to improve the situation is to bin sequences according to their fitness. This increases the density of states and decreases the dimensionality at the expense of losing the ability to resolve between different sequences in the same fitness class. Using a very simple fitness function $r = \frac{1}{L}\sum \sigma_i$, we obtain

$$\frac{d}{dt}n_r = n_r(r-\bar{r}) + \mu\left[r(r+\frac{1}{L})n_{r+1/L} - rn_r + (1-r)(r-\frac{1}{L})n_{r-1/L}\right] \tag{1.2}$$

If $\sqrt{n_r} \sim 1$ for some $r > \bar{r}$, as is the case for a population evolving up a fitness function, then Eq.1.2 will not apply to the most fit individuals at the leading edge. Because those individuals grow exponentially faster than everyone else, this turns out to be a serious error. The fundamental problem is underscored by analyzing an approximation of Eq.1.2 in which the r dependent terms in brackets are treated as constants and $L \to \infty$. In this case, $\bar{r}$ diverges in finite time [BLT91]. The conclusion is that the $r - \bar{r}$ term is deeply flawed because it neglects large fluctuations in the most important part of the evolving fitness pulse.

It thus seems that a full stochastic treatment is extremely difficult and that mean-field approximations are qualitatively incorrect. Recent work [RWC03, DF07] has demonstrated the possibility of treating populated fitness classes deterministically, treating the sparsely populated regions stochastically, and somehow matching together the separate answers. A related, though more heuristic approach, is to simply impose a growth cutoff in the leading edge until the number of cells in that region is $O(1)$. This is accomplished by replacing $r - \bar{r}$ with $(r-\bar{r})\theta(n-n_c)$, where θ is the Heaviside step function [BD97, TLK96a].

In chapter two, I employ this cutoff approach in the context of front propagation in two dimensions. In chapter four the approach is used again in the context of evolution.

The methods in chapter three are in some sense complementary to the cutoff mean-field approach described above. The cutoff approach accurately describes the dynamics in populated regions and heuristically treats the highly stochastic region. By

contrast, the strategy in chapter three involves a detailed, stochastic analysis of certain rare cells (the mutators). Once they become more common, the mutator dynamics are treated stereotypically.

2 Two dimensional front propagation

2.1 Introduction

Several well known processes in spatially extended systems exhibit fronts that propagate through space. Most of these processes that have been considered to date occur in media in which the governing dynamics are spatially uniform. Recently, however, some interesting findings have been made concerning fronts propagating in systems with spatially heterogeneous dynamics. In particular, the simple infection model $A+B \rightarrow 2A$ on a lattice with equal hopping rates and a linear reaction rate gradient has been studied[CKL05a, CKL05b]. Two versions of this system have been examined in some detail: one in which the gradient is defined with respect to the medium itself (the "absolute gradient"), and another in which the gradient is defined relative to the front's interface and travels along with the front (the "quasi-static gradient"). One can imagine numerous systems that can be described by the absolute gradient, e.g. a chemical reaction occurring in a temperature gradient. The quasi-static gradient is more analytically tractable and also arises naturally in models of biological evolution[TLK96b, RWC03].

The usual way to analytically study a system with a propagating front, such as the infection model mentioned above, is within a mean field, reaction-diffusion framework. The simplest MF analog to our infection model is the usual Fisher equation [Fis30], with a spatially varying reaction rate:

$$\frac{\partial \phi}{\partial t} = D\nabla^2\phi + r(x)\phi(1-\phi) \tag{2.1}$$

For our simple infection model, Eq.2.1 (the "naive MFE") fails to capture many of the qualitative aspects of the stochastic problem with either absolute or quasi-static

gradients. These failures, as well as many other issues involving the MF description of similar front propagation problems, are largely remedied [CKL05a, CKL05b, CKL05c, CK06, CKL06] by introducing a cutoff factor in the reaction term [TLK96a, BD97, KL98a]:

$$\frac{\partial \phi}{\partial t} = D\nabla^2\phi + r(x)\phi(1-\phi)\theta(\phi-\phi_c) \tag{2.2}$$

This added factor causes the reaction rate to abruptly drop to zero in regions far into the front's leading edge where ϕ drops below a critical level ϕ_c, and is meant to roughly mimic the effect of finite number fluctuations in the stochastic process. In other words, the discrete nature of individual particles implies that a sufficiently small value of the density field $\phi < \phi_c \sim 1/N$ corresponds, in an average sense, to zero particles present and thus zero reaction rate. In previous work, we showed how this modified MF treatment gives a quantitatively accurate prediction of the stochastic model in one dimension.

The purpose of this paper is to extend these investigations to the two-dimensional system. We will work in a channel geometry, with no-flux conditions on the sidewalls, such that the front propagates down the channel. In particular, we are interested in the patterns generated by the system, due to an instability to transverse fluctuations.

As mentioned previously, this system can be viewed as being analogous to certain problems in biological evolution. In this context, the relevant equation is similar to Eq. 2.2, but with a simpler rate term:

$$\frac{\partial \phi}{\partial t} = D\nabla^2\phi + (x-\bar{x})\phi \cdot \theta(\phi-\phi_c) \tag{2.3}$$

Here, ϕ represents the fraction of individuals in a population with a given fitness x. If the size of the population is fixed, the growth rate of individuals with a particular fitness is proportional to $x-\bar{x}$, where $\bar{x}$ is the mean fitness in the population. The diffusion term represents the effect of mutation, and the dynamics of the system corresponds to the population evolving towards greater mean fitness. The transverse y coordinate, being orthogonal to the fitness x, represents the frequency of some selectively neutral trait. Instability of a planar pulse would then correspond to evolution toward a non-uniform frequency distribution of this neutral trait. Due to the difference in the structure of

the rate term, Eq. 2.3 describes an evolving *pulse* whereas Eq. 2.2 describes a *front*. However, this difference should not alter the stability properties of the system since, as we shall see, these properties are determined by the leading edge where the front and the pulse are identical. The cutoff term is appropriate in this context because members of a population, like particles, are quantized.

In this study, we turn our attention to the quasi-static gradient in two dimensions and ask how finite number fluctuations and the related cutoff approach affect the stability of planar fronts propagating in a rectangular channel. In what follows we will see that in contrast to the predictions of the naive MFE, the results of stochastic simulations point to unstable planar fronts. Furthermore, once again the cutoff term will rescue the effectiveness of the mean field description of the stochastic process. We first study the cutoff mean-field equations, both numerically and analytically, showing the instability. We then turn to the stochastic model, demonstrating the instability there as well. An appendix contains details about the numerics.

2.2 Mean-field stability calculation

The full equation of motion governing the quasi-static gradient in the MF cutoff framework is Eq. 2.2 with

$$\begin{gathered}
\phi(x,y,t) \equiv N_A/N \\
r(x) \equiv \max(r_{min}, r_o + \alpha(x-\bar{x})) \\
\bar{x}(t) \equiv \tfrac{1}{b}\int \phi(x,y,t)dxdy \\
\phi_c = k/N \\
\partial_y\phi(x,0,t) = \partial_y\phi(x,b,t) = 0
\end{gathered}$$

Here x is the direction parallel to the channel's long axis. N_A is the number of A's at a given site and N is the equilibrium number of A particles per lattice site. k is some $O(1)$ fitting parameter. $\bar{x}$ serves to define the interface position of the front by essentially comparing the front's profile to a step function, and b is the cross-channel width. r_{min} merely serves to keep the reaction rate from going negative far behind the front and plays no role in the front dynamics.

To investigate numerically the stability of the planar front, we start with a front which is a slightly perturbed planar front, with

$$\phi(x,y,0) = \theta\left(0.01\cos\left(\frac{\pi y}{b}\right) - x\right) \tag{2.4}$$

with $\theta(x)$ again the Heaviside step function. Direct numerical integration of a spatially discretized version (with lattice spacing unity) of the time dependent Eq. 2.2 shows that planar fronts are in fact unstable to transverse fluctuations. For a sufficiently wide channel, perturbed planar fronts develop into long, though finite, fingers whose length increases with increasing channel width. An example of such a finger is shown in Fig. 2.1. We see that there is a deep narrow "notch" on the trailing side of the finger, so that the width of the interface is much greater here than for the rest of the finger. Defining the finger length by $\int [\phi(x,0) - \phi(x,b)]\,dx$, the data for finger length versus channel width is presented in Fig. 2.2. We now turn toward an analytic understanding of this result.

Due to the translational invariance of the system, it is natural to investigate first steady-state propagating planar front solutions. Plugging into Eq. 2.2 the traveling wave form, $\phi_0(x,y,t) = \phi_0(x - vt)$, with velocity v, we obtain

$$D\phi_0'' + v\phi_0' + r(z)\phi_0(1-\phi_0)\theta\left(\phi_0 - \frac{k}{N}\right) = 0 \tag{2.5}$$

in terms of the comoving coordinate $z \equiv x - vt$. A quick analysis of the linearized version of Eq. 2.5 provides insight into the role of the cutoff. As $z \to -\infty$, $\phi_0 \to 1$. Linearizing around $\phi_0 = 1$, we find two exponential solutions, but one must be discarded since it decreases with increasing z. Similarly, as $z \to \infty$, $\phi_0 \to 0$. Linearizing around $\phi_0 = 0$, in the region past the cutoff, once again we find only one acceptable, decaying solution. This leaves our solution with a total of two undetermined constants. Fixing translational invariance reduces this number to one. Requiring continuity of ϕ_0 at the cutoff determines the remaining coefficient, and continuity of ϕ_0' determines the velocity. Thus, mathematically, the cutoff fixes the velocity by overdetermining the boundary conditions, i.e. converting Eq. 2.5 into an eigenvalue problem. An analysis for large N yields the leading order result [CKL05a]:

$$v = \left[24D^2\alpha\ln(N/k)\right]^{1/3} \tag{2.6}$$

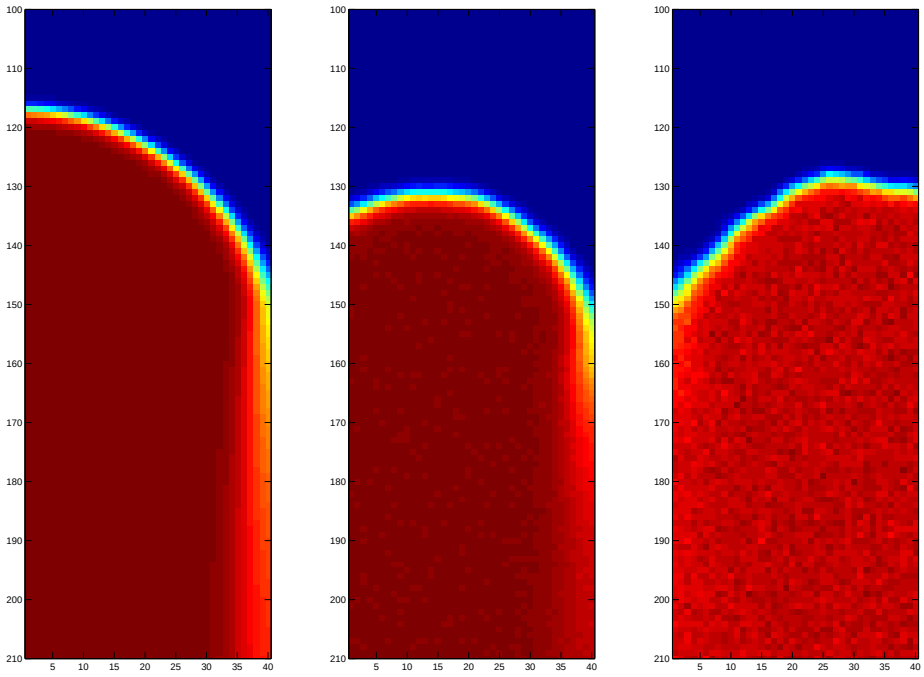

Figure 2.1: Snapshots of the growing finger for the cutoff MFE compared to that for the stochastic model. The parameters are $D = 1$, $r_0 = 6$, $\alpha = 0.3$. Lengths are expressed in units of the lattice spacing $l = 1$. Left: The cutoff MFE with $k/N = 8.7 \times 10^{-5}$. Center: The stochastic model with $N = 90801$. Right: The stochastic model with $N = 2881$.

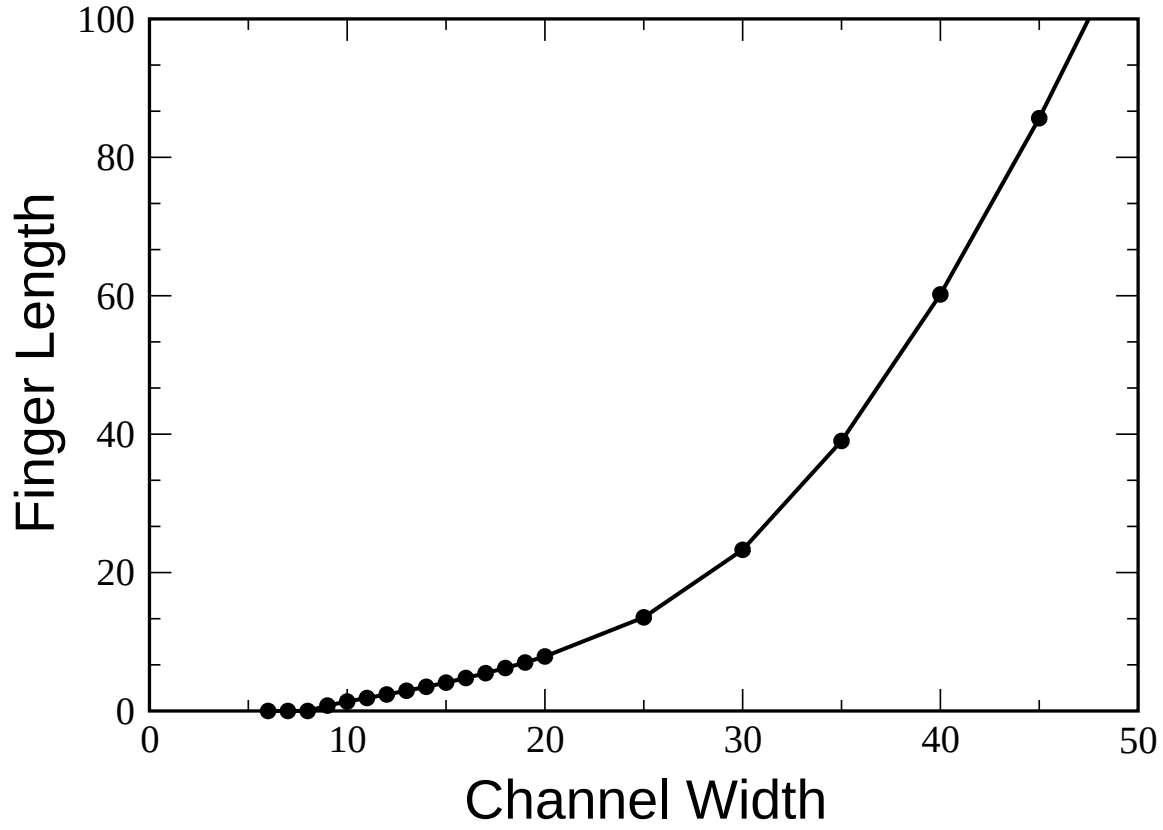

Figure 2.2: Finger length (as defined in the text) versus channel width for the cutoff MFE. The parameters are: $D = 1$, $r_0 = 6$, $\alpha = 0.3$, $k/N = 8.7 \times 10^{-5}$, $l = 1$.

In the limit $k/N \to 0$ we regain the naive MF approach, in which $v \to \infty$. Thus the naive MF and the cutoff MF predict qualitatively different results with respect to velocity. Not surprisingly, stochastic fronts in fact approach a (finite) steady-state velocity that agrees well with that given by the cutoff MF.

Turning now to 2D fronts, we wish to study the linear stability of the planar solution to transverse perturbations. We write $\phi(x,y,t) = \phi_0(z) + \tilde{\phi}(z,y,t)$ and linearize Eq. 2.2 with respect to $\tilde{\phi}$. The invariance of the system with respect to translations in time and the transverse spatial direction y implies $\tilde{\phi}(z,y,t) = e^{\omega t} e^{iqy} \eta(z)$. The governing equation for $\eta(z)$ is then:

$$D\eta'' + v\eta' + \eta r(z)\left[(1-2\phi_o)\theta(\phi_0 - k/N) + \phi_0(1-\phi_0)\delta(\phi_0 - k/N)\right] = \Omega\eta \qquad (2.7)$$

with

$$\Omega \equiv Dq^2 + \omega \qquad (2.8)$$

The delta function arises from differentiating the step function and is due to the shift in z_{cut} caused by the perturbation $\tilde{\phi}$. We have assumed here that $q \neq 0$ so that $\int \tilde{\phi}(z,y,t)dy = 0$. The case $q = 0$ has to be treated separately, but in any case the least stable mode should be the translation mode with $\Omega = 0$. Notice that Eq. 2.8 implies a simple stabilizing quadratic dependence of the growth rate ω on q. Thus the least stable mode is that with the smallest non-zero q, which, assuming a zero-flux sidewall boundary condition, is $q_{min} = \pi/b$. This implies a minimum channel width b^* below which even the longest wavelength mode has too much curvature for any instability to exist:

$$b^* = \pi\sqrt{\frac{D}{\Omega_{max}}} \qquad (2.9)$$

where Ω_{max} is the largest (positive) eigenvalue of the stability operator, Eq. 2.7.

Like the steady-state problem, insight can be gained into Eq. 2.7 by considering the boundary conditions at $z \to \pm\infty$. We require that $\eta \to 0$ as $z \to -\infty$. As $\phi_0 \sim 1$ in this region, we find two exponential solutions for η: one growing with increasing z and the other decaying. The latter must of course be excluded. If we perform the same procedure past the cutoff, as $z \to \infty$, we find two decaying modes. However, one of the modes decays more slowly than the steady-state solution and thus dominates it for sufficiently large z. This is unacceptable behavior for a perturbation and therefore

this solution is discarded. Thus, our solution has two arbitrary constants, one of which may be chosen arbitrarily since Eq. 2.7 is linear in η. The remaining constant is fixed by requiring continuity of η at the cutoff. Matching η' at the cutoff determines the eigenvalues Ω. Thus, once again the cutoff has played a central role in determining the problem's interesting quantities.

As with the steady-state problem, we can make analytic progress in the limit of large N. In this case, the cutoff is at large z, in the region where ϕ_0 is small. If we consider Eq. 2.7 in the region where $\phi_0 \ll 1$ and $z < z_{cut}$, and fix the translation invariance by setting $\bar{z} = 0$ for the unperturbed state, we obtain

$$D\eta'' + v\eta' + \eta(r_0 + \alpha z) = \Omega\eta \tag{2.10}$$

Up to a similarity transformation, this is the Airy equation, with the general solution

$$\eta = e^{-\frac{vz}{2D}}\left[A\mathrm{Ai}\left(\frac{\Gamma - z}{\delta}\right) + B\mathrm{Bi}\left(\frac{\Gamma - z}{\delta}\right)\right] \tag{2.11}$$

with

$$\Gamma \equiv \frac{v^2/4D - r_0 + \Omega}{\alpha}$$
$$\delta \equiv \left(\frac{D}{\alpha}\right)^{1/3}$$

We argue that the Bi term must vanish by considering the large v limit of Eq. 2.7 and matching onto Eq. 2.11. As shown in [CKL05b], in the large v limit, the diffusion term in Eq. 2.5 can be ignored, and the solution in the region where $\phi_0 \ll 1$ is

$$\eta \sim e^{-\frac{1}{v}[(r_0 - \Omega)z + \frac{1}{2}\alpha z^2]} \tag{2.12}$$

Expansions of *Ai* and *Bi* for large argument show that the diffusionless result Eq. 2.12 matches onto Eq. 2.11 only if the *Bi* term is absent. The constant A may be arbitrarily set to unity since the problem is linear. Thus we have for $z \lesssim z_{cut}$

$$\eta = e^{-\frac{vz}{2D}}\mathrm{Ai}\left(\frac{\Gamma - z}{\delta}\right)$$

We have to match this result to the simple exponential solution for $z > z_{cut}$. Thus,

$$e^{-\frac{vz_{cut}}{2D}}\mathrm{Ai}\left(\frac{\Gamma - z_{cut}}{\delta}\right) = Ce^{\left[-\frac{vz_{cut}}{2D}\left(1+\sqrt{1+\frac{4\Omega_0 D}{v^2}}\right)\right]} \tag{2.13}$$

The derivative of η must also match properly at the cutoff. Looking back to Eq. 2.7, we see that the delta function term causes a discontinuity in η' at z_{cut}:

$$\eta'_{right} - \eta'_{left} = \frac{r(z_{cut})}{D}\frac{\frac{k}{N}(1-k/N)}{\phi_0'(z_{cut})} = -\frac{r(z_{cut})}{v}(1-k/N) \tag{2.14}$$

Computing the derivatives in (12) and dividing by (11), we obtain

$$\frac{v}{2D}\sqrt{1+4D\Omega/v^2} - \frac{1}{v}(r_0+\alpha z_{cut})(1-k/N) = \frac{1}{\delta}\frac{Ai'(\frac{\Gamma(\Omega)-z_{cut}}{\delta})}{Ai(\frac{\Gamma(\Omega)-z_{cut}}{\delta})} \tag{2.15}$$

This equation determines Ω if the quantities v and z_{cut} are known. Now, for large v the LHS of (12) is also large. For the RHS to balance it, the Airy function in the denominator must be small. Thus, $\frac{\Gamma-z_{cut}}{\delta} \approx \xi_0$, where $\xi_0 \approx -2.3381$ is the first zero of the Airy function. For the position of the cutoff, we quote another result from [CKL05a] obtained by matching the linearized steady-state equation at the cutoff:

$$z_{cut} \approx \frac{v^2/4D - r_0}{\alpha} - \xi_0\delta - \frac{2D}{v} \tag{2.16}$$

Plugging this expression into Eq. 2.15, expanding around ξ_0, and dropping higher order terms, we obtain the leading order result valid for large v:

$$\Omega = \frac{2D\alpha}{v} \tag{2.17}$$

This result is tested in Fig. 2.3, where we plot the eigenvalue Ω versus velocity determined by an exact numerical solution of Eq. 2.7, together with the numerical solution of the matching condition, Eq. 2.15, and the leading order result, Eq. 2.17. We see that indeed the leading order result approaches the exact results as v increases.

Our leading-order result, Eq. 2.17, yields the interesting conclusion that planar fronts become stable in the limit as $v \to \infty$, i.e. $N \to \infty$, i.e. the cutoff disappears. Eq. 2.17 can be interpreted as saying the that Ω is proportional to the ratio of the diffusive length scale (D/v) to the length scale over which the rate changes appreciably ($1/\alpha$). Thus, heuristically incorporating the effects of finite number fluctuations qualitatively changes the system's stability properties by limiting the front's velocity, which in turn makes the diffusive length scale finite. In practice, however, without a cutoff, an initial front which is compact (or decays sufficiently rapidly) will act as a time-dependent cutoff [KNS98], so that at least initially transverse fluctuations will grow. The fluctuation

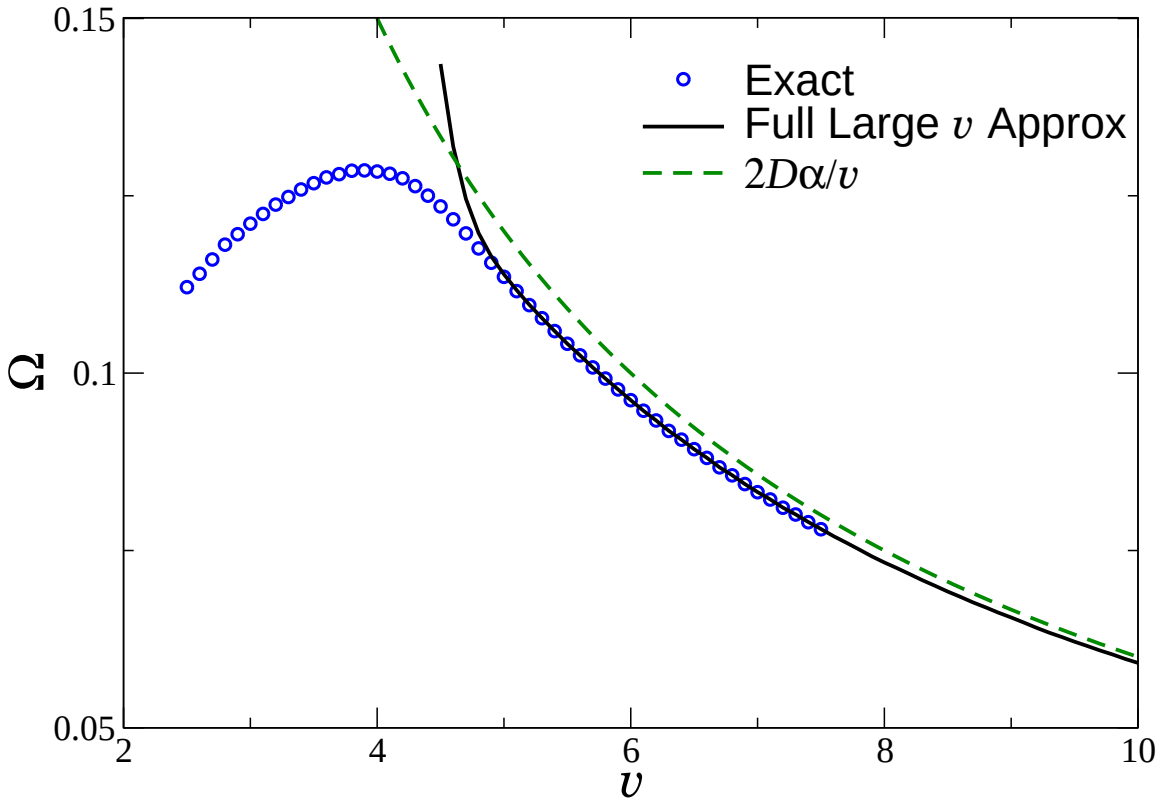

Figure 2.3: The circles represent the exact numeric solution of Eq. 2.7. The solid line is the exact numeric solution of Eq. 2.15 which is itself a large v approximation. Exact numerically generated values of N and z_{cut} were used to generate this approximation. The dashed curve is the analytic approximation Eq. 2.17. The parameters are $D = r_0 = 1$, $\alpha = 0.3$.

induced instability in this system is similar to that in [KL98a], where it was found that that a coupled reaction diffusion system with no reaction gradient, but with unequal diffusion coefficients, is unstable with a cutoff but stable without one. Furthermore, Eq. 2.17 shows that the fronts become stable as $\alpha \to 0$, for any value of N. This is consistent with the stability shown in [KL98a] in the case of equal diffusion coefficients.

Thus, once again, the presence of the cutoff qualitatively changes the simple mean field predictions. If the cutoff approach indeed captures the effect of finite number particle fluctuations, we should expect to see some analog of this front instability in the stochastic, discrete infection model discussed earlier, to which we now return.

2.3 Stochastic system

We ran simulations in which the lower rectangular portion of the channel was initially populated with N type A particles per lattice site and the upper rectangular portion of the channel was populated by N type B particles per lattice site. During each time step, a binomially distributed random number of particles hops to adjacent sites. Furthermore, A particles probabilistically cause some B particles to change into A particles . The reaction probability and hopping rates were chosen so that the discretized, stochastic equation for ΔN_A reduces to Eq. (2.1) (with the quasi-static form for $r(x)$) when the expectation value is taken in the small time, small lattice spacing limit. In particular, for the hopping probability we took $P_{hop} \sim D\frac{dt}{l^2}$, where dt is the simulation time step and l is the lattice spacing. The number of particles reacting during each time step was chosen as a binomially distributed random variable characterized by N_A repetitions of a Bernoulli process with individual event probability $1-(1-\frac{r(x)dt}{N})^{N_B}$.

The simulation results are easiest to interpret when the channel width b and the average number of particles per lattice site, N, are large. For fixed large N, there is some b beyond which there is a pronounced finger which survives for very long times. An example of such a finger is seen in the middle frame of Fig. 2.1, where N was chosen to correspond to the cutoff chosen for the MF simulation seen in the leftmost frame. The overall similarity of the patterns is clear. As N is reduced for the same b, the statistical fluctuations become larger, as expected, and give the finger a clearly finite lifetime before it succumbs to the noise. The pattern eventually regenerates, sometimes with opposite parity, and the cycle of destruction and regeneration starts anew. Such a noise-roughened finger in seen in the rightmost frame of the Figure. The very visible effect of the noise is striking given the still quite large value of N employed, underscoring the extreme sensitivity to fluctuations of our system.

For very narrow channels, on the other hand, the interface appears to be essentially planar, with random short-lived fluctuations. All this is in accord with our expectations based on our study of the cutoff MF dynamics. What is more subtle, however, is a quantitative measurement of the critical value of b for the onset of the pattern. On the small b side of the transition, the pattern is not exactly planar due to noise. On the large b side, the pattern is smeared out due to noise. This problem is exacerbated by

the supercritical nature of the transition, such that the pattern has very small amplitude near the transition. In order to compare the stochastic system to the MF prediction, we need a way to distinguish this random roughening of the interface from the genuine pattern forming mechanism discussed in the previous section. We present below two tests

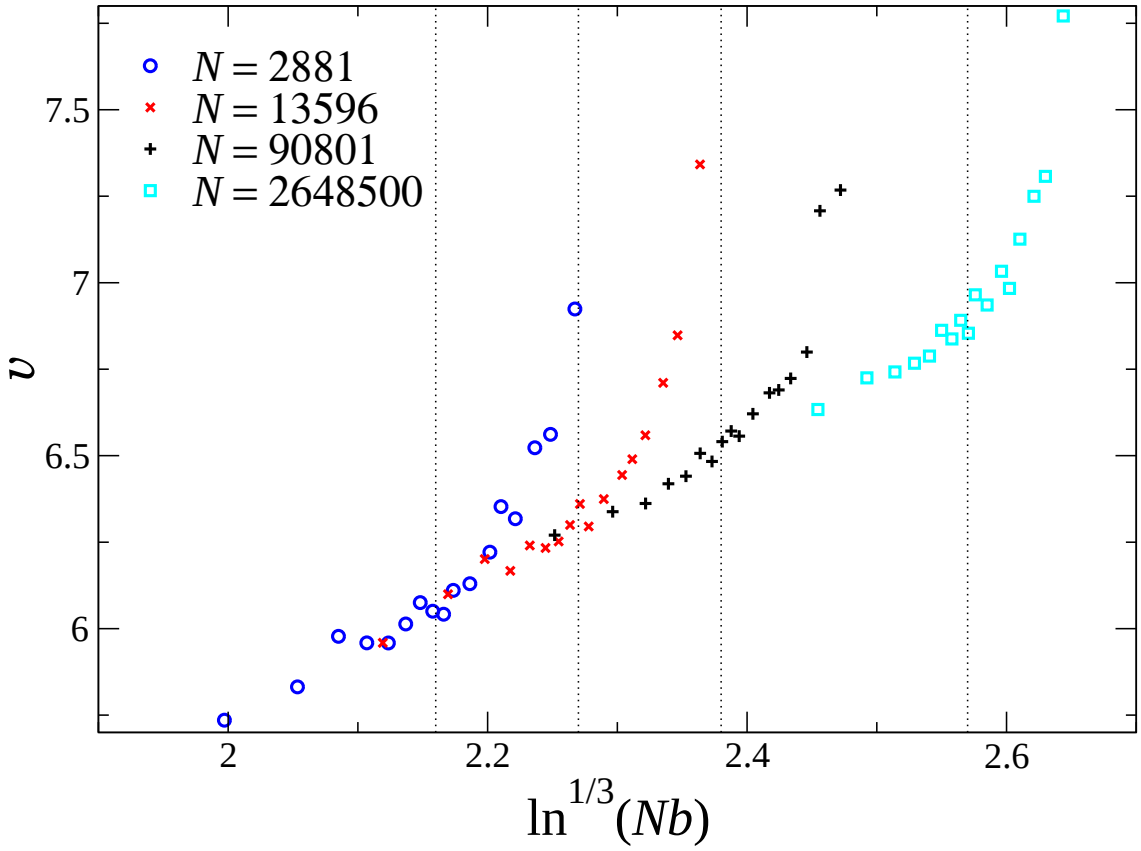

Figure 2.4: Evidence of the transition to instability. The linear envelope of the different curves demonstrates the N renormalization $N_{eff} \sim Nb$ required by widening the channel. The dotted lines show the b^* resulting from the corresponding deterministic, MF cutoff simulation (k=.25). Each data point represents an ensemble average of three long trials (100 time units each). The parameters are $D = 1$, $r_0 = 6$, $\alpha = 0.3, l = 1$

Both of these tests exploit the predicted transition between stable and unstable states that occurs when the channel width exceeds a critical value b^*, as stated in Eq.(2.9). First, we measured the ensemble averaged velocity of the mean interface

$\overline{z} \equiv \sum_{i,j} \frac{A(i,j)}{Nb}$ as a function of b (Fig. 2.4). The increasing trend along the envelope of the different curves can be understood as a result of wider interfaces presenting an effectively larger number of particles N_{eff}. In fact, since in the steady-state, $v \sim (\ln N)^{1/3}$, we see from the figure the remarkably simple result $N_{eff} \sim Nb$. This simple dependence continues until b approaches b^* (dotted vertical lines), where the velocity suddenly increases. This increase can be understood as a result of the system spending much of its time in a configuration in which one side of the interface significantly leads in front of the other. The lagging side then effectively stalls while the leading side is in a region of large reaction rate, and thus propagates quickly. The overall effect is an increase in the velocity averaged over the width of the channel. The fact that the change occurs so near the b^* calculated earlier suggests that the cutoff approach is effectively capturing the stochastic dynamics.

As a second test, we plot the mean roughness of the interface W vs b (Fig. 2.5). W is defined in the standard way

$$W^2 \equiv \langle \overline{\left[\left(\sum_j A(i,j)/N\right) - \overline{z}\right]^2} \rangle$$

where $\langle\rangle$ denotes ensemble average and the bar denotes average over the transverse direction. For $b < b^*$ we see power law scaling reminiscent of that discovered by Kardar, Parisi, and Zhang [KPZ86] for a growing interface. However, the data shows no sign of a universal exponent. It may be that the very weak stability of the interface near b^* is responsible for a long crossover. This issue clearly requires more extensive study. For a fixed b, W decreases with increasing N, consistent with the hypothesis that interface roughness is noise driven in this regime. However, for $b \gtrsim b^*$ this simple dependence is lost. The curves converge near b^*, showing that particle number and its associated noise are no longer the relevant factor in determining interface roughness. Past this intersection, there is no apparent correlation between W and N. We interpret this as a crossover from noise driven interface roughness to gradient driven pattern formation occurring very near the b^* predicted from the cutoff MF approach.

Thus, the cutoff MF approach is quantitatively successful in predicting the transition of the width and velocity observed in ensemble averaged stochastic fronts when the channel is widened. In contrast, the naive MF approach predicts no such transition and an infinite steady-state velocity, in stark qualitative disagreement with the simula-

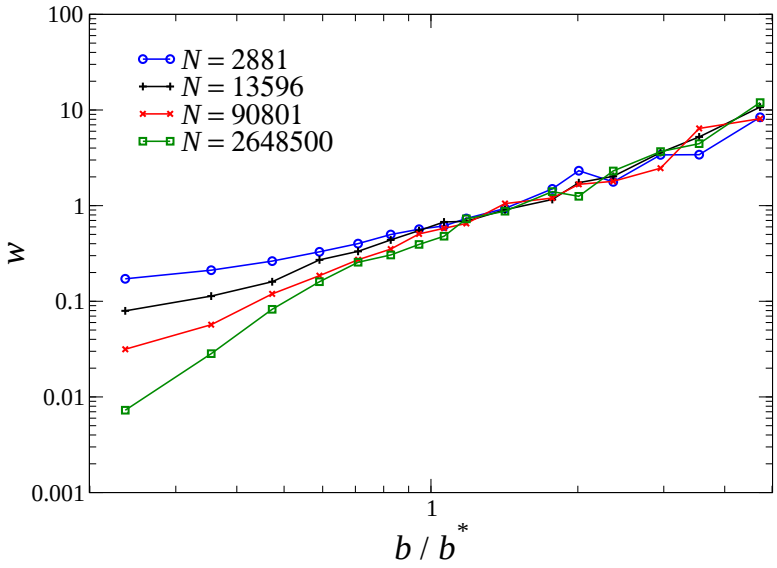

Figure 2.5: Noise driven roughness scaling for $b < b^*$, gradient driven scaling thereafter. Each data point represents an ensemble average of three long trials (100 time units each). Parameters are $D = 1$, $r_0 = 6$, $\alpha = 0.3, l = 1$.

tion results. The cutoff MF approach also predicts the velocity of the average interface for $b < b^*$, provided we take $N \to Nb$.

Another aspect of the stochastic system which one would like to predict is the ensemble-averaged shape. We find that qualitatively this behaves as expected; namely, for small channel width the average shape is flat, and above the critical width, a nontrivial shape is apparent. The amplitude of the averaged pattern continues to increase with increasing width. However, we do not know how to quantitatively relate the average pattern to the results of the cutoff MF equations. One obvious impediment is the fact that the stochastic system switches parity at random, with the right and left sides alternating as the leading edge. Thus, a naive ensemble average produces a shape which is highest in the center, clearly at odds with the deterministic calculation. Another aspect of the problem that we would like to correlate with the deterministic calculation is the growth rate of the pattern near onset. This problem is also difficult because the width, measured in the usual way, consists of a contribution from noise driven roughening and one from pattern formation. Clearly, the usual MF approach can only make predictions about the contribution from patterning and thus the stochastic results and MF predictions are

intrinsically difficult to compare. Even though the noise decreases with increasing N, the dominance of the dynamics by the leading edge where fluctuations are unavoidably present makes this a nontrivial task, even at large N. These questions remain challenges for the future.

2.4 Acknowledgements

The text and data of chapter two, in full, has been published in “C. S. Wylie, D. A. Kessler, and H. Levine, “Fluctuation-induced instabilities in front propagation up a comoving reaction gradient in two dimensions”, *Physical Review E*, 74, 2006. The dissertation author was the lead investigator and author of this article.

3 Mutation rate evolution

3.1 Introduction

The most evolutionarily important characteristic that an individual inherits from its parents is the average number of offspring that it will leave in the next generation, i.e. its fitness. But, is fitness the *only* evolutionarily relevant heritable trait? The ultimate fate of an individual depends not only on its immediate properties, but on those of its entire lineage of descendants. Therefore, the genetic system that shapes the statistical properties of this lineage is also an evolutionarily relevant, selectable trait.

In this article we study one such property, namely a globally elevated mutation rate. In practice this property is inherited via a mutated copy of a gene, called a mutator allele, involved in DNA copy or repair. We ask the following basic question: *What is the fixation probability of an initially rare mutator?* This is a generalization of the classic population genetic calculation for the fixation probability of a static mutant with selection coefficient s [Fis30]. If the fixation probability of a mutator allele differs from that of a neutral one (i.e. $1/N$), then the average mutation rate of the population will be under selective pressure.

The selective forces acting on mutators is not purely a theoretical issue. Natural populations quite often contain a mixture of wild-type and mutator strains [LLPC96, LCB$^+$00, GMT$^+$01, MRT$^+$97, dCMdlP$^+$04, BSF$^+$04, OCC$^+$00, PML$^+$03, RYPS02, WBS04]. Furthermore, the somatic tissues of multicellular sexual organisms comprise populations of asexually reproducing cells possessing opportunities for an increased growth rate. Correspondingly, tumoregenesis has been associated with mutator alleles [Loe91]. Even more strikingly, laboratory-scale evolution experiments [SGL97, MLLM97, TSB54, Miy60] have resulted in examples of spontaneous mutator

fixation. Several experimental studies [GMT+01, CC83, LPG+05, SDS+02, MLLM97] indicate that mutators achieve fixation because of the adaptive mutations they generate and not because of any intrinsic fitness advantage. Thus, selection on mutator alleles occurs via an indirect mechanism. One of the goals of our work is to make semi-quantitative contact between our model of indirect selection and the existing data of mutator fixation in laboratory experiments.

The evolution of mutation rate is a problem that dates back to the 1930's. The general issue was articulated by Sturtevant [Stu37], and important theoretical contributions date back to Kimura [Kim67] and Leigh [LJ70]. Theoretical studies proliferated during the last decade, and the field is reviewed in [SGJS00] and also in [DM06]. Given the abundance of existing theoretical articles, it is critical to understand how our work relates to and improves upon this body of literature. We address this issue in detail in the Discussion section. For now, we merely provide a brief sketch. First, we neglect the complicating influences of recombination and environmental fluctuations. This allows for a direct and comparatively precise treatment of the simplest situation: a strictly asexual population adapting in a constant environment. Even this simplest scenario has rich and often counterintuitive behavior. Secondly, our methods naturally treat both strong (e.g. 100 fold) mutators and weak modifiers of mutation rate. Thirdly, unlike most previous work, we combine fully stochastic simulations with an analytic approach. Our analytic results for weak modifiers are a generalization of previous work by Andre and Godelle [AG06], but we find that both approaches often fail to match simulations. However, our work for strong mutators *does* match simulations over the expected parameter range. The simulations thus provide vital checks and guidance for the analytic approach. Conversely, the analytic approach deepens our understanding of mutator fixation and makes predictions in parameter regimes that are computationally inaccessible via simulation. Finally, unlike previous work, our diffusion based analytic approach captures the effects of random genetic drift. This not only allows for exploration of regimes where random drift is important, but also a quantitative understanding of when it can be neglected.

The outline of this article is as follows. We begin with a heuristic discussion of mutator dynamics. Next, we construct and simulate a stochastic model of asexual

Table 3.1: Notation used in chapter 3.

Symbol	Usage
N	Total population size
μ_-	Wild-type mutation rate per genome
μ_+	Mutator mutation rate per genome
U	Mutation rate into mutator state
L	Length of genome
b	Number of 1's in genome
δ	Fraction of mutations that are lethal
x	Mutator frequency
$\bar{\mu} \equiv (1-x)\mu_- + x\mu_+$	Average mutation rate per genome
$R \equiv \mu_+/\mu_-$	Mutator strength
$r \equiv b/L$	Growth rate per individual per simulation time-step
$s = 1/b$	Selection coefficient of non-lethal mutation
$\alpha \equiv 1 - b/L$	Fraction of 0's in the genome
$\alpha_e \equiv \alpha(1-\delta)$	Fraction of mutations that are beneficial

populations that include mutator alleles. We do not explicitly allow for the formation of mutators, merely the competition between mutators and wild-type strains once mutators arise. Afterward, steered by the outcome of simulations, we develop a quantitative understanding of the results of the stochastic simulations. Although a full mathematical treatment turns out to be intractable, we are able to devise an approximation scheme that captures many features of the simulation results. We then solve our approximation scheme, both numerically and analytically. The resulting expressions allow a comparison to the *E. coli* experiments of Lenski and co-workers [SGL97].

3.2 Heuristic analysis

In this section, we briefly explain the conceptual factors underlying mutator fixation. The equations in this section should be considered merely as heuristic guides and not formal results.

Since mutator alleles do not directly affect fitness, their dynamics must be guided by association with other genes which do have a direct fitness effect. In asexuals, all loci sharing the same genome with a sweeping beneficial mutation will also become

fixed via "hitchhiking" [MSH74]. Whereas most alleles hitchhike completely passively, the mutator allele plays a somewhat active role in facilitating its own hitchhiking by increasing the probability of a beneficial mutation elsewhere in the genome. This well known mechanism occurs in our simulations and is evident in Fig.3.1.

At the same time, the wild-type subpopulation also generates advantageous mutations. When this occurs, mutators become extinct due to fixation of their counterpart wild-type alleles. Although the wild-type generates mutations more slowly on a per capita basis, if it vastly outnumbers the mutator subpopulation, then the *total* mutation rate in the wild-type background may be larger. Along these lines, it is tempting to think of the number of mutators as initially constant, and that the mutator will achieve fixation if and only if it generates a sweeping beneficial mutation before the wild-type background does. This means that

$$P_{fix} = x_o \frac{\mu_+}{\bar{\mu}} = \frac{x_o \mu_+}{x_o \mu_+ + (1 - x_o)\mu_-} \tag{3.1}$$

where x_o is the initial frequency of mutators and μ_+ (μ_-) is the genome-wide mutator (wild-type) mutation rate. This equation has striking qualities. First, it is independent of the following *prima facie* important parameters: population size N, selection coefficient of mutations s, and the fraction of mutations which are beneficial versus deleterious. Secondly, and more subtly, the equation is *explicitly frequency dependent*. It will turn out that Eq.3.1 arises as a limiting form of our analytic expression, but does *not* typically match the results of simulations.

In contrast to the frequency dependent Eq.3.1, a classic result from population genetics [Fis30] is the fixation probability of a mutant with a simple selective advantage:

$$P_{fix} = \frac{1 - e^{-N x_o S}}{1 - e^{-NS}} \tag{3.2}$$

This result holds for haploid populations using Moran process dynamics, and merely requires factors of two in the exponents to handle diploids or Wright-Fisher dynamics. In Eq.3.2, P_{fix} depends on the frequency of mutants only via the product Nx_o, i.e. the initial *number* of mutants. Thus, Eqs.3.1,3.2 scale differently with population size. The form of Eq.3.2 implies that (when $NS \gg 1$), $P_{fix} \approx 1 - e^{-N x_o S} \approx 1 - (1 - S)^{N x_o}$ and we can think of each mutant as an independent "trial" with fixation probability S. In other

words, if the fraction x_o is kept constant and N is increased, Eq.3.1 says that P_{fix} should remain unchanged whereas Eq.3.2 says that P_{fix} should increase. On the other hand, if Nx_o is held constant as N is increased, Eq.3.1 predicts a decrease in P_{fix} whereas Eq.3.2 predicts that P_{fix} remains unchanged. Since mutators achieve fixation by hitchhiking with mutations which are themselves governed by Eq.3.2, perhaps we should *a priori* view Eq.3.1 with suspicion. Indeed, our simulation data and analytic methods will show that mutator fixation is often governed by an equation with the form of Eq.3.2.

While Eq.3.1 completely neglects deleterious mutations, they are the basis for another heuristic line of thought. In any realistic biological population, regardless of how maladapted, deleterious mutations vastly outnumber advantageous ones. Because of this, upon first thought, one might think that the mutator allele will do more harm than good and therefore be selected against. Although it is true that an elevated mutation rate will quite likely cause an immediate decrease in the population's mean fitness, evolution does not always act to maximize this quantity. The situation is understood more clearly in the following game theoretical context. A beneficial mutation often greatly increases the probability that a lineage will achieve complete evolutionary success by sweeping through the entire population, whereas a deleterious mutation only slightly decreases the low probability of a neutral sweep. More quantitatively, we can think of the "payoff" for a sweeping advantageous mutant as the entire population size N. For this to occur, the mutator must generate a beneficial mutation which must then survive in spite of random drift. In contrast, the payoff for a deleterious mutant is merely a single individual who is destined to die out with near certainty. The mutation strategy is favored when its expected payoff is greater than zero, i.e.

$$N \cdot \pi(s) \cdot \mu_{ben} - 1 \cdot \mu_{del} > 0 \tag{3.3}$$

where $\pi(s)$ is the fixation probability of a simple mutant, given by Eq.3.2 and μ_{ben} (μ_{del}) are the beneficial and deleterious mutation rates, respectively. Note that this expression weights beneficial mutations $N \cdot \pi(s)$ times more heavily than deleterious ones, underscoring their asymmetric effects. Later in this article, we show that Eq.3.3 also follows from a rigorous mathematical analysis.

Thus far we have argued that the fate of mutators is in principle limited both by competition with wild-type and by their increased load of deleterious mutants. Addi-

tionally, random genetic drift is commonly a potent force acting on rare subpopulations. Each mutator begins its existence selectively neutral. It can be shown that random drift eliminates neutral alleles from the population with a high probability $= 1 - 1/N$, and that the average time taken to do so is merely $\sim \ln(N)$ generations [Cro70b]. Although we cannot write down a "back of the envelope" estimate of this effect, we will later derive a formula that fully incorporates random drift and specifies the parameter regimes in which it dominates mutator fixation.

Our analytic work results in a formula for the mutator fixation probability in terms of simple parameters. Examining this expression yields a quantitative sense of the relative importance of random drift, deleterious mutations, and beneficial mutations. This allows us to define "strong-effect" and "weak-effect" mutator regimes in terms of the model parameters. In the strong-effect regime, mutations in the wild-type background do not affect mutator success and our analytic approach works well. In the weak-effect regime, mutations in wild-type backgrounds are predicted to be the dominant influence on mutator fixation. However, in the case of weak-effect mutators, we will show that our analytic approach, like existing work by Andre and Godelle [AG06], typically overestimates the competitive effects of mutations in wild-type backgrounds. When this is true, Eq.3.1 provides a poor description of mutator fixation. We now turn toward a discussion of our stochastic simulations, that provide an invaluable reference to which we compare our analytic work.

3.3 Description of stochastic simulations

We model haploid asexual populations of fixed size N undergoing stochastic processes of birth, death, and mutation. Initially, a fraction $x_o \ll 1$ of the population are mutators and all individuals have the same fitness. The birth-death-mutation process is iterated until the population consists entirely of either mutators or wild-type. Transitions between the mutator and wild-type states are not allowed. We do not model environmental changes explicitly, thereby assuming that the process of mutator fixation occurs on a time-scale much shorter than that associated with environmental changes.

Our stochastic simulations are based on the well known "Moran Process" [Mor92].

The following sequence of actions occurs every discrete timestep:

1. A randomly selected individual is chosen as a potential parent.

2. The chosen individual gives birth with probability proportional to its fitness. If it does not give birth, the simulation advances to the next timestep.

3. A randomly chosen individual, other than the baby, is killed.

4. The baby undergoes a deleterious (beneficial) mutation with probability equal to its deleterious (beneficial) mutation rate. This mutation rate of course depends on whether the baby is a mutator or a wild-type. Mutations between mutator and wild-type alleles are not allowed. In effect, this assumes that mutators are generated on a time-scale much longer than that of the entire "competition experiment".

We model the genome of each individual as a string of L bits [Cro70a, WH96, TLK96b]. A fraction δ of these bits correspond to critical sites in the genome that, when mutated, cause a lethal phenotype. In this case, the baby is never born, and the simulation simply advances to the next time-step. Changing the value of δ in effect allows for some adjustment of the distribution of deleterious mutational effects. The birth probability per unit time, which we denote r, is proportional to the log-fitness of the chosen individual and equals the fraction of 1's in the genome, denoted by b/L. Key parameters are $\alpha \equiv 1 - b/L$ and $\alpha_e \equiv (1-\delta)\alpha$, i.e. the fraction of sites that would be beneficial if mutated. Thus, all non-lethal mutations have the same strength and genes do not interact. This scheme for assigning fitness to genotypes is known as a "multiplicative Fujiyama" fitness landscape, and is the $K = 0$ version of Kaufman's "NK" model [Kau93]. This toy landscape is obviously a useful mathematical simplification. Additionally, recent experimental work [HSHK06, DFM07] shows that some dynamics of real bacteria and yeast populations can be captured by considering mutations of only a single strength.

Mutation is implemented by "flipping" bits with a probability $\frac{\mu_\pm}{L}$ per bit per birth event, depending on whether the baby is a mutator $(+)$ or a wild-type $(-)$. The total number of flips is determined by drawing a binomially distributed random number with success probability $\frac{\mu_\pm}{L}$ and number of trials L. Each mutation has a probability δ

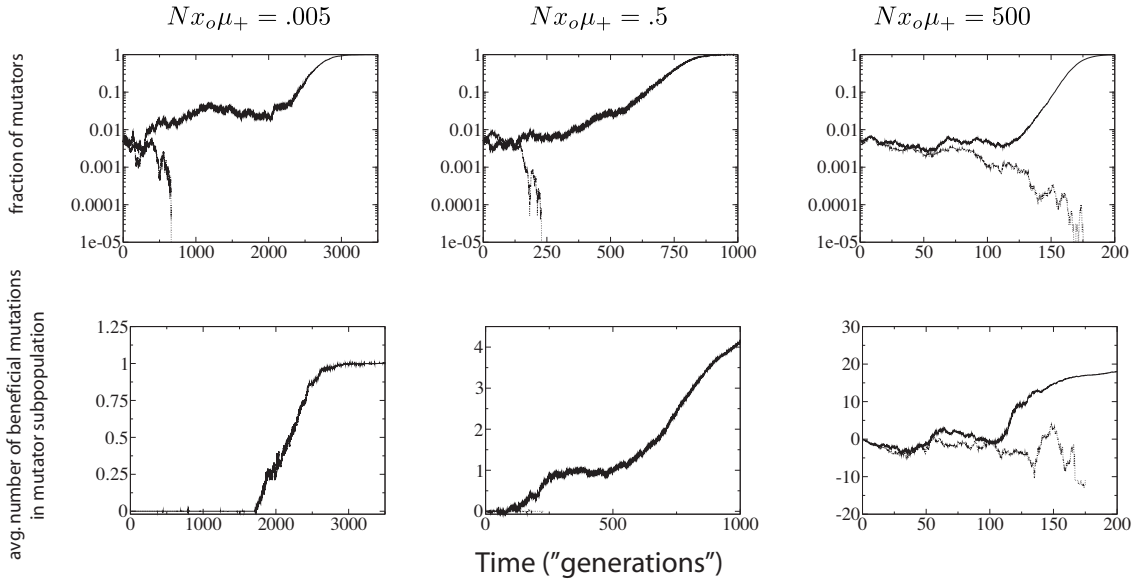

Figure 3.1: Some sample runs from simulations where the wild-type mutation rate is zero. The top panels depict the number of mutators in the population vs. $\frac{rt}{N}$, where r is the birth probability per time step which is proportional to the (initial) mean population fitness. The bottom panels show the average number of beneficial mutations in the mutator subpopulation. The dark lines resulted in fixation of the mutator allele, whereas the lighter lines resulted in its loss. When the mutation rate of the mutators (μ_+) is not too large, the mutator hitchhikes to fixation with a single beneficial mutation (left panels). When μ_+ is larger, many beneficial mutations occur during the fixation process (center and right panels). Our analytic approximation scheme assumes that the fixation process is *triggered* by merely the first beneficial mutation to survive drift. Note that in each case the population is always far from the fitness maximum when the mutator achieves fixation since there are 80 possible beneficial mutations. Parameters are $N = 10^5, x_o = .005, \delta = 0$, wild-type mutation rate $\mu_- = 0$, and $\mu_+ = 10^{-5}$ (left), $\mu_+ = 10^{-3}$ (center), $\mu_+ = 1$ (right). $\alpha = .4, s = 1/120$ (initial values).

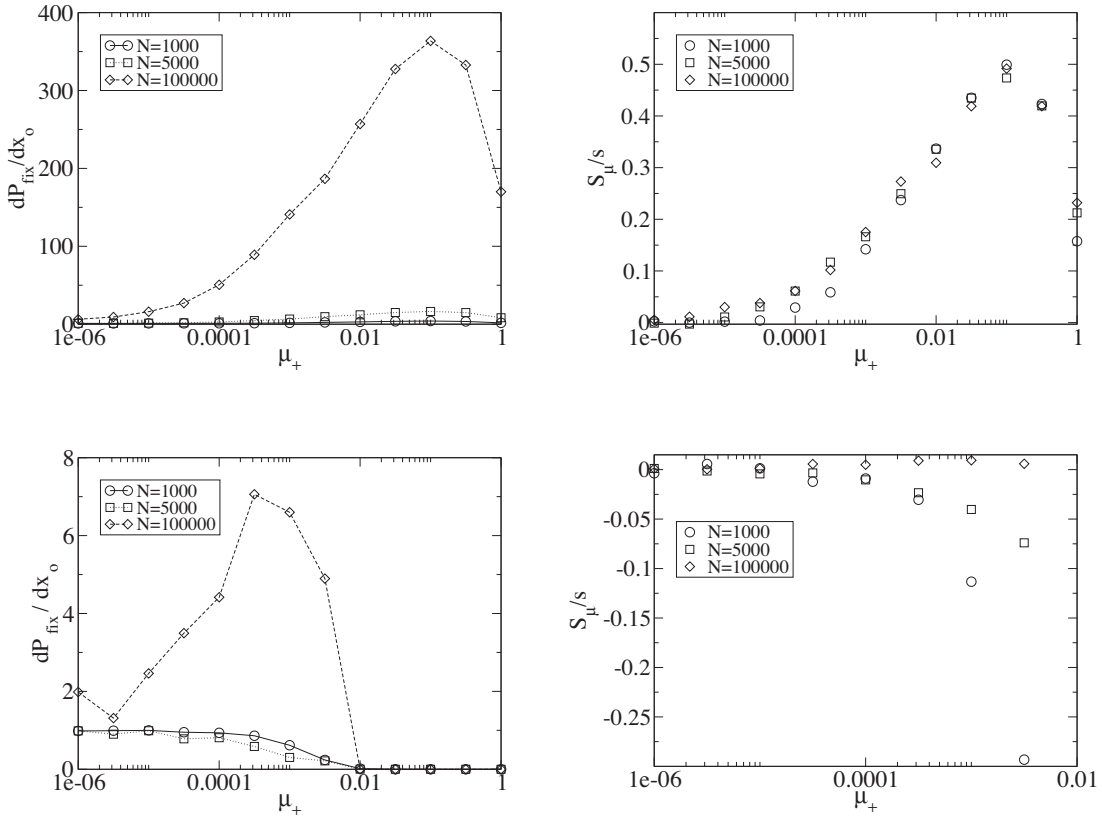

Figure 3.2: Averaged results of simulations, and the utility of S_μ as the measure of mutator success. When $P_{fix} \ll 1$, P_{fix} increases linearly with x_o (data not shown). The left panels show the (least squares) slope of said linear increase when the population is well adapted (bottom) and poorly adapted (top) to its environment. The data on the bottom row are quite noisy because of the small number of trials resulting in fixation. The panels on the right express the same data, but in terms of the effective selection coefficient S_μ of the mutator allele obtained by inverting Eq.3.2. Whereas the values from the left obviously depend on N, the values on the right panels are *independent of* N when $NS_\mu \gg 1$. This suggests that S_μ, which exposes an underlying simplicity to the simulation results, is a more natural measure of mutator success than P_{fix}. Notice that when the mutator is favored, S_μ is always less than the selective advantage s of a single beneficial mutation; this is due both to deleterious mutations and loss due to random drift. Parameters are $s = 1/120, \mu_- = 0, \delta = 0, \alpha = .4$ (top) and .008 (bottom). See Supplementary Information for details concerning averaging.

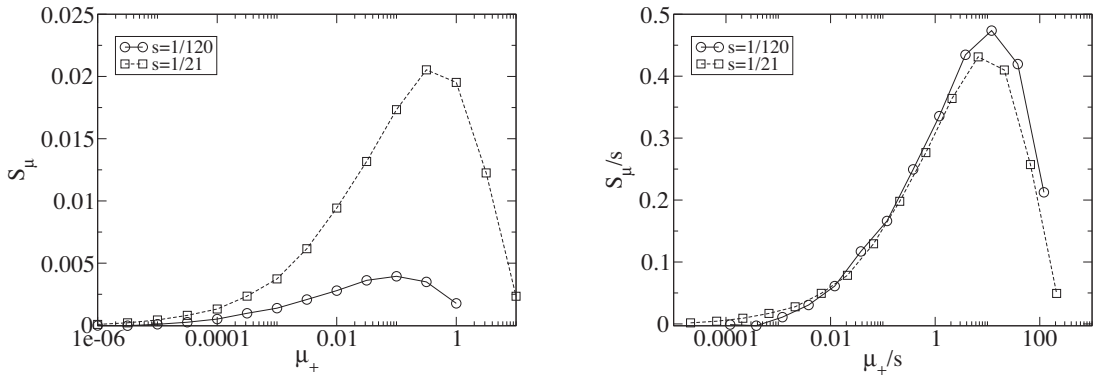

Figure 3.3: Dependence on the underlying selective advantage s. The data corresponding to two values of s, i.e. two values of L, approximately collapse onto a single curve when S_μ and μ_+ are each scaled by s. The scaling of the independent variable underscores the fact that mutator success for fixed α is largely controlled by the ratio of timescales for mutation $(1/\mu_+)$ and selection $(1/s)$. In particular, the sharp decrease in S_μ at large μ_+ occurs when these timescales become comparable, i.e. when deleterious mutations accumulate in an expanding lineage before it has sufficient time to achieve fixation. Parameters are $N = 5000$, $\mu_- = 0$, $\alpha = .4$, $\delta = 0$.

of being lethal. If no mutations are lethal, the number that are beneficial is determined by drawing another binomially distributed random number with success probability α and number of trials equal to the number of flips. Unless $\mu_\pm$ is $O(1)$, the probability of more than one mutation occurring during a single birth event is negligible and we will refer to the genome-wide mutation rate as $\mu_\pm$.

Another useful parameter is $s = \frac{1}{L}/(1-\alpha)$ which, like α and α_e, changes throughout the simulation as the population evolves. We emphasize that this fitness dependent value of s does not represent an epistatic effect. Rather, it is a consequence of mutations which result in a fixed, additive increment in "log-fitness."

A consequence of our genomic model is that both the beneficial and deleterious mutation rates will be larger than values encountered in biological populations unless L is extremely large. While this may seem like an unnecessary and undesirable restriction, it will turn out that our analytic results, which readily handle arbitrary values of the mutation rates, are insensitive to these details of our bit string simulation model.

3.4 Simulation results

To simplify matters, we first investigate the case where the wild-type mutation rate is zero; results for the more general case will be given later. Fig.3.1 shows typical runs for this case. These graphs make it clear that if the mutator mutation rate, μ_+, is sufficiently small, the mutator allele hitchhikes to fixation with a single beneficial mutation. This simple observation reminds us that mutator fixation or loss is not the result of winning the race up the fitness landscape, but rather hitchhiking with beneficial mutations. Thus, mutator alleles are better thought of as *consequences* of asexual evolution than *causes* of more rapid evolution [SGJS00]. When μ_+ is larger, the dynamics are more complex. Despite this complexity, we will later show, via the success of our analytic approximation scheme, that the fixation process is triggered mostly by the first beneficial mutation to escape random drift.

3.4.1 Dependence on μ_+:

Fig.3.2 presents simulation results for three different population sizes and two different degrees of adaptation. The fundamental measured quantity is the fixation probability P_{fix} of an initially rare mutator. When $P_{fix} \ll 1$, the mutators are completely independent of one another and P_{fix} increases linearly with x_o (data not shown). To normalize against the effect of x_o, we consider the slope of said linear increase, dP_{fix}/dx_o, which equals the mean number of mutator descendants left by each mutator, as our preliminary measure of mutator success. Fig.3.2 (left panel) shows how dP_{fix}/dx_o depends on μ_+. The small and large μ_+ limits make qualitative sense: as $\mu_+ \to 0$, the mutator phenotype is "turned off" and therefore neutral, resulting in $dP_{fix}/dx_o \to 1$. On the other hand when $\mu_+ \gtrsim 1$, a mutation occurs nearly every birth event and the fitness of an evolutionary line of individuals takes a biased random walk toward the much lower fitness of a completely random genome. Thus, although it is computationally prohibitive to measure a negligible fixation probability, it is clear that the mutator allele is nearly lethal at sufficiently large μ_+.

3.4.2 Dependence on N, and mutator effective selection coefficient:

Fig.3.2 also shows that dP_{fix}/dx_o increases with increasing N. This behavior is incompatible with Eq.3.1, which is independent of N, but is fully consistent with Eq.3.2:

$$P_{fix} = \frac{1 - e^{-Nx_oS}}{1 - e^{-NS}}$$

We now quantitatively consider whether Eq.3.2, which applies to mutants with a *direct* fitness advantage, also describes mutators with *indirect* fitness effects. For this to be the case, the fixation probability measured from simulations with differing values of N and x_o would all correspond to a single value of $S_\mu(\alpha, s, \mu_+, \mu_-, \delta)$. Using the values of P_{fix} measured from simulations, we used a computer to invert Eq.3.2, thereby obtaining corresponding values of S_μ. Fig.3.2(right) shows that, when $NS_\mu \gg 1$, there indeed exists an underlying quantity S_μ, which we call the "effective mutator selection coefficient," that remains invariant as N, x_o, and P_{fix} change.

There are several advantages to using S_μ as the measure of mutator success. First, it allows Eq.3.2 to determine in advance how P_{fix} depends on N and x_o, thereby reducing our number of parameters by two. Secondly, it allows us to apply aspects of our conceptual understanding of direct mutants to the fixation of indirect mutators. For example, when $NS_\mu \gg 1$, P_{fix} for a single mutator becomes independent of N, i.e. the notion of a frequency independent per capita fixation probability makes sense. Thirdly, the existence of S_μ, in the sense of Eq.3.2, invites future questions. For example, one may wonder whether S_μ, in addition to determining P_{fix}, also describes the average *dynamical* behavior of the mutator subpopoulation, e.g. whether $\langle x(t) \rangle \sim e^{S_\mu t}$ when rare. In this article we do not apply such an interpretation on S_μ. Rather, we merely interpret it as a succinct descriptor of mutator success.

3.4.3 Dependence on strength of mutations:

Fig.3.3 shows how S_μ depends on the strength of the mutations on our fitness landscape, as measured by s. Fig.3.3 (left) shows that as s is increased, S_μ also increases, and reaches its maximum value at a faster mutation rate. Fig.3.3(right) demonstrates that the curves in the left panel are not as different as they appear: when S_μ and μ_+ are each scaled by s, the curves become nearly identical. This means that S_μ is directly

proportional to s, and that S_μ is governed by the single composite parameter μ_+/s rather than μ_+ and s separately. Thus, an examination of the simulation data has allowed us to reduce our number of parameters by three.

3.5 Instantaneous single locus approximation (ISLA)

Stochastic simulations provide valuable signposts along the way to understanding mutator fixation. However, a deeper understanding, as well as the ability to probe computationally prohibitive regions of parameter space, requires an analytic approach as well. At a given time, the state of the population is fully specified by (i) the number of mutators, (ii) the fitness distribution of the wild-type subpopulation, and (iii) the fitness distribution of the mutator subpopulation. A complete solution to the stochastic process requires an enumeration of the transition probabilities between each of these states at each point in time. The problem with such an approach is the extremely large number of possible fitness distributions and the correspondingly high dimensionality of the resulting governing differential equations. In order to make progress, we note the heuristic rule that deleterious mutations are rapidly removed from the population, whereas beneficial mutations, and all loci linked to them, become rapidly fixed. This observation motivates the following approximations that handle mutations, which are the ultimate source of the aforementioned daunting multiplicity of fitness distributions.

Approximation 1 (A1): We assume that when a beneficial mutation arises, it instantly becomes fixed with a probability given by the classical fixation probability π of a beneficial mutation in a static, homogeneous environment. For our Moran process dynamics, this probability is simply s if $s \ll 1$ and $Ns \gg 1$. All loci in the genome in which the beneficial mutation arose also achieve fixation via hitchhiking. This represents the most common process by which the mutator allele achieves fixation or loss.

Approximation 2 (A2): The remaining fraction $1-s$ of beneficial mutations are simply ignored and treated as if no mutation occurred. This approximation is necessarily somewhat awkward. On the one hand, A2 is unnatural in that it allows lineages which are destined to be extinguished by random drift to remain in the population and potentially generate their own beneficial mutants. An alternative, which we call A2*, is to

immediately kill the beneficial mutants which do not sweep, which is clearly too harsh. These two alternatives lead to a trivial difference in our formulas, and are discussed in Supplementary Material.

Approximation 3 (A3): Deleterious mutations are treated as effectively lethal, since their descendants are quickly removed from the population. This results in an effective reduction in the birthrate of the mutator strain.

3.5.1 Derivation of diffusion equations

Since the approximations (A1-A3) preclude fitness polymorphism over finite time intervals, they allow us to describe the dynamics of the entire population by the frequency of the mutator allele $x \in \{0, \frac{1}{N}, \frac{2}{N}, ..., 1\}$. Let $T_{\uparrow}(x)$ denote the probability that the system makes a transition from the state with a fraction x of mutators to the state with a fraction $x + \frac{1}{N}$ of mutators. This may occur in one of the following two ways:

1. A mutator is selected for birth, a wild-type is selected for death, and no mutation occurs.

2. A mutator is selected for birth, a wild-type is selected for death, a beneficial mutation occurs, and this mutation is part of the fraction $1-s$ that is destined for loss by random drift .

Computing these probabilities in the order listed, we arrive at the following expression for $T_{\uparrow}(x)$

$$\begin{aligned} \frac{T_{\uparrow}(x)}{r} &= x(1-x)(1-\mu_+) + x(1-x)\mu_+\alpha_e(1-s) \\ &= x(1-x)\left[1-\mu_+\left(1-\alpha_e(1-s)\right)\right] \end{aligned} \tag{3.4}$$

The factor of r on the LHS is just the birth probability per time-step which, according to A1-A3 is common to all members of the population and will soon be scaled out. In a similar way we calculate $T_{\downarrow}(x)$, the probability that the system makes a transition from the state with a fraction x mutators to the state with a fraction $x - \frac{1}{N}$ mutators. In fact, we may simply interchange $x \leftrightarrow 1-x$ and $\mu_+ \leftrightarrow \mu_-$ in Eq.3.4 which results in

$$\frac{T_{\downarrow}(x)}{r} = x(1-x)\left[1-\mu_-\left(1-\alpha_e(1-s)\right)\right] \tag{3.5}$$

Within the framework of A1-A3, the population may also make large, non-local transitions to the "absorbing" $x = 0$ and $x = 1$ states if the mutator or wild-type strains produce an advantageous mutant which is marked for fixation. This gives rise to

$$\frac{T_{fix}}{r} = x\mu_+\alpha_e s \tag{3.6}$$

$$\frac{T_{loss}}{r} = (1-x)\mu_-\alpha_e s \tag{3.7}$$

The probability that the population undergoes no change during a timestep is simply what remains

$$\frac{T_o}{r} = 1 - T_\downarrow(x) - T_\uparrow(x) - T_{fix} - T_{loss} \tag{3.8}$$

These transition probabilities allow us to write down the so called forward and backward Kolmogorov diffusion equations which describe the time dependent probability density $P(x,t)$ that the mutator frequency is x at time t. The forward equation reads:

$$\begin{aligned}\frac{\Delta P(x,t)}{\Delta t} = &- \left[T_\downarrow(x) + T_\uparrow(x)\right] P(x,t) \\ &+ T_\downarrow(x+\frac{1}{N})P(x+\frac{1}{N},t) + T_\uparrow(x-\frac{1}{N})P(x-\frac{1}{N},t) \\ &- \left[T_{fix}(x) + T_{loss}(x)\right] P(x,t)\end{aligned} \tag{3.9}$$

A pictorial representation of this equation can be seen in Fig.3.4. Taking the continuum limit and plugging in the specific expressions for transition probabilities, we obtain for the forward equation

$$\begin{aligned}\frac{\partial P}{\partial t} = &\frac{1}{N}\frac{\partial^2}{\partial x^2}\left[x(1-x)P\right] \\ &+ (\mu_+ - \mu_-)\left[1-\alpha_e(1-s)\right]\frac{\partial}{\partial x}\left[x(1-x)P\right] \\ &- N\alpha_e s\left[x\mu_+ + (1-x)\mu_-\right]P\end{aligned} \tag{3.10}$$

where t has been rescaled by N/r so that the units are now "generations."

Each of the three lines in Eq.3.10 has a straightforward physical interpretation. The first line represents "random genetic drift." The second line represents the mutational load of the mutator. The final line represents the "decay" of probability from the open interval $x \in (0,1)$ due to beneficial mutations that instantaneously sweep.

An approximation to a limited version of Eq.3.10 is solved in appendix D. However, we can write an equivalent "backward Kolmogorov" equation which is often more

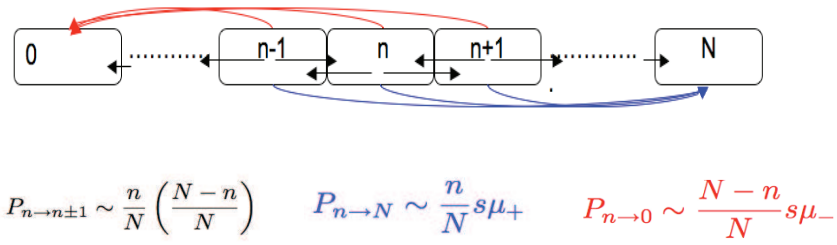

Figure 3.4: Diagrammatic representation of ISLA. The black arrows correspond to local transitions representing random genetic drift. Although these transitions are locally symmetric they are smaller near the $n = 0, N$, leading to the accumulation of probability at these endpoints. The blue arrows represent the fixation process of mutators, which ISLA caricatures as an instantaneous, nonlocal jump to the state $n = N$. Likewise, the red arrows correspond to the instantaneous fixation of a beneficial mutation in the the non-mutator (wild-type) background, which drives the mutator extinct.

mathematically convenient than Eq. 3.10. Defining $G(x_o,t)$ as the probability that the mutator has been *lost* by time t, given that $x = x_o$ at $t = 0$, we find

$$G(x_o,t+\Delta t) = T_{\downarrow}G(x_o-\frac{1}{N},t) + T_{\uparrow}G(x_o+\frac{1}{N},t) + T_oG(x_o,t) + T_{loss}(x_o) \qquad (3.11)$$

The backward equation is especially useful in its steady state form. Defining $G(x_o,t\rightarrow\infty)\equiv G_\infty(x_o)$ and taking the continuum limit, we obtain the ODE

$$\begin{aligned} 0 &= \frac{1}{N}\frac{d^2}{dx_o^2}G_\infty \\ &- (\mu_+-\mu_-)\left[1-\alpha_e(1-s)\right]\frac{d}{dx_o}G_\infty \\ &- N\mu_+\alpha_e s\frac{G_\infty}{1-x_o} + N\mu_-\alpha_e s\frac{1-G_\infty}{x_o} \end{aligned} \qquad (3.12)$$

3.5.2 Solution and analysis without wild-type mutations

We return for now to the simpler case $\mu_- = 0$, deferring until later the more general situation. Eq.3.12 can be solved exactly in terms of the Whittaker M function[AS65]. This exact solution is however not immediately instructive (and in any case cannot be generalized to the case of finite wild-type mutation rate). It is simpler in practice to solve Eq.3.12 numerically (see Supplementary Information). It is also possible to extract some useful information directly from the differential equation.

First, we note that a simple analysis reveals when the mutator allele will be favored. For notational convenience we define the constants

$$\begin{aligned} B &\equiv \mu_+\left[1-\alpha_e(1-s)\right] \\ C &\equiv \mu_+\alpha_e s \end{aligned}$$

According to ISLA, the mutator is neutral *for all* μ_+ when $G_\infty(x_o) = 1-x_o$. Plugging this into Eq.3.12, we find that this requires $B = NC$, or

$$\alpha_e^{crit} = \frac{1}{1+(N-1)s} \approx \frac{1}{1+Ns} \qquad (3.13)$$

First note that Eq.3.13 is equivalent to our heuristic guess, Eq.3.3, if $Ns \gg 1$. Examining Eq.3.13, we see that conditions which favor the emergence of mutators (at least

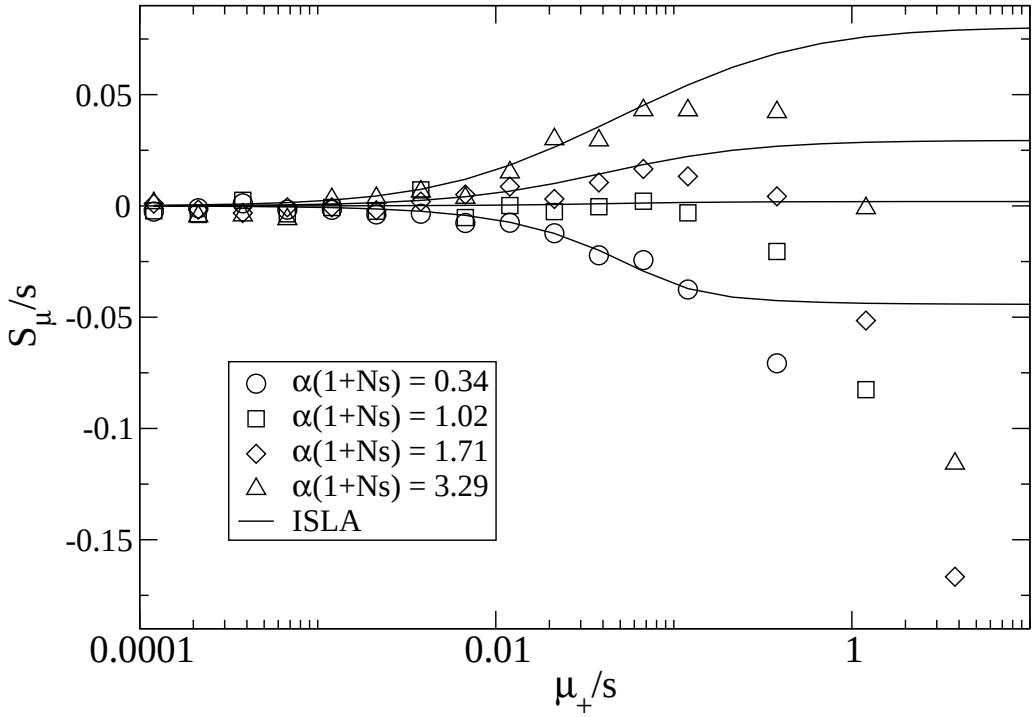

Figure 3.5: Behavior near the transition from favored to disfavored mutators. When α_e is greater than a critical value α_e^{crit}, the mutator allele is favored ($S_\mu > 0$) for small enough μ_+. Our analytic approach (ISLA) predicts that the transition occurs at $(Ns+1)\alpha_e^{crit} = 1$, which agrees extremely well with simulation data. Parameters are $N = 5000, s = 1/120, \mu_- = 0, \delta = 0$. The number of available beneficial mutations are, in order of decreasing mutator success: 10, 5, 3, and 1.

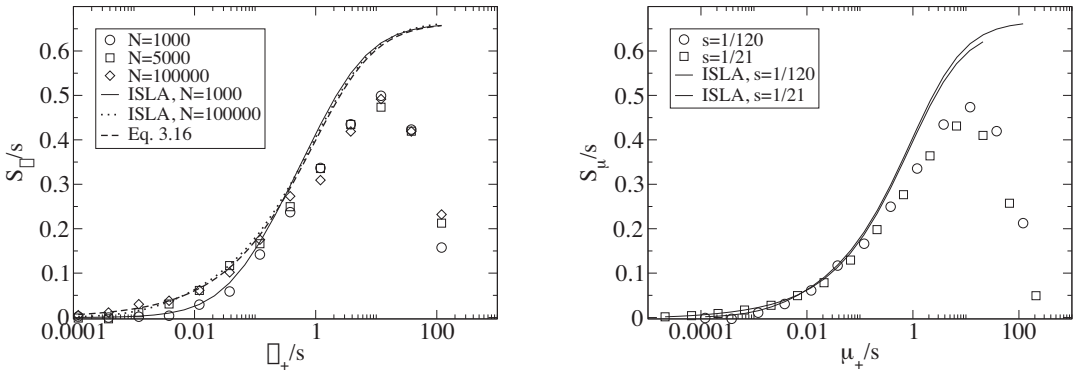

Figure 3.6: Comparison of simulation, numerical solution of Eq.3.12, and the analytic approximation Eq.3.16. The exact numeric solutions to our ISLA Eq.3.12 for different N converge to the analytic approximation Eq.3.16 when $NS_\mu \gg 1$ (left). Solutions to Eq.3.12 show, in agreement with simulation, that S_μ/s depends on μ_+/s rather than μ_+ and s seperately (right). Parameters are those used in Figs. 3.2, 3.3.

when the resident mutation rate μ_- is negligibly small) are large population size, potent mutations, and a relatively large fraction α_e of sites that would be beneficial if mutated, perhaps due to an environment to which the organism is not well adapted. The fact that large α_e favors mutators is obvious. The dependence on N is simply a result of the fact that as population size increases, the neutral fixation probability $1/N$ becomes an easier benchmark to exceed. The qualitative dependence on s is also straightforward in hindsight, given A1-A3: increasing s increases the fraction of beneficial mutations that achieve fixation, but does not affect the fate of deleterious mutations, all of which are treated as lethal. Also notice that for sufficiently large N the mutator is always favored, although its fixation probability may be very small: it is favored only in the sense that it fares better than a neutral allele whose fixation probability is $1/N$. Fig.3.5 demonstrates the success of Eq.3.13 when $\mu_+/s \ll 1$. The failure of ISLA for larger μ_+/s will be discussed later. We next develop approximate solutions to Eq.3.12, with $\mu_- = 0$.

Strongly Favored Mutators ($NS_\mu \gg 1$)

In this regime, we expect P_{fix} to increase rapidly with x_o. Therefore, we expect the loss probability $G_\infty(x_o)$ to decrease rapidly, and $1/(1-x_o)$ to differ significantly

from 1 only when $G_\infty \approx 0$. Then, for $x_o \ll 1$, we can approximately take $1 - x_o \to 1$, and the solution to Eq.3.12 with $\mu_- = 0$ is simply

$$\begin{aligned} G_\infty(x_o) &= e^{-Nzx_o} \\ z &\equiv \frac{\sqrt{B^2+4C}-B}{2} \end{aligned} \tag{3.14}$$

Our approximation is self consistent if indeed G_∞ decays rapidly, i.e. $Nz \gg 1$. This solution does not satisfy the boundary condition at $x_o = 1$ since our solution is only valid for $x_o \ll 1$. Beyond this region the structure of the solution is more complicated, which need not concern us here since fixation is essentially total in this regime. We then have for the fixation probability of the mutator

$$P_{fix}(x_o) = 1 - e^{-Nzx_o} \qquad (Nz \gg 1) \tag{3.15}$$

A comparison with Eq.3.2 shows that, according to A1-A3 and in the limit $Nz \gg 1$, the mutator effectively behaves like a simple advantageous mutant with a well defined selection coefficient $S_\mu = z$:

$$S_\mu = z = \frac{\sqrt{B^2+4C}-B}{2} \approx \frac{\mu_+}{2}\left[\sqrt{(1-\alpha_e)^2 + 4\alpha_e s/\mu_+} - (1-\alpha_e)\right] \qquad NS_\mu \gg 1 \tag{3.16}$$

A comparison of the stochastic simulation data with both a numerical solution of Eq.3.12 and this approximate analytic expression (Eq.3.16) is given in Fig.3.6. We see that our approximate S_μ/s only depends on μ_+/s rather than μ and s separately, as we noted in the Simulation Results section.

For small $\mu_+ \ll \alpha_e s$, $C \gg B^2$ and $S_\mu \approx \sqrt{C} = \sqrt{\mu_+ \alpha_e s}$, and thus only advantageous mutations are relevant to mutator success. This result (which is directly supported by Fig.3.10 to be discussed later), shows that in this regime, random drift, and not deleterious mutations, is the only check on mutator success.

In the complementary regime where $\mu_+ \gg \alpha_e s, |S_\mu|$ approaches its maximum value S^*_μ with respect to μ_+. Here, the solution is the same as if the second derivative term, which represents random drift, were dropped from Eq.3.12 (see below). Therefore, random drift is irrelevant in this regime and deleterious mutations alone limit mutator success, giving

$$S^*_\mu = \frac{C}{B} \approx \frac{\alpha_e}{1-\alpha_e} s \tag{3.17}$$

The factor in Eq.3.17 multiplying s is the ratio of beneficial mutations to deleterious and lethal mutations. In real biological populations, this ratio is certainly less than one, and hence $S^*_\mu \ll s$.

Marginal Mutators ($NS_\mu \lesssim 1$)

We can readily make progress in this regime if $N\mu_+ \gg 1$ and $N^2\mu_+\alpha_e s \gg 1$. In this case, the B and C terms dominate Eq.3.12 and the solution for G_∞ is simply

$$G_\infty(x_o) \approx (1-x_o)^{NS^*_\mu} \tag{3.18}$$

with a fixation probability $P_{fix}(x_o) \approx Nx_oS^*_\mu$. In obtaining this solution, we dropped the second derivative term in Eq.3.12, which could in principle introduce large errors near $x_o = 1$, where $G''(x_o)$ from Eq.3.18 is in fact large. Nonetheless, it turns out that Eq.3.18 satisfies the boundary condition at $x_o = 1$ and thus remains a valid leading order approximation for all x_o. Since P_{fix} is comparable to $1/N$ in the present marginal case, we cannot interpret S^*_μ as a mutator selection coefficient here. Rather, we have $P_{fix} = x_o(1 + NS_\mu/2)$, from which we obtain $NS_\mu = 2\frac{\alpha_e(Ns+1)-1}{1-\alpha_e}$, independent of μ_+. The numerator of this expression makes clear the agreement with our previous estimate for the critical value of α_e given by Eq.3.13.

The case where $N\mu_+ \lesssim 1$ and $NS_\mu \lesssim 1$ requires a more lengthy analysis, and is presented in appendix B.

3.6 Effect of wild-type mutations

We now turn our attention to the more complicated case when mutations in wild-type backgrounds are allowed, i.e. $\mu_- > 0$. We begin by solving Eq.3.12 for $\mu_- > 0$ in the large $N\mu_\pm$ limit, where the second derivative term can be neglected. Working in this limit simplifies the mathematics, and is sufficient for illustrating the points that we intend to make. An approximation that incorporates the second derivative term and

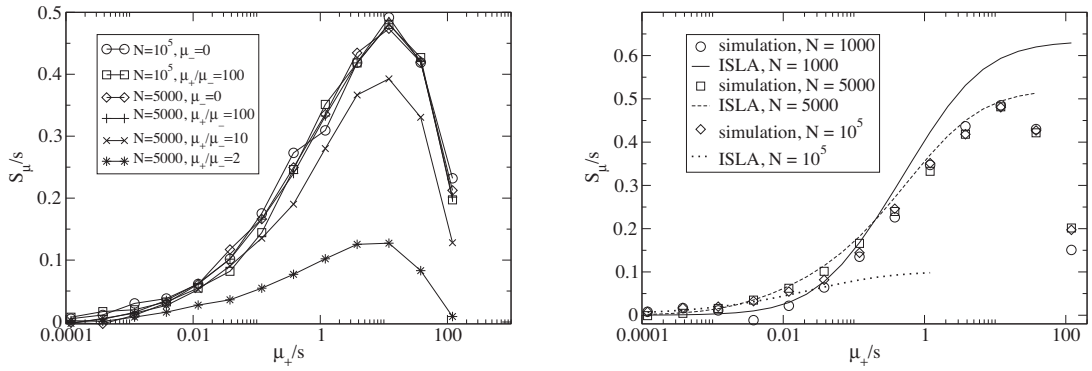

Figure 3.7: Small effect of mutations arising in wild-type backgrounds. ISLA predicts that these mutations will become important in the weak-effect mutator regime defined by $\frac{R(1-\alpha_e)}{N\alpha_e s} \lesssim 1$, where $R \equiv \mu_+/\mu_-$. However, the simulation data show that mutations in wild-type backgrounds sometimes have a negligible impact even in the weak-effect mutator regime. In the panel on the right, $\frac{R(1-\alpha_e)}{N\alpha_e s}$ has the values 18, 3.6, and .18, respectively, as N is increased. Accordingly, ISLA predicts a decrease in S_μ, but S_μ did not change in simulations. The panel on the left shows that beneficial mutations in wild-type backgrounds eventually decrease S_μ for large enough R, though the decrease here is smaller than what ISLA predicts. Parameters are $\alpha = .4, s = 1/120, \delta = 0$, and $\mu_+/\mu_- = 100$ (right).

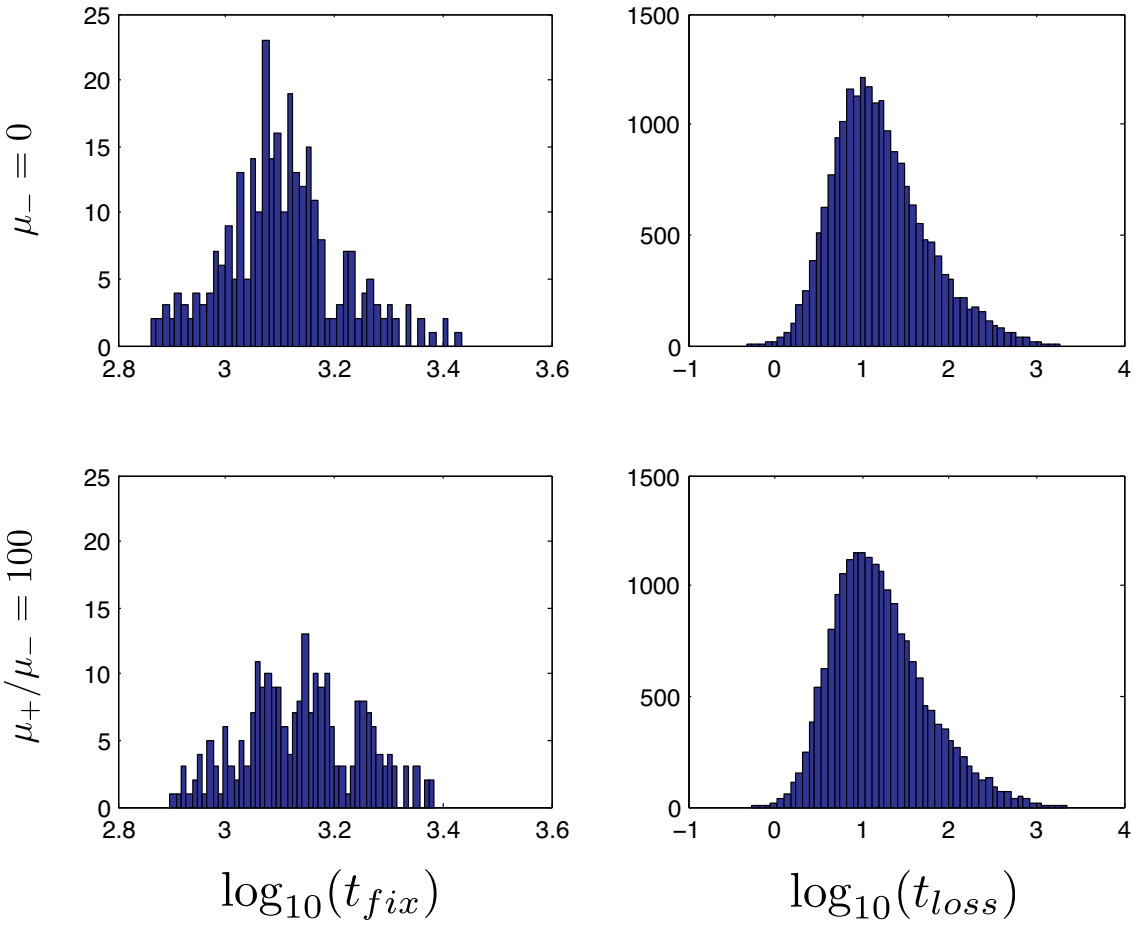

Figure 3.8: The distributions of fixation and loss times for cases where $P_{fix} \approx 1\%$. The left (right) column shows the distribution of fixation (loss) times. The top row corresponds to $\mu_- = 0$ and the bottom row to $\mu_+/\mu_- = 100$. Notice the logarithmic scale and the extremely long tails on the t_{loss} distributions. The two t_{loss} distributions have the same mean $\bar{t}_{loss} \approx 40$ generations, which is of the same order as $\bar{t}_{drift} = Nx_o \ln(1/x_o) \approx 92$ generations. The t_{fix} distributions have means $\bar{t}_{fix} \approx 1300$ generations ($\mu_- = 0$) and $\bar{t}_{fix} \approx 1400$ generations ($\mu_+/\mu_- = 100$). Since $t_{sweep} \sim \frac{ln(Ns)}{s} \approx 800$ generations are required for an advantageous mutant to sweep the population, we see that $500 - 600$ generations passed before a beneficial mutant destined for fixation was generated. Thus, when mutator fixation occurs, such beneficial mutations are typically generated early compared to $\bar{t}_{mut} \equiv (\alpha s \mu_+ N x_o)^{-1} = 3 \times 10^4$ but late compared to $\bar{t}_{drift}$. S_μ is determined mostly by the probability that the mutator survives the long drift period and this is barely affected by wild-type beneficial mutant fixation events. Parameters are $N = 10^5, s = 1/120, \alpha = .4, x_o = 10^{-4}, \delta = 0, \mu_+ = 10^{-3}$. Note that the initial *overall* mutation rate in the wild-type population is $100\times$ that in the mutator subpopulation.

random drift is included in appendix E. In the large $N\mu_{\pm}$ limit,

$$\begin{aligned} 0 = & - (\mu_+ - \mu_-)\left[1-\alpha_e(1-s)\right]\frac{d}{dx_o}G_\infty \\ & - N\mu_+\alpha_e s\frac{G_\infty}{1-x_o} \\ & + N\mu_-\alpha_e s\frac{1-G_\infty}{x_o} \end{aligned}$$

This first order, linear ODE can be solved by standard methods. Defining $R \equiv \mu_+/\mu_-$, we obtain

$$P_{fix} \approx Nx_o s\frac{\alpha_e}{1-\alpha_e}\left(1+\frac{\alpha_e(Ns+1)-1}{R(1-\alpha_e)}\right)^{-1} + O(x_o^2) \tag{3.19}$$

The prefactor in Eq.3.19 is identical to our previous expression for the $\mu_- = 0$ case (Eqs.3.17,3.18) when $x_o \ll 1$. Recall that the sign of the quantity $\alpha_e(Ns+1)-1 \approx N\alpha_e s - 1$ determines whether mutators are favored (Eq.3.13). Therefore, mutations in wild-type backgrounds decrease P_{fix} when mutators are favored and *increase* P_{fix} when they are disfavored. This latter effect occurs because mutating is generally a losing strategy when $\alpha_e(Ns+1)-1 < 0$ (see Eq.3.3): the small persistent cost of deleterious mutations exceeds the huge occasional benefit of a selective sweep. Thus, in this regime the wild-type aids the mutator by participating in this losing strategy.

Eq.3.19 also determines when R is sufficiently large to ignore mutations in wild-type backgrounds. In other words, Eq.3.19 allows us to define natural "strong-effect" and "weak-effect" mutator regimes. For weak-effect mutators, $\frac{\alpha_e(Ns+1)-1}{(1-\alpha_e)} \approx N\alpha_e s \gg R$, and Eq.3.19 reduces to $P_{fix} = x_o R$, which is *independent of* N. This is the same as Eq.3.1 for $x_o \ll 1$. Thus, in this regime, ISLA predicts that mutational competition with the wild-type is the dominant factor limiting mutator fixation, and we recover the explicitly frequency dependent heuristic picture. In the opposite extreme of strong-effect mutators, regardless of the sign of $\alpha_e(Ns+1)-1$, we recover our $\mu_- = 0$ result (Eqs.3.17,3.18) where deleterious mutations are the dominant factor limiting mutator fixation.

These are pleasing mathematical results that seem to reconcile opposing heuristic viewpoints. However, they do not always match simulations in the weak-effect mutator regime. Fig.3.7 (right) shows numerically generated solutions to Eq.3.12 (Eq.3.19 gives the large μ limit of these curves) as compared to the outcome of simulations.

The disagreement is obvious: ISLA drastically overestimates the effect of the mutations in wild-type backgrounds. Fig.3.7 shows that beneficial mutations in wild-type backgrounds eventually decrease S_μ for large enough R, though the decrease here is smaller than what ISLA predicts. The small effect of these mutations persisted even when we used parameters such that the wild-type subpopulation generated mutations at a rate $N(1-x_o)\mu_-$ that was equal to or even greater than the corresponding rate $Nx_o\mu_+$ in the mutator subpopulation. Although we do not fully understand this discrepancy, we can point to its source: There is a subtle error involving the final term of both Eqs.3.10,3.12 which states that during a single time-step, the mutator has a probability $(1-x)\mu_-\alpha_e s$ of becoming *instantly* lost. This is incorrect. The correct statement is that $(1-x)\mu_-\alpha_e s$ is the probability that during one time-step, the wild-type generates a beneficial mutation that will *eventually* escape loss to random drift. Such mutations sweep through the population during a mean time interval $t_{sweep} \sim \frac{\ln(Ns)}{s}$ generations which is typically much longer than the time to extinction of a mutator due to random drift $\bar{t}_{drift} \approx \ln(N)$ [Cro70b]. A more detailed picture is gained by examining the distribution of fixation and loss times of the mutator allele. Fig.3.7 shows that these distributions are barely affected by μ_-, suggesting that these mutations play a very small role in the mutator fixation process.

Despite these complications, for sufficiently large s, t_{sweep} is small, A1 becomes a better approximation, and ISLA more closely matches simulations. An example of this agreement is presented in Fig.3.9, where $s = 1/3, N = 1000, \alpha_e = .4, R = 10$. Thus, ISLA provides accurate results except in the weak-effect mutator regime with sufficiently small s. Unfortunately, we do not have a quantitative sense as to how large s must be in order to achieve accuracy. We plan to address this issue in future work.

3.7 Comparison of ISLA to simulation

We now return to the case $\mu_- = 0$, where the results of ISLA agree with simulations when $R \equiv \mu_+/\mu_-$ is sufficiently large. Figs.3.5,3.6 illustrate the agreement between ISLA Eq.3.12 and simulations, whenever μ_+/s is not too large. However, for larger μ_+/s, we see the emergence of two qualitatively distinct discrepancies between

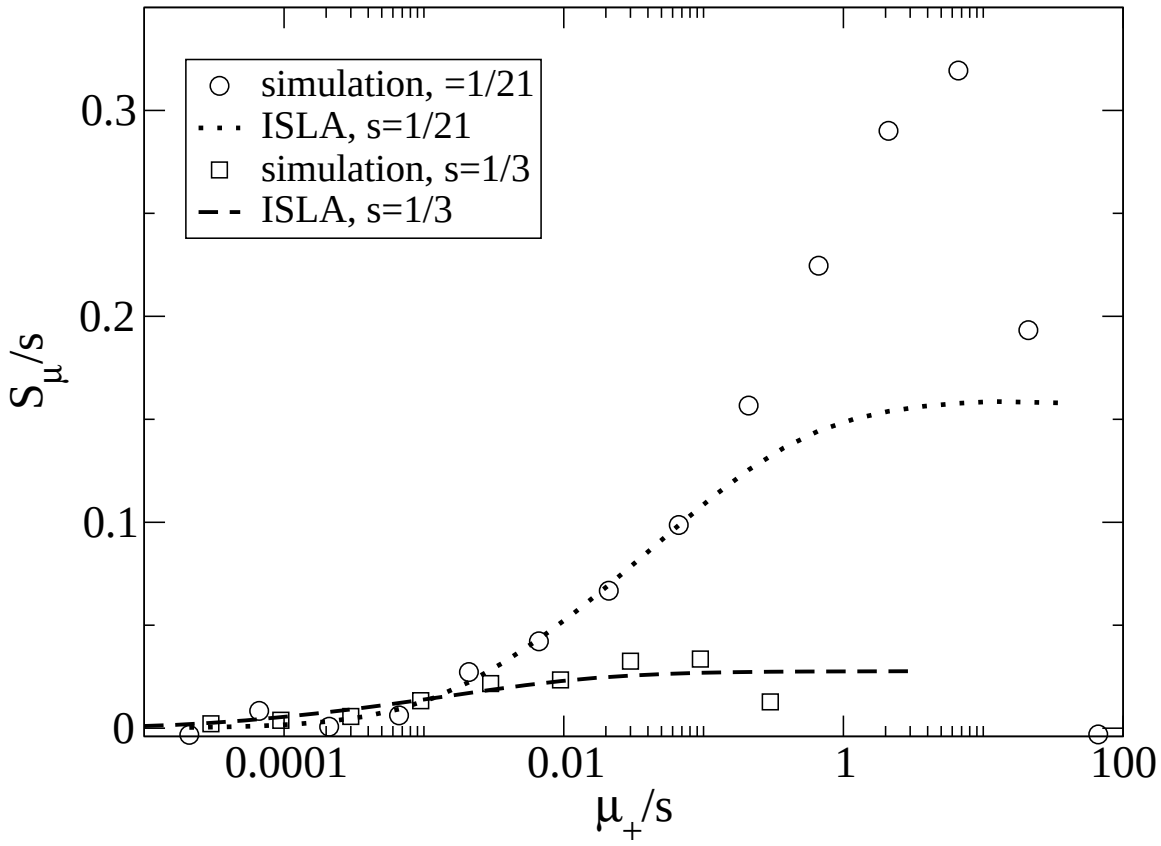

Figure 3.9: Simulation data for very large s. When $s = 1/21$, ISLA greatly overestimates the the effect of mutations in wild-type backgrounds, whereas the agreement is much better when $s = 1/3$. Parameters are $N = 1000$, $\mu_+/\mu_- = 10, \alpha_e = .4, \delta = 0$

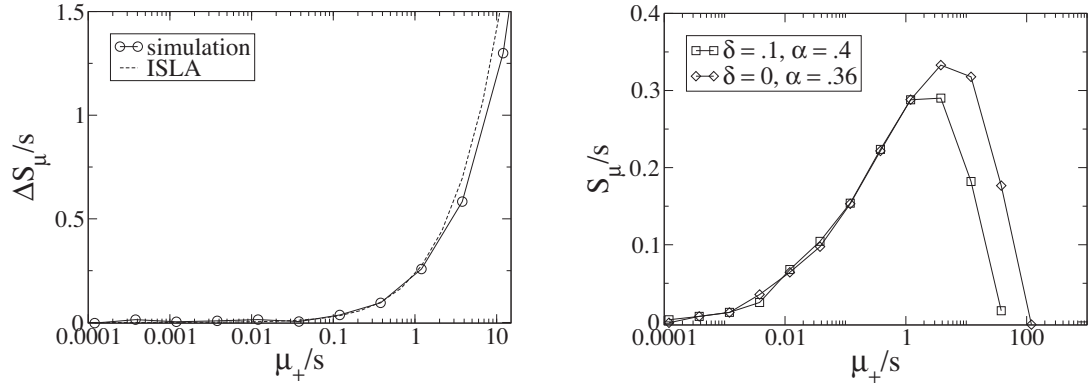

Figure 3.10: The role of non-lethal deleterious mutations. We "turned off" deleterious mutations, both in simulations and in ISLA, by setting the deleterious mutation rate to zero and leaving the beneficial mutation rate unchanged (left). The difference between these results and the corresponding ones *with* deleterious mutations is plotted on the vertical axis on the left. For $\mu_+/s \lesssim 1$, deleterious mutations have the same effects in ISLA Eq.3.12 as in simulations (left). ISLA essentially treats deleterious mutations as lethal (A3), instead of merely having a selective disadvantage $-s$. We tested this approximation directly in simulations by varying the parameters α and δ while holding the product $\alpha(1-\delta) \equiv \alpha_e$ constant (right). Parameters are $s = 1/120, N = 5000, \mu_- = 0$ and $\alpha = .4, \delta = 0$ (left only).

ISLA and simulations. For $\mu_+/s \lesssim 1$, a relatively small difference accumulates, whereas when μ_+/s reaches values of $O(1)$, a drastic difference emerges. In this section, we analyze the sources of these discrepancies.

The broad reason that ISLA and simulation do not agree for all μ_+ is simply that A1-A3 and the resulting transition probabilities are only an approximation of the complex stochastic process executed by the simulations. Indeed, strictly speaking, the simulation does not even undergo a Markov process with respect to the variables x,t: one must also consider the fitness distributions of the subpopulations in order to write down the exact transition probabilities. When viewed this way, it is perhaps surprising that A1-A3 work as well as they do. We now specifically point out the errors introduced as a result of A1-A3, all of which are associated with mutational processes.

A3 is accurate when $\mu_+/s \lesssim 1$

We first analyze the way that ISLA treats deleterious mutations, which includes both A3 (which treats all deleterious mutations as lethal) and A1 (which does not allow deleterious mutations to arise in the course of fixation of an "evolved" clone). Fig.3.10 (right) compares simulation results from two sets of parameters with identical beneficial mutation rates ($\alpha_e\mu_+$) but different allocations of lethal and deleterious mutations via a difference in the parameter δ. The results are essentially identical as long as $\mu_+/s \lesssim 1$. This shows that as far as mutator fixation is concerned, mutations of effect $-s$ can be considered lethal, i.e. A3 is accurate in this regime.

A1 is accurate when $\mu_+/s \lesssim 1$

Furthermore, we can test all the effects of deleterious mutations by removing them from both the simulations and ISLA: the deleterious mutation rate is set to zero whereas the advantageous mutation rate is left unchanged. The results of this case are presented in Fig.3.10 (left). Predictably, S_μ increases monotonically with μ_+ in this case (data not shown). To compare the effect of deleterious mutations in simulations against those same effects according to ISLA, Eq.3.12, we plot the difference $\Delta S_\mu \equiv S_{\mu,no-deleterious} - S_{\mu,deleterious}$ between results with deleterious mutations "off" and those with deleterious mutations "on" in the two cases. We see in Fig.3.10 (left) that

ΔS_μ from ISLA matches that from simulation until $\mu_+/s \to 1$. Also note that $\Delta S_\mu \approx 0$ for $\mu_+/s \ll .1$, illustrating the negligible effect of deleterious mutations in this regime. Thus, both A1 and A3 are accurate when $\mu_+/s \lesssim 1$.

A2 fails when $\mu_+/s \lesssim 1$

Since A1 and A3 remain valid in this regime, the mild discrepancy between simulations and ISLA must originate in A2, which handles beneficial mutations. Specifically, the fraction $(1-s)$ of advantageous mutants that are lost to random drift are treated as neutral mutators which can later give rise to beneficial mutants that may sweep through the population. In some sense, this overstates the potential of these mutants because, in fact, they are typically lost to random drift within a few generations [Cro70b]. There is no simple remedy for this deficiency in A2, but an alternative, which we denote A2*, is to immediately kill these advantageous mutants, thereby treating them equivalently to deleterious and lethal mutants. Whereas A2 overestimates S_μ in this regime, A2* underestimates it. Thus, the simulation data is bounded by the predictions of A2 and A2* when $\mu_+/s \ll 1$. See Supplementary Information for a graphical comparison and further discussion of A2*.

A1 fails when $\mu_+/s \sim 1$

We now turn to the large discrepancy between ISLA and simulations when μ_+/s is $O(1)$, as seen in Fig.3.10. Roughly speaking, this occurs when the time-scales of (deleterious) mutation and selection become comparable. In this regime, members of an expanding "evolved" clone are "lost" due to deleterious mutations faster than they are "added" due to selection. Consequently, the fixation probability of an advantageous mutant in a homogeneous genetic background $\pi(s) < s$ and A1 fails. Semi-quantitatively, we expect this effect to set in when $(1-\alpha_e)\mu_+/s \sim 1$. The α_e dependence can be seen by comparing Figs.3.5,3.6.

Table 3.2: Values of relevant parameters for non-mutators in *E. coli*, as reported in various references. We assume that all mutation rates are $100\times$ greater in mutators. Mutation rates are per genome per replication. "Selection coefficient" refers to that of advantageous mutations only.

Reference	μ_{ben}	μ_{del}	U	$\tilde{s}$
[HSHK06]	2.0×10^{-7}			0.054
[LRST91]	2.8×10^{-10}			0.10
[PFMG07]	2×10^{-8}			0.023
[IS01]	4×10^{-9}			0.02
[RdVG02]	5.9×10^{-8}			0.0235
[KL96]		1.9×10^{-4}		
[KEW99]		1.6×10^{-3}		
[TMGR97]			5×10^{-7}	
[BDK$^+$00]			5×10^{-6}	

3.8 Comparison to experiment

As mentioned previously, the spontaneous emergence of mutator alleles has been documented in laboratory evolution experiments with *E.coli* [SGL97, SDS$^+$02]. In this experiment, mutator alleles with $R\approx100$ became fixed in 3 out of 12 independently evolving *E.coli* populations within 10,000 generations. The total number of mutators generated among 12 lines during 10,000 generations is approximately $N_e\times U\times(10^4\times12)$, where U is the mutation rate into the mutator state and N_e is the effective population size [WG01, WGSV02]. U has been measured between 5×10^{-7} [TMGR97] and 5×10^{-6} [BDK$^+$00], and we find $N_e=6.3\times10^7$ (see Appendix C). Since three of these mutators achieved fixation, the experimental fixation probability $P_{fix,expt}$ is approximately given by $3/(N_e\times U\times10^4\times12)$ and bounded by

$$7.9\times10^{-8}<P_{fix,expt}<7.9\times10^{-7} \tag{3.20}$$

This value is 5-50 times that of a neutral allele ($1/N_e$).

In order to compare this value to the predictions of ISLA, we need experimental values for the parameters μ_+,α_e, and s. It turns out that the equivalent set of parameters s, the beneficial mutation rate $\mu_{ben,+}=\alpha_e\mu_+$, and the deleterious mutation rate $\mu_{del,+}=(1-\alpha_e)\mu_+$ are more readily available in the literature. A survey of these parameter values is presented in table 4.1. Presently, we use the beneficial mutation rate

$\mu_{ben} = 2.8 \times 10^{-8}$ and selection coefficient $s = .1$ obtained by Lenski and co-workers [LRST91]. Following reference [KEW99], we take $\mu_{del} = 1.6 \times 10^{-1}$. These mutation rates are based on the measured wild-type values and assume $R = 100$. Since $N_e \mu_{del,+} \gg 1$, $N_e^2 \mu_{ben,+} s \gg 1$, and $N_e \alpha_e s \ll R$, these populations are in the drift-less, strong-effect mutator regime. Therefore, the appropriate formula is either Eq.3.18 or Eq.3.19, which give the same results. Plugging our parameter values into ISLA, we obtain

$$P_{fix,isla} = 1.8 \times 10^{-8} \tag{3.21}$$

in reasonable agreement with the rough experimental value (Eq.3.20). Other choices for parameter values, particularly $\mu_{ben,+}$, would result in less impressive agreement with experiment.

The interpretation of "beneficial mutation rate" deserves careful attention. In biological populations, mutants with a spectrum of beneficial effects are generated at specific rates $\mu_{bp}\rho(s)ds$, where $\rho(s)$ is likely a decreasing function of s [Orr03, EWK07]. The weakest mutants are generated frequently, but are unlikely to achieve fixation because (i) their intrinsic fixation probability $\pi \sim s$ is small, and, (ii) in reasonably large populations, several of these mutations exist simultaneously and thus compete with one another. Conversely, stronger mutants are seldom generated, but likely achieve fixation. These conflicting influences result in beneficial mutations of some intermediate size $\tilde{s}[\rho(s), N, \mu_{bp}]$ typically achieving fixation [GL98, DFM07, HSHK06]. These mutants are generated at a per capita rate $\mu_{ben} \approx \mu_{bp} \int_{\tilde{s}}^{\infty} \rho(s)ds$. The dependence of μ_{ben} and $\tilde{s}$ on N has been theoretically predicted [GL98, DF07] and directly observed experimentally [PFMG07]. Thus, whenever the population size is large enough for the aforementioned effects to play a strong role, the microscopic parameters μ_{bp} and $\rho(s)$ result in the *macroscopic parameters* $\tilde{s}$ and μ_{ben}. These are the parameters that we list in table 4.1 and plug into our model.

It is also interesting to note that, according to these experimental parameters, $N\alpha_e s \approx 1.1$, indicating that these *E. coli* populations only very marginally favored mutators. This could explain why no mutators fixed during the next $25,000$ generations: $N\alpha_e s$ had decreased below the threshold value of one as fewer, and less potent, beneficial mutations became available.

Due to the relatively large population size $N_e = 6.3 \times 10^7$ and the anticipated small fixation probability, we cannot obtain an accurate measurement of P_{fix} using our simulation method. However, for these experimental parameters, $\mu_+(1-\alpha_e)/s = \mu_{del,+}/s$ is $O(1)$ and therefore we expect the data to lie in the decreasing portion of curves such as Fig.3.6. Thus, our ISLA estimate of P_{fix} is possibly much larger than what simulations would yield. We briefly return to this issue in the Discussion.

3.9 Discussion

3.9.1 Relation to Previous Theoretical Work

As mentioned in the introduction, there are many existing theoretical models of mutator evolution. In this section we briefly review the existing body of knowledge and place our present work in this larger context. Studies are discussed roughly in order of increasing similarity to our present work.

Models with explicit environmental change

Leigh [LJ70] endeavored to calculate the mutation rate that maximizes the growth rate of its corresponding modifier locus. An infinite population with this wild-type ("resident") mutation rate is evolutionarily stable in the sense that it cannot be invaded and swept by any modifier of mutation rate. Such an evolutionarily stable strategy (ESS) is referred to as the ESS mutation rate. Leigh developed a simple two locus, two allele model of mutator dynamics in an environment that regularly alternates between two states. One locus is under selection, and its two alleles are alternately favored in the two different environments. The second locus is not under direct selection and merely modifies the mutation rate at the selective locus. The dynamics of the mutator allele are deterministically governed by two effects. First, immediately after the environment changes, the mutator increases its frequency because the small population of mutants, which is favored in the new environment, is over-represented in the mutator background. This favors the higher mutation rate. Secondly, after the mutant sweeps through the population, the frequency of the mutator decreases due to association with the deleterious

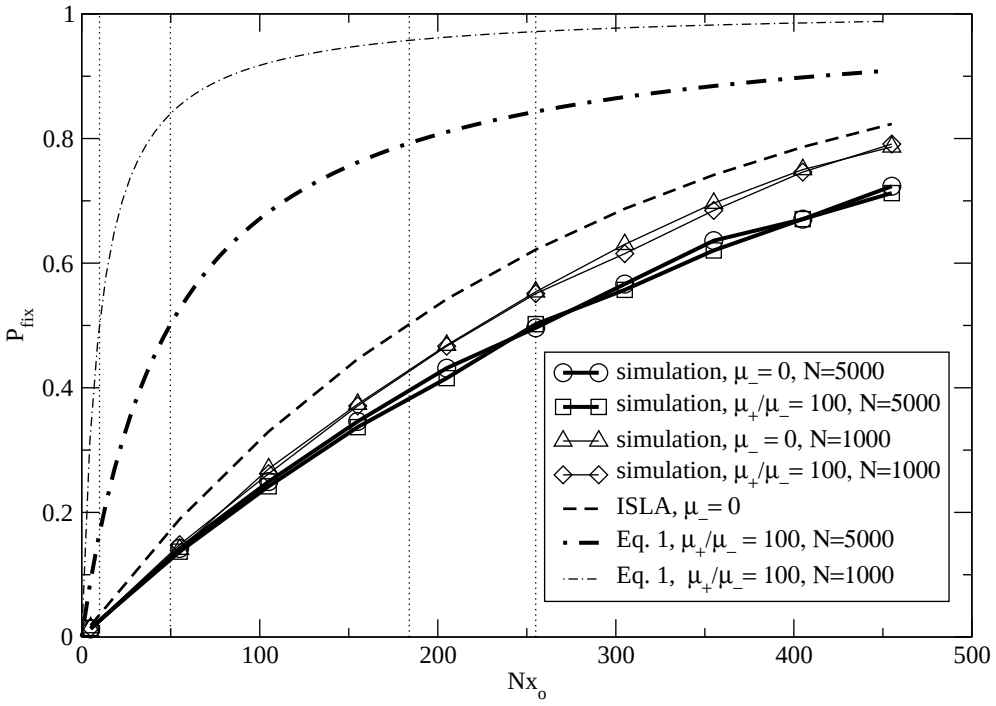

Figure 3.11: The scaling behavior of Eq.3.1 and ISLA are *qualitatively* different. If the initial number of mutators Nx_o is kept constant while N is increased, then ISLA predicts that P_{fix} remains invariant, whereas the frequency dependent Eq.3.1 predicts a large change. Simulations are in better accord with ISLA than Eq.3.1. These scaling predictions could be experimentally tested by observing whether the "threshold" number of initial mutators changes with N. Here, we have defined the threshold as the number of mutators for which $P_{fix} = 1/2$, and depicted these values with vertical dotted lines. Parameters are $\alpha = .4, \delta = 0, \mu_+ = s = 1/120$.

mutants that it generates at its new fitness peak. This favors lower mutation rate. The cycle repeats itself many times, and Leigh finds that the long term ESS mutation rate is equal to the rate of environmental change. Over the years, this basic model was improved by incorporating the effects of timing of environmental changes, varying selective coefficients [IMIS89], intermediate genotypes [TT02], and multiple mutable sites [PL06].

While these models doubtless provide valuable insight into certain biological scenarios, they are rather orthogonal to our work. Three differences seem especially important. First, most obviously, mutator success requires repeated environmental changes in these models. In contrast, our model shows that environmental change is only *necessary* for mutator fixation insofar that it provides a rationale for having a population displaced from its fitness peak. Secondly, they endeavor to find the global ESS mutation rate whereas we focus on quantifying, via fixation probability, the probabilistic result of a single competition experiment. While full knowledge of $P_{fix}(N, s, \alpha, \mu_+, \mu_-, \delta)$ implies the value of the ESS, the converse is not true. Thirdly, their mechanism of mutator success is very different from ours. Whereas they rely upon the alternating selective effects of existing mutants to boost mutator frequency, our model analyzes the dynamic, stochastic interplay between random drift, deleterious mutations, and advantageous mutations in a constant environment. We propose that, on the whole, our model contains fewer special assumptions than models with explicit environmental change. Regardless of whether fluctuating or constant environments are more biologically informative, our results constitute an important null model of mutator fixation.

Constant environment models

Work by Tanaka and co-workers [TBL03] also involves a changing environment. However, unlike the models described in the previous section, theirs contains no alternating selective effects: when the environment changes, the mutations acquired during the previous environmental cycle simply become neutral. Thus, as in our work, all beneficial mutants are generated *de novo*. In further similarity with our work, they pursue, via quasi-stochastic simulations and analytic approximations, an understanding of the long term mutator behavior by concentrating on a single environmental cycle, i.e. by exam-

ining populations in a constant environment. These authors were interested primarily in the case when $Nx_o\mu_+ \ll N(1-x_o)\mu_-$, where the fixation of mutators is in some sense unlikely. With this in mind, instead of P_{fix}, they measure and calculate the (much larger) probability P_{gain} that the initially rare mutator increases its frequency by the end of a "time cycle." These cycles are defined to end when an expanding clone in a wild-type background reaches a size of $O(N)$, at which point the simulation is halted. Their most interesting result is that P_{gain} is substantial even when $Nx_o\mu_+ \ll N(1-x_o)\mu_-$. In other words, mutators can still "break even" if the wild-type background generates the first beneficial mutation, which is important if the environment changes. Nonetheless, without environmental change in their model, mutators will always be doomed unless they are the first to generate a beneficial mutation. Furthermore, they model birth and death processes deterministically, in a way that precludes extinction. For these reasons, our P_{fix} and their P_{gain} are truly distinct quantities, and no direct comparison can be made with our work.

We next discuss a simple calculation by Lenski [Len04] based on indirect mutation-selection equilibrium of the mutator subpopulation. If the dominant processes occurring in the population are mutation into the mutator state and creation of deleterious mutations by mutators, then the frequency of mutators approaches an equilibrium value. This frequency is easily calculated if, as in A3 of ISLA, deleterious mutations are treated as immediately lethal:

$$x_{eq} = \frac{U}{(1-\alpha_e)(\mu_+ - \mu_-)} \approx \frac{U}{\mu_+(1-\alpha_e)}$$

The time taken for the population to reach this equilibrium state, as well as a much more careful calculation of x_{eq}, was investigated in reference [Joh99b], but presently we assume that this simple estimate is sufficient. In equilibrium, beneficial mutations therefore arise at a rate $Nx_{eq}\mu_+\alpha_e$ from the mutators, and rate $N(1-x_{eq})\mu_-\alpha_e$ from the wild-type. If all beneficial mutants of equal effect have the same probability of achieving fixation, regardless of whether they originate in a mutator or wild-type background, then the *fraction of substitutions* linked to a mutator is approximately

$$\frac{U}{\mu_+(1-\alpha_e)}\frac{\mu_+}{\overline{\mu}} = \frac{U}{\overline{\mu}(1-\alpha_e)} \tag{3.22}$$

Plugging in reasonable values, Lenski [Len04] finds that $\approx 1\%$ of substitutions should

be linked to mutators. Furthermore, given that each line of *E. coli* in experiments from reference [SGL97] generated 10-20 substitutions, this calculation is impressively consistent with the observation that $3/12$ lines became mutators.

In order to relate this approach to our own, we must reintroduce dynamics into the picture. We can interpret the quantity $x\frac{\mu_+}{\bar{\mu}}$ as the conditional probability that a mutator achieves fixation, given that a selective sweep occurs during its lifetime. Our quantity P_{fix} is this conditional probability multiplied by the probability that a selective sweep occurs during the lifetime of a mutator. Assuming that selective sweeps and death each occur as Poisson processes with rates $N\bar{\mu}\alpha_e s$ and $(\mu_+ - \mu_-)(1-\alpha_e)$, respectively, it is straightforward to show that the probability that at least one selective sweep occurs before death is given by

$$\frac{N\bar{\mu}\alpha_e s}{(1-\alpha_e)(\mu_+ - \mu_-)}\left(1+\frac{N\bar{\mu}\alpha_e s}{(1-\alpha_e)(\mu_+ - \mu_-)}\right)^{-1}$$

Multiplying this expression by the conditional probability $x\frac{\mu_+}{\bar{\mu}} \approx xR$, we obtain Eq.3.19. Thus, the approach suggested by Lenski [Len04] is the equilibrium version of ISLA, in the limit where mutational processes occur frequently enough to overwhelm random genetic drift. Thus, remarkably, even though this approach frames the problem of mutator fixation in terms of competition with beneficial mutations in wild-type backgrounds, R cancels out of the solution in the strong-effect mutator regime: $R \gg N\alpha_e s/(1-\alpha_e)$.

It is also worthwhile to examine the conditions under which we expect the equilibrium assumption to hold. Let us imagine that an evolution experiment is conducted for T generations, during which H substitutions occur. ISLA predicts that the expected number of mutator fixations is $NP_{fix}UT$, whereas according to Eq.3.22, the equilibrium approach yields a value equal to $H\frac{U}{\bar{\mu}}$. Setting these two values equal to one another, and plugging in (from Eq.3.17) $P_{fix}(x_o = 1/N) = s\frac{\alpha_e}{1-\alpha_e}$, we obtain

$$H = Ns\bar{\mu}T\frac{\alpha_e}{1-\alpha_e} \approx N\bar{\mu}\alpha_e sT$$

This expression merely states that the (mostly wild-type) population is in the "successive mutations regime", i.e. only a single beneficial mutation spreads at a time. Alternatively, one could imagine turning this argument around and asking what P_{fix} must equal given that the equilibrium approach is valid and that the population accumulates substitutions

"one by one". In that case, one would, remarkably, arrive at $P_{fix}(x_o = 1/N) = \alpha_e s$, which (for small α_e and $NS_\mu \gg 1$) is what we obtained earlier (Eq.3.17) by more sophisticated methods.

Turning to another study, Tenaillon and co-workers [TTLN$^+$99] investigated, via stochastic simulations and very brief analytic arguments, multi-locus mutator evolution in a constant environment. These extensive simulations are a generalization of earlier work [TRMS$^+$97] and are partly amenable to comparison with our work. Some noteworthy differences with our simulations are that they scan a larger range of N, they have a more realistic implementation of mutation, and, most importantly, they allow flux into and out of the mutator state. Thus, mutators are never absolutely fixed during their trials, which necessitates a different termination condition than ours: They declare a trial "over" when the population reaches its maximum fitness, whereas we declare it "over" when the mutator is completely and permanently fixed or lost. Upon termination of the trial, they consider the mutator "fixed" if its frequency is $> 95\%$. They measure the fraction of trials that terminate with mutator frequency $> 95\%$ and denote this quantity the "frequency of mutator fixation," which differs from our P_{fix} because of reasons discussed below.

One important consequence of their method is that the total number of mutators *generated* during a trial varies with the choice of parameters. This is because each replication event presents a chance for the creation of a new mutator, and the number of replication events that occur before termination clearly depends on N, s, μ_+, μ_-, and the number of mutational steps required to reach the peak. Thus, a change in the value of any of these parameters may alter the "frequency of mutator fixation" simply because it changes the number of mutators that are typically created during the trial. Our P_{fix}, on the other hand, remains invariant under such changes and allows us to filter out this background effect. Their system is doubtless a more literally accurate representation of biological reality, which has its virtues but also major costs, which we discuss below in the context of two important examples.

First, they measure that the "frequency of mutator fixation" increases with N. This is an interesting and potentially practical result, but their method makes it very difficult to determine the extent to which the increase is simply due the background effect

that more mutators were created in the larger populations. ISLA, on the other hand, unambiguously states that when $NS_\mu \gg 1, P_{fix}$ for a single mutator becomes independent of N. Therefore, ISLA predicts that the dependence of mutator fixation frequency on population size observed by those authors is entirely driven by the simple background effect.

A second example has even more dramatic conceptual consequences. These authors ask whether P_{fix} is determined by the number of potentially advantageous mutations (steps away from the peak) or merely by the *rate* that such mutations are generated. In order to investigate this question, they devised two sets of simulations. In one set, there were 12 available advantageous mutations, accessible at a rate of 10^{-8} each. In the other set, there was a single mutation of the same effect, accessible at a rate of 12×10^{-8}. The explicit difference between these sets of simulations is the number of steps to the fitness peak, but an additional, implicit difference is that the set with 12 beneficial mutations runs for more generations. Therefore, more mutators are created in that set of simulations. Now, ISLA predicts that P_{fix} depends only on the advantageous mutation *rate*, and that therefore the two simulations should result in the same P_{fix}. In seeming contrast, they found the "frequency of mutator fixation" to equal approximately .5 for the first situation and approximately zero for the second. This observation led them to conclude that mutators succeed because of their advantage in rapidly creating genomes which carry multiple beneficial mutations, which is fundamentally different from our conceptual picture. We propose that this simulation finding might be explained by the simple background effect that far more mutators are created en route to acquiring 12 beneficial mutations than to acquiring a single beneficial mutation. ISLA completely neglects multiple beneficial mutations, and its success, both near the peak (Fig.3.5) and far from it (Fig.3.6), suggests that the multiple mutations effect proposed by those authors in fact plays a very minor role in mutator fixation. However, it should be noted that we did not investigate cases where the mutator is *favored* and only a single beneficial mutant is available. It could be the case that multiple beneficial mutations in the same genome are implicitly important in that they are what allows the mutator to overcome competition with wild-type beneficial mutations. This hypothesis should be explored in future work.

Whereas reference [TTLN$^+$99] focused almost exclusively on stochastic simulations, work by Andre and Godelle [AG06] relies almost exclusively on analytic methods. In work that bears many similarities to ours, those authors studied, mostly via an analytic approach, the long term trajectory of mutation rate evolution. A key insight of theirs is that, in a finite asexual population, the frequency of a mutator undergoes strong fluctuations, with values covering the entire range from zero initially to one upon a selective sweep by a linked locus. Thus, they point out that studies which assume that mutators are rare during all generations, either because of infinite population size [LJ70] or sexual recombination [Joh99a], are qualitatively different than finite asexual populations. Andre and Godelle remedy this problem by calculating the *fixation probability* of an initially rare mutator. We now briefly summarize their method of solution and show that, with minor modification, it corresponds to the $N\mu \to \infty$ limit of our results. In what follows, we take some liberty in changing their notation and using continuous time.

Their initial condition is identical to ours: a clonal population is seeded with a small number of otherwise identical mutators. They then temporarily ignore beneficial mutations and analyze how the *expected* number of mutators changes with time. In agreement with reference [Joh99b], they find that after a waiting time $1/s$, the mutator subpopulation declines exponentially, i.e. $E[x(t)] = x_o e^{-(\mu_+ - \mu_-)(1-\alpha_e)(t-1/s)}$. They then construct their key equations (their Eq. 19)

$$\begin{aligned}
\frac{d}{dt}P_{fix}(t) &= (1 - P_{fix}(t) - P_{loss}(t)) \cdot N\bar{\mu}\alpha_e s \cdot \frac{\mu_+}{\bar{\mu}} \cdot E[x(t)] \\
\frac{d}{dt}P_{loss}(t) &= (1 - P_{fix}(t) - P_{loss}(t)) \cdot N\bar{\mu}\alpha_e s \cdot \frac{\mu_-}{\bar{\mu}} \cdot (1 - E[x(t)])
\end{aligned}$$

We have written these equations in a somewhat peculiar way, and replaced their symbol K with $N\bar{\mu}\alpha_e s$ in order to facilitate translating between our notation and theirs. These equations are very similar to ISLA in that they represent the instantaneous fixation of beneficial mutations which originate from a time dependent mutator subpopulation. However, there are two disturbing features about these equations. First, they assume that the only cause of mutator extinction is beneficial mutations in the wild-type background. In fact, mutators also become extinct due to (i) their mutational load and (ii) random drift. In their equations, $E[x(t)]$ declines exponentially, but this decline erroneously does not contribute to P_{loss}. Both (i) and (ii) cause an overestimate of P_{fix}.

The second disturbing feature of these equations is the appearance of expectation values on the RHS. With this move, those authors replaced the random variable $x(t)$ with its mean value, which is a very substantive approximation. The distribution of $x(t)$ is in fact diffusing, i.e. random drift is in fact occurring. Nevertheless, we expect that their representation of $x(t)$ as a deterministic quantity to be approximately valid when the timescale of this diffusion is slower than the timescales due to mutation and selection. Unlike our approach, theirs cannot quantify when it is safe to neglect random drift. Looking back to Eq.3.12, we see that the diffusive process, i.e. random drift, can be neglected when $N\mu_+(1-\alpha_e)s \gg 1$ and $N^2\mu_+\alpha_e s \gg 1$. It just so happens that these criteria will often be met in microbial populations.

We now explicitly demonstrate some important parallels between our work and that of Andre and Godelle in the large $N\mu$ limit. Since, in our model, deleterious mutations are as strong as advantageous ones, the best comparison is made with their "ruby in the rubbish" hypothesis. The relevant solution is their Eq.A5

$$P_{fix} = x_o \frac{N\bar{\mu}\alpha_e s}{1-(1-N\bar{\mu}\alpha_e s)\cdot e^{-(\mu_+-\mu_-)(1-\alpha_e)}} \cdot \frac{\mu_+}{\bar{\mu}} \tag{3.23}$$

Simplifying the denominator by taking $\exp[-(\mu_+-\mu_-)(1-\alpha_e)] \approx 1-(\mu_+-\mu_-)(1-\alpha_e)$ and neglecting the term $-N\bar{\mu}\alpha_e s\mu_+$, we recover our large $N\mu$ result from ISLA (Eq.3.19). The neglected term inflates the value of P_{fix}, and is a result of these authors not treating extinction of the mutator due to its mutational load. This has important consequences for the next topic.

3.9.2 Long term mutation rate evolution:

Although our work primarily addresses the plain issue of calculating P_{fix}, we briefly contemplate implications for the more grand question of long term mutation rate evolution.

μ_{conv} is proportional to the rate of sweeps

Thus far we have considered selective sweeps to be initiated by *de novo* beneficial mutations. Let us now briefly apply our results to the case where sweeps are instead triggered by an environment that changes at rate K. This merely requires transcribing

$N\bar{\mu}\alpha_e s \leftrightarrow K$. Following those authors we expand the fixation probability (Eq.3.23) in powers of $\mu_+ - \mu_-$ and denote the first order coefficient in this series by $Sel(\mu_-)$. The roots of $Sel(\mu_-)$ give the "convergence stable resident mutation rate." Using Eq.3.19, we find $\mu_{conv} = K/(1-\alpha_e) \approx K$, which is the classical result [LJ70]. Using Eq.3.23, they find a qualitatively different result: $\mu_{conv} = \frac{K}{(1-\alpha_e)(1-K)}$, which diverges as $K \to 1$. The reason for this discrepancy is that those authors did not allow for extinction due to mutational load. ISLA naturally averts the need for this assumption and leads to the classical result. However, ISLA approximates deleterious mutations as being lethal, whereas these authors also treated the more realistic non-lethal case. It may be possible to demonstrate, via further analysis, the claim that non-lethal deleterious mutants cause μ_{conv} to diverge for some parameter values.

Equilibrium mutation rate

We find that $Sel(\mu_-) = \frac{1}{\mu_-}\frac{\alpha_e(Ns+1)-1}{N\alpha_e s}$, whereas Andre and Godelle find $Sel(\mu_-) = \frac{1}{\mu_-}\frac{\alpha_e(Ns+1)-1}{N\alpha_e s} + 1 - \alpha_e$. Our expression indicates that there are no equilibrium mutation rates: for all μ_-, weak mutators are favored when $\alpha_e(Ns+1) \approx N\alpha_e s > 1$ and disfavored in the opposite case. This threshold is clearly in agreement with our Eq.3.13. Thus, as far as ISLA is concerned, populations with $N\alpha_e s < 1$ should continually evolve toward the minimum attainable mutation rate. On the other hand, populations with $N\alpha_e s > 1$ should evolve an ever higher mutation rate. Our expression for $Sel(\mu_-)$ is clearly inaccurate for very small μ_- (because random drift dominates in that regime) and also for very large μ_- (since our simulations show that there is a maximum mutation rate that can achieve fixation).

3.9.3 Limitations of present work:

Real biological populations possess many features that this article either neglects or severely constrains. We now briefly discuss the most striking limitations.

Initial Conditions

Both ISLA and our simulations suppose that "initially" all members of the population have the same fitness. If this assumption is false and mutators arise randomly in a population with pre-existing fitness variation, this might act to decrease mutator success: unless the mutator happens to emerge from the fittest subclass of the population, the advantageous mutations it generates will already be present in more abundant subclasses which could out-compete the rare mutator. This point is especially relevant since, in comparing ISLA to experiment, we essentially assumed that each mutator that arose during the course of the experiments did so in a population consisting of a single fitness value.

Strict Asexuality

Our simulations and ISLA do not allow any mechanisms of horizontal gene transfer or recombination. These events would decouple mutator alleles from the advantageous mutations that they generated, and thereby result in significantly decreased mutator success. This effect is especially important since some genes associated with a mutator phenotype also exhibit hyper-recombination [DM06].

Simple Fitness Landscape

Our simulations assume that mutations all fall into one of three classes: lethal, beneficial with effect $+s$, or deleterious with effect $-s$. As mentioned previously, and discussed in Supplementary Information, it may be true that, in large populations, beneficial mutations of a fixed size $\tilde{s}$ are the ones that typically reach appreciable frequency [GL98, DFM07, HSHK06]. However, this simplification is certainly not possible when considering deleterious mutants, whose distribution is likely complicated and bimodal, with many mutations being nearly neutral and many being lethal [EWK07]. Fig.3.10 suggests that increasing the strength of deleterious mutations has effects only at large μ_+/s, where it increases both the peak value of S_μ and the value μ_+/s at which the peak occurs. Along these lines, a simulation model that included a class of weakly deleterious mutations would likely continue this trend. This would delay the large discrepancy be-

tween the simulations and ISLA until even larger μ_+/s. This issue could help to explain the previously mentioned fact that μ_+ in experiments of reference [SGL97] seem very close to the maximum allowable value. Including mildly deleterious mutations would also prolong the lifetime of genomes which carry them. In this case, it might be necessary to incorporate a time delay before these deleterious mutations are "enforced," along the lines explored in reference [Joh99b].

3.9.4 Suggestions for further research

This article leaves many questions unanswered, but also points to interesting theoretical and experimental opportunities.

Theoretical directions

A satisfactory analytic description of our stochastic simulations remains incomplete. Two key issues remain unresolved. First, we do not understand the mechanism by which mutators continue to succeed when faced with intense mutational competition from the wild-type background (Fig.3.7). Our work and that of Andre and Godelle both imply that mutations in wild-type backgrounds should become important when $N\alpha_e s \sim \mu_+/\mu_-$, but this is not borne out in the simulations unless s is "sufficiently large." Secondly, it is clear that ISLA fails to match simulations when the mutation rate is very large $(1-\alpha_e)\mu_+ \gtrsim s$. Quantifying the success of mutators in this regime is especially relevant to studies of long term mutation rate evolution.

Another issue that we did not address is the full dynamics of mutator fixation. Our analytic results are mostly derived from Eq.3.12, which is relevant to the eventual fate of mutators. An approximate solution to the time dependent forward diffusion (Eq.3.10), with $\mu_- = 0$, is given in Supplementary Information. This solution provides some dynamical information, but, like the entire ISLA approach, it assumes that selective sweeps occur instantaneously. In this sense, Eq.3.10 predicts incorrect dynamics. Furthermore, we showed that mutator success is compactly represented by an effective selection coefficient S_μ. For simple advantageous mutants, S contains information not only about P_{fix} but also about the average dynamics: $\langle x(t)\rangle \sim e^{St}$ when rare. Perhaps that is the case with mutators as well.

Experimental ideas

Our work shows that, in most regimes, P_{fix} is not explicitly frequency dependent. Rather, P_{fix} depends on the initial *number* of mutants Nx_o. This scaling behavior could be tested experimentally. Suppose that competition experiments in a chemostat carrying a population of size N_1 showed that, when the initial frequency of mutators exceeded a threshold value of x_1, mutator achieved fixation with a high probability. One could decrease the population size to N_2 and again inoculate with mutators at a frequency of x_1. Our results predict that mutators would not achieve fixation in this case because N_2x_1 is less than the threshold number N_1x_1. In fact, very similar experiments were recently performed [LCFT06], which support the notion that P_{fix} scales with Nx_o and not with x_o alone. However, these competition experiments were done under a lethal selective pressure, which selected for pre-exiting resistant mutants. Here we propose competitions between initially isogenic (aside from the mutator allele) mutator and wild-type strains adapting to a new environment. In addition to this scaling behavior, ISLA predicts a testable value for this threshold that differs significantly from the frequency dependent picture represented by Eq.3.1. These ideas are presented in Fig.3.11.

It would also be interesting to experimentally investigate the decline in mutator success seen for very large mutation rates when $(1-\alpha_e)\mu_+ \sim s$. As mentioned previously, during the first few thousand generations of experiments in reference [SGL97], $N\alpha_e s \approx 1.1$. The reason why no mutators achieved fixation after the first $10,000$ generations could be that this parameter decreased below the threshold value of one during the course of its evolution. A similar effect was previously discussed by Kessler and Levine [KL98b]. An alternative explanation is that μ_+ was near the theoretical maximum $(1-\alpha_e)\mu_+ \sim 1$ suggested from our simulations. As noted in reference [GCPS07], once could test these competing explanations by founding several new lineages with a clone from of one of the mutator populations, and growing these mutator lineages in a novel environment. The new environment should be one in which $N\alpha_e s > 1$. If no "double mutators" arose, then the hypothesis of a maximum allowable mutation rate would be supported.

3.10 Acknowledgements

The text and data of chapter three, in full, has been published in C. S. Wylie, C. Ghim, D.A. Kessler, and H. Levine “The fixation probability of rare mutators in finite asexual populations”, *Genetics*, 181, 2009. The dissertation author was the lead investigator and author of this article.

4 Evolution of competence in bacteria

4.1 Introduction to competence

Under certain stressful conditions, some bacterial species such as *B. subtilis* undergo a differentiation process in which a *finite subpopulation* ($\sim 10\%$) transiently and stochastically expresses the "competence" phenotype, characterized by the following properties:

1. *Recombination*: Competent cells import, chromosomally incorporate, and express foreign DNA fragments in a process called "transformation." This is the defining feature of competence. If the foreign DNA originates from another species, the process is called "horizontal gene transfer" and may result in the dramatic acquisition of a new (set of) gene(s). Comparative genomic studies demonstrate that important evolutionary events have occurred as a result of HGT [GT05]. However, HGT is probably not the typical outcome of competence. The incorporation of DNA is accomplished by recombination that is facilitated by base pairing between the donor fragment and acceptor genome [Red01]. Furthermore, most extracellular DNA probably originates from members of the same species and population. This suggests that a more likely process is the incorporation of different alleles originating from the same species. This chapter only addresses this conspecific, homologous recombination and not HGT.

2. *Reduced growth*: The following observations of are based on movies made by the Elowitz laboratory [SGOLE06]. While expressing competence, cells elongate but do not divide. After ≈ 20 hours in the competent state [SKD$^+$07], the single elongated cell fragments into ~ 10 vegetatively growing cells, thus completing

the bout of competence. By contrast, a vegetatively growing cell doubles approximately every 3.3 hours [SGOLE06], giving rise to $2^{20/3.3} \approx 67$ descendants during a 20 hour interval [SGOLE06]. Thus, competent cells have a growth rate disadvantage relative to vegetatively growing cells. The general phenomenon of growth reduction/arrest in the competence state has also been reported in other studies [NS63, HHHD01].

3. *Decreased susceptibility to antibiotics*: Perhaps as a consequence of reduced growth, competent cells are refractory to penicillin [Nes64, JDL09] and possibly other antibiotics.

4. The conditions that trigger competence often trigger the sporulation pathway as well. Vegetative cells can sporulate but competent cells cannot [SHA00]. Spores are completely dormant over timescales which are short compared to those of drastic environmental change.

Properties 2,3 taken together are an example of the more general phenomenon called "persistence," in which slowly replicating cells are able to survive stress [Big44, BMC$^+$04, JDL09].

The elaborate competence system involves ~ 150 chromosomal genes [SPA06], and is thus probably selected and maintained by evolution. Three well known, non-exclusive hypotheses concerning the adaptive value of competence are [Dub99]:

- Imported DNA provides a nutrient source.
- Imported DNA serves as a template for DNA repair.
- Homologous, conspecific recombination is selected because of the pattern of genetic diversity that it generates.

While it is intuitively clear that nutrients and DNA repair have value for bacteria, the same is not *prima facie* true of recombination. This chapter focuses on the interaction between the four features of competence outlined above. Using stochastic simulations and an semi-deterministic approximations we show that, even in a constant environment,

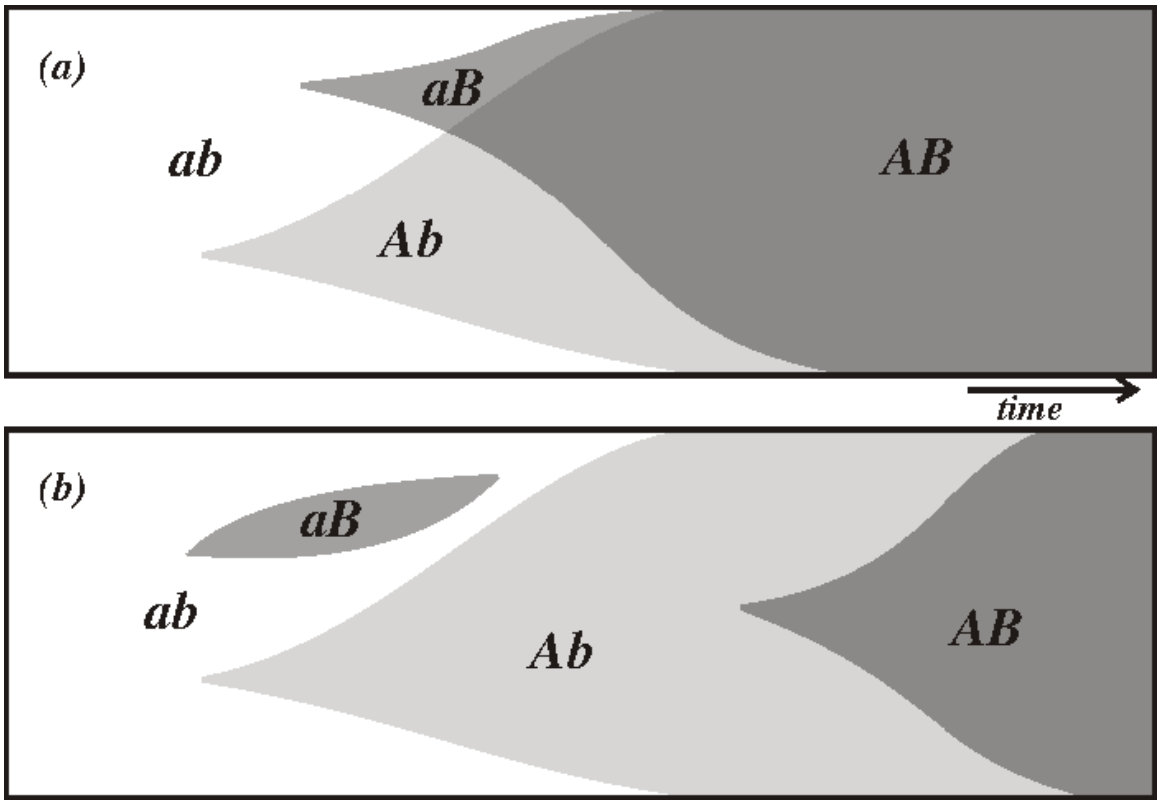

Figure 4.1: The Fisher-Muller effect provides an advantage to recombination when the time between originations of beneficial mutations is shorter than that required for a selective sweep. (a) Recombination increases the speed of adaptive evolution by combining beneficial mutations ($a \rightarrow A$ and $b \rightarrow B$) that originate in different genetic backgrounds. (b) By contrast, in a strictly asexual population, one of the simultaneously spreading beneficial mutation is "wasted." (figure taken from wikipedia.org)

there are evolutionary forces selecting for a mixed population of competent and vegetative cells. We do not address arguments surrounding the nutrition or repair hypotheses. These can be found in the literature [Dub99, Red01].

4.2 Heuristic effects of recombination

The essential effect of recombination is to reduce the correlations between alleles at different loci. These correlations are known as "linkage disequilibrium" (LD). To see what this means, consider two loci i, j each holding an allele $a \in \{0,1\}$. LD between the alleles at loci i and j (D_{a_i,a_j}) is determined by their joint and marginal frequencies in the

population: $D_{a_i,a_j} \equiv freq(a_i, a_j) - freq(a_i) \cdot freq(a_j)$. For example, LD between two alleles is negative if they are found on the same chromosome less often than they would be if placed independently in random members of the population. In this case, the effect of recombination is to drive LD closer to zero by joining together the two alleles from different chromosomes. In the absence of LD, recombination can have no average effect on the population's genetic structure.

There are three relevant situations that can give rise to LD. The first is the effect of gene interaction on fitness, known as epistasis. Epistasis is classified according to the interactions between deleterious mutations. If the combined effect of two deleterious mutations is greater than expected based on their individual effects, the epistasis is known as "synergistic." In the opposite case it is known as "antagonistic." These cases are illustrated in Fig.4.2. Of course, these two concepts only capture the simplest kind of epistasis– in reality, many genes may interact jointly, and the interaction between a given pair may be antagonistic or synergistic depending on the state of the rest of the genome. Experimental evidence shows that both forms of epistasis are widespread but that neither predominates [Ric02].

When epistasis is synergistic, the population is deficient in both very fit and very unfit genomes. Recombination removes this deficiency, thereby increasing the variance in fitness which, by "Fisher's fundamental theorem," increases the rate of adaptation. Several studies [Kon84, Cha90, Bar95, OF97] show that, with some caveats, this effect favors recombination in infinite populations. By contrast, recombination decreases the variance in fitness under antagonistic epistasis, and these studies find that recombination is disfavored in this situation.

As a second situation leading to LD, consider a large asexual population acquiring multiple beneficial mutations (Fig.4.1). If the second beneficial mutation does not occur in the same background as the first, which is likely, then the frequency of the double mutant is zero. Thus, the double mutant is clearly underrepresented and negative LD prevails between the single mutations. This is known as the "Fisher-Muller effect" [Fis30, Mul32]. In this situation, recombination dramatically increases the speed of evolution and decreases linkage equilibrium (LD=0) by combining the beneficial mutations into a common chromosome [Fel74, CKL05c]. Note that the assumptions underlying

the Fisher-Muller effect do not hold in a truly infinite population, in which all possible genomes are always finitely populated.

A third source of LD is inescapable in finite populations. Asexual reproduction results in parent and daughter cells which are genetically identical, apart from a small number of mutations ($\sim 1/300$) [DCCC98]. This induces correlations between the genomes of different cells, which manifests as LD that is qualitatively similar to that generated by synergistic epistasis [BO05]. In very small populations, LD due to finite N has strong effects related to Muller's ratchet [Mul32]. Additionally, recent studies show that this effect is strong enough to favor recombination in large, finite populations. Perhaps surprisingly, this remained true with none or even mildly antagonistic epistasis [KO06, GC08].

This chapter corroborates and extends these recent developments in several ways. First, somewhat superficially, our model reflects an interest in bacterial transformation as opposed to meiotic recombination. Secondly, we investigate both populations undergoing adaptive evolution (sometimes called "positive selection") as well as those at mutation-selection equilibrium. Thirdly, we find that when the four properties of competence (discussed in the introduction) are combined, an optimal mixed strategy emerges. Finally, we formulate an approximation scheme that semi-quantitatively agrees with simulation data and sharpens our understanding of important dynamical issues.

4.3 Model

4.3.1 A single phenotype

We stochastically model logistic birth and death in the presence of mutation, recombination, and phenotypic switching. The deterministic birth and death dynamics of a single phenotype, neglecting mutation and recombination, are given by

$$\frac{dN}{dt} = Nr(1 - N/\kappa) - N\delta. \tag{4.1}$$

κ is the carrying capacity of the environment, which reflects the availability of nutrients and/or space. As the number of cells N approaches κ, the *logistic factor* $\mathscr{L} \equiv (1 - N/\kappa)$ depresses the birth rate from its intrinsic value r. Cell death occurs at a constant per

Table 4.1: Commonly used notation in chapter four.

Symbol	Usage
a_i	"Value" of allele at locus i
λ	Number of genomic fragments (bits) in genome
$b \equiv \sum_i a_i/\lambda$	Fraction of 1's in a genome
G_b	Number of vegetative (growing) cells in class b
C_b	Number of competent cells in class b
κ	Population carrying capacity
N_o	Total number of cells at beginning of competition experiment
$\mathscr{L}$	$1-\frac{1}{\kappa}\sum_b(G_b+C_c)$ (Logistic factor)
r	Birth rate of vegetative cells (when $\mathscr{L}=1$)
δ	Death rate of vegetative cells
γ	Factor by which birth and death are slower in the competent state
$\mu_{\rightarrow}$	Probability per locus per replication of $0 \rightarrow 1$ transition
$\mu_{\leftarrow}$	Probability per locus per replication of $1 \rightarrow 0$ transition
$\sigma_{in}(\sigma_{out})$	Switching rate into (out of) the competent state

capita rate δ. At steady state, the number of cells in the population is $N_{eq} = \kappa(1-\delta/r)$. Instead of density dependent birth and constant death, some logistic models do the reverse, leading to $\frac{dN}{dt} = Nr - N(1+N/\kappa)\delta$. Some stochastic population genetic quantities (e.g. fixation times) have been shown to be identical in either formulation of the density dependence [PQP08]. There are both obvious differences and reassuring similarities between our logistic model and Moran's process (used in chapter three):

- Unlike Moran's process, birth and death are decoupled in the logistic model. This allows for stochastic fluctuations in N.

- In the logistic model, N_{eq} depends on the ratio δ/r, whereas it is a fixed parameter in Moran's process. During adaptive evolution δ/r clearly decreases which causes N_{eq} to increase.

- In Moran's process, during adaptive evolution the average birth rate and death rate each increase through time. By contrast, both these quantities remain near the constant δ.

- The fixation probability of a rare mutant with a growth rate advantage is approximately the same in either model, when $N \approx N_{eq}$ [PQ07a].

We believe that the three differences listed above do not qualitatively affect any of the main results in this chapter. Nevertheless, we expect that, to the extent that bacteria in the wild are ever in a steady ecological state, the logistic model is more appropriate than Moran's model. Moran's model is likely better suited to laboratory experiments, particularly in a chemostat.

4.3.2 Two phenotypes

For our purposes, the real utility of the logistic model is that it decouples birth and death. If the total number of cells is near N_{eq}, this scheme allows for two coexisting phenotypes with different birth (r_{comp}, r_{veg}) and death ($\delta_{comp}, \delta_{veg}$) rates. Up to a deterministic approximation, the two phenotypes are competitively neutral if they separately lead to the same value of N_{eq}, i.e. $r_{veg}/\delta_{veg} = r_{comp}/\delta_{comp}$ [PQ07b]. We enforce this condition by requiring that both the birth and death rates of competent cells be lower than those of vegetative cells by a factor $\gamma < 1$. It should be emphasized that each of the above statements applies only to the birth and death process, neglecting mutation, recombination, and phenotypic switching.

These choices are motivated by experiment. As mentioned in the introduction, competent cells in Elowitz's movies elongate for ≈ 6 doubling periods, then fragment into ~ 10 daughters upon return to the vegetative state. For simplicity, we model this unusual process as simple replication at a reduced rate compared to vegetative cells. On its own, this would impose an enormous fitness cost to competence. This is compensated by requiring that competent cells also die more slowly than vegetative ones. The experimental rationale for this is twofold. First, the natural environments that trigger competence may plausibly contain antibiotics. In this case, the persister effect of competence results in slow death for these cells. Secondly, some vegetative cells may sporulate under the same conditions that stimulate competence. On time scales that are short compared to drastic environmental changes, spores are effectively dead, thereby imposing a relatively large death rate to vegetative cells.

4.3.3 Simulation proceses

The simulations consist of model genomes (see subsection 4.3.4) undergoing the following dynamical changes in continuous time:

1. *Phenotypic transition*: There are two allowed phenotypes: competent and vegetative. Competence is defined by a nonzero probability of recombination ($\rho > 0$), as well as birth and death rates that are each lowered by a factor $\gamma < 1$. Competent (vegetative) cells switch to the other phenotype with probability $\sigma_{out} dt$ $(\sigma_{in} dt)$.

2. *Replication*: A vegetative cell replicates with probability $r(1 - N/K)dt$, where N is the total number of bacteria in the population. Competent cells replicate in the same way, but with reduced rate $\gamma r(1 - N/K)dt$.

3. *Mutation*: Upon replication, mutations may occur. Beneficial and deleterious mutations are represented as $0 \rightarrow 1$ and $1 \rightarrow 0$ transitions that occur with probabilities $\mu_{\rightarrow}$ and $\mu_{\leftarrow}$ per locus per replication.

4. *Death*: A vegetative (competent) cell is annihilated with probability $\delta\ dt$ $(\gamma\delta\ dt)$.

5. *Recombination*: A competent cell undergoes a transformation-like event with probability $\rho\ dt$. See Fig.4.3.5 and subsection 4.3.4 for a description of the recombination process.

4.3.4 Genome and recombination model

We model the bacterial chromosome as λ loci $\{a_i\}$, each of which has either a more fit (one) or less fit (zero) allele (Fig.4.3). Each locus represents the same number of nucleotides as is typically incorporated during transformation. For *B. subtilis*, this is $\sim 10^4$ base pairs [Dub99]. Recombination by transformation occurs with rate ρ between a living cell (the acceptor) and a pool of extracellular DNA (the donor) that represents the contents of recently lysed conspecific cells. In reality, these lysates could be derived mainly from less fit cells. However, for simplicity the allele frequencies in the extracellular pool are assumed to be identical to those in the population of living cells.

4.3.5 Birth rate functions

For simplicity we assume that only the birth rate (r), and not the death rate (δ), depends on the genome. Because the effects of recombination are known to depend crucially on epistasis, we used three different birth rate functions corresponding to synergistic, antagonistic, and no epistasis:

$$r_{syn} = \max\left(0, 1+\frac{1}{2}\ln(2b-1)\right) \quad (4.2)$$

$$r_{ant} = \frac{1}{2}\left[1+\exp(-2(1-b))\right] \quad (4.3)$$

$$r_{lin} = b, \quad (4.4)$$

where b is the fraction of ones in the genome. These functions are plotted in Fig.4.2. They have identical slopes near $b = 1$, which means that the first deleterious mutation has the same effect on birth rate in each of the three functions. In Eq.4.4, mutations make *independent* contributions to fitness in the sense that no linkage disequilibrium is generated in an infinite population [Smi68].

At this stage it is helpful to clarify a confusing point concerning birth rate functions. In the population genetics literature, non-epistatic birth rate functions often have the multiplicative form $r_{mult} = (1-\frac{1}{\lambda})^{\lambda(1-b)}$. How is this consistent with the claim that Eq.4.4 corresponds to non-interacting mutations? The answer is related to the fact that most population genetic studies employ a discrete time, non-overlapping generations ("Wright-Fisher") process, whereas we employ a continuous time process. A simple calculation presented in appendix I reveals that, once this difference is taken into account, Eq.4.4 is essentially equivalent to a multiplicative function. This point is crucial in comparing this work to existing literature.

4.4 Results

In order to explore the evolutionary forces acting on the four properties of competence (see introduction), we first constructed several "strains" of *in silico* cells that isolate these properties:

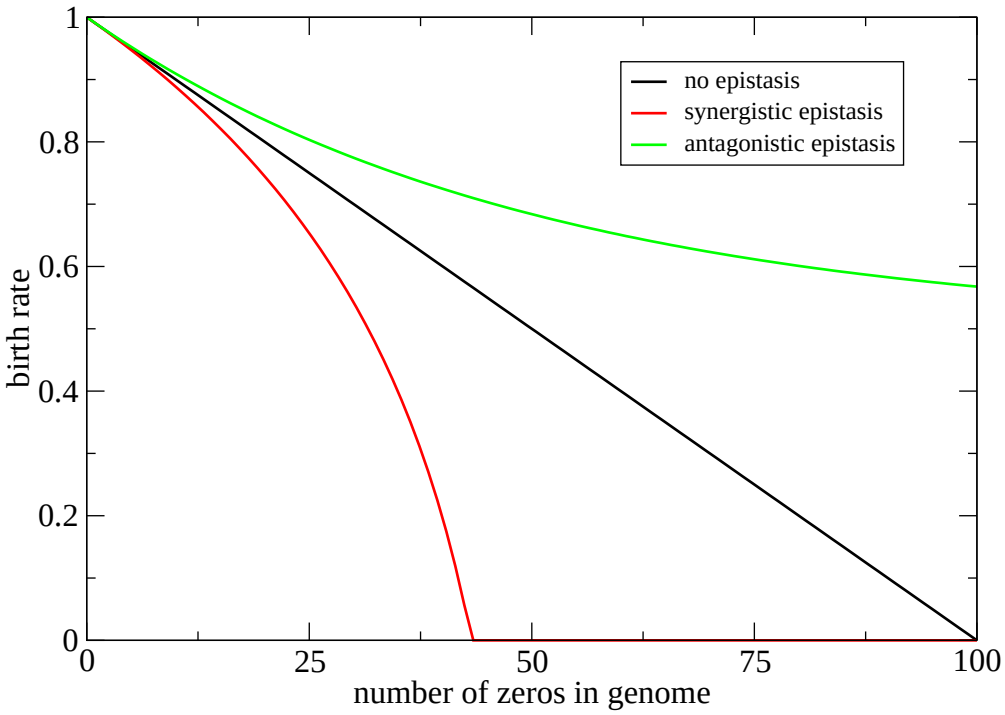

Figure 4.2: Fitness functions. Deleterious mutations interact either "synergistically" (red), "antagonistically" (green), or not at all (black). The first deleterious mutation decreases the birth rate by $\approx 1\%$ in each case.

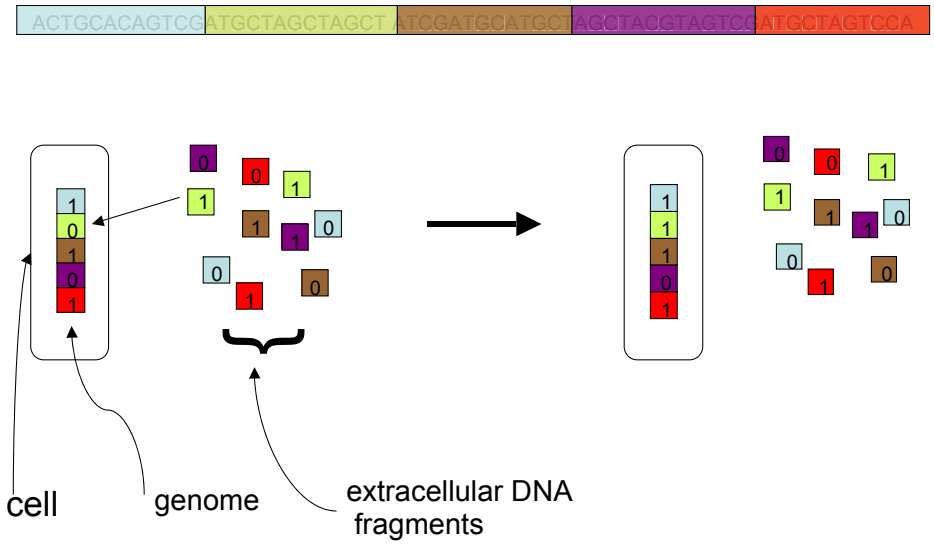

Figure 4.3: Representation of bacterial genome and recombination model. The genome consists of *L* loci, represented by different colors. Either a more fit (one) or less fit (zero) allele resides at each locus. Upon recombination, the acceptor allele is replaced by a homologous (same color) donor allele drawn randomly from the extracellular DNA pool. The allele frequencies in the extracellular pool are assumed to be identical to those among the population of living cells. The genetic change is non-reciprocal: the acceptor allele is presumed degraded and not placed in the extracellular pool.

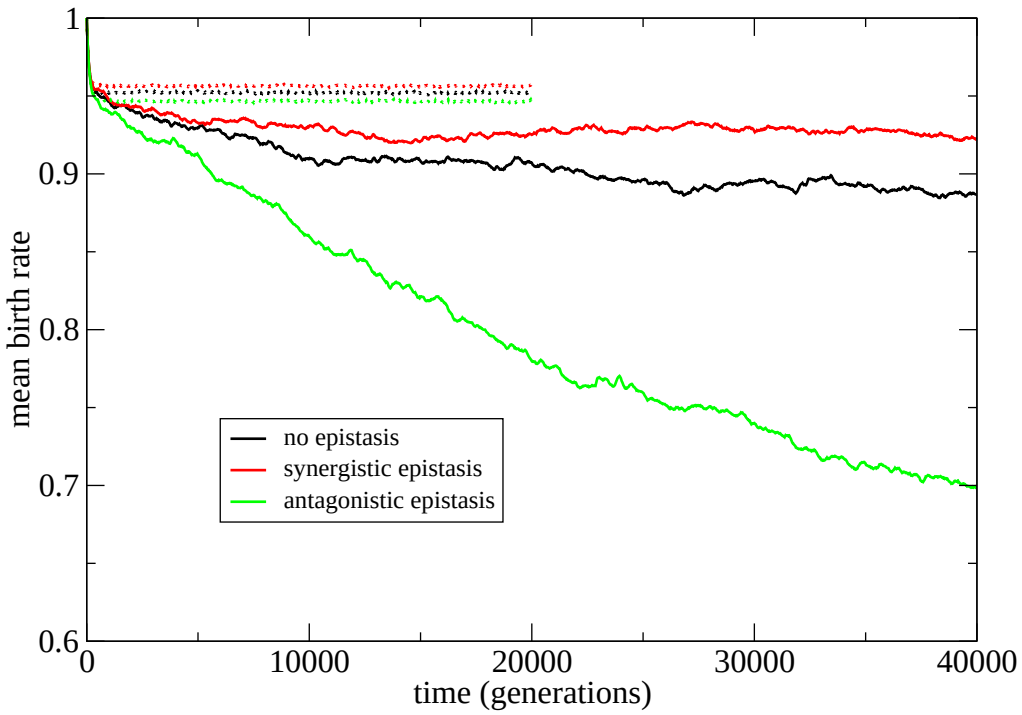

Figure 4.4: Approach to equilibrium. Dotted lines represent C strain residents, whereas solid lines represent G strain residents. Relaxed selection on antagonistically interacting deleterious mutations causes their continual accumulation (Muller's ratchet) in the absence of recombination (solid green). Finite N effects also reduce the equilibrium birth rate in G strains below the deterministic prediction $r(N \to \infty) \approx 0.95$ when synergistic (solid red) or linear (solid black) fitness functions are used. Parameters are $\lambda = 100, \mu_{\rightarrow} = 10^{-5.3}, \mu_{\leftarrow} = 10^{-3.3}, \kappa = 10^5, \delta = 0.2, \gamma = 0.5, \rho = 1, \sigma_{in} = \sigma_{out} = 0.1$.

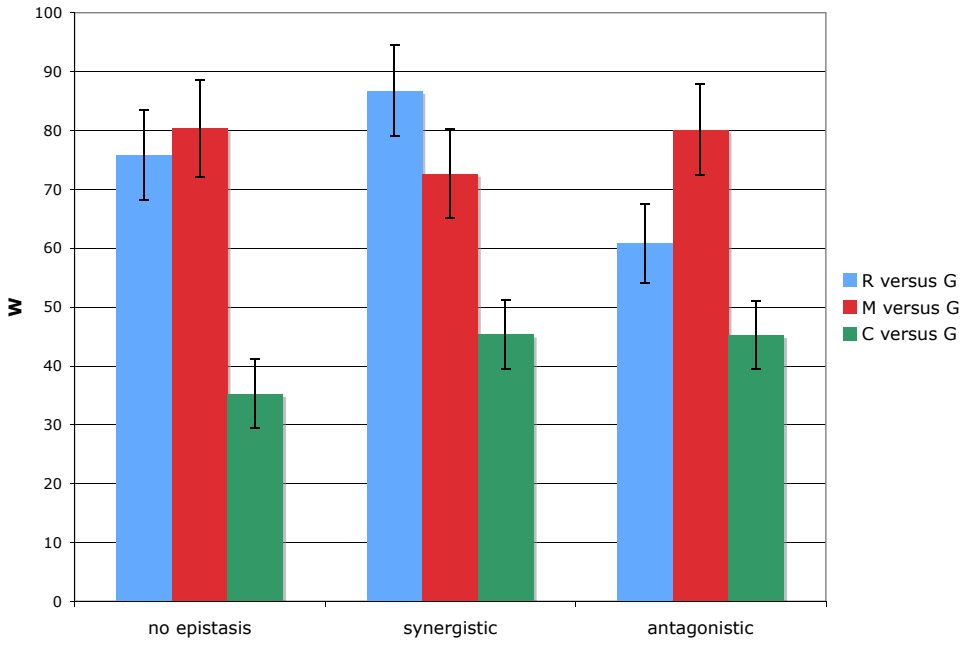

Figure 4.5: Competitions near the fitness peak. Recombination is favored since all recombining strains (R,M,C) can invade the asexual vegetative strain (G). M strains are approximately twofold more effective than C strains at invading G strains, indicating that a mixed strategy is superior to a purely competent one. Parameters are the same as in Fig.4.4. Error bars represent one standard error.

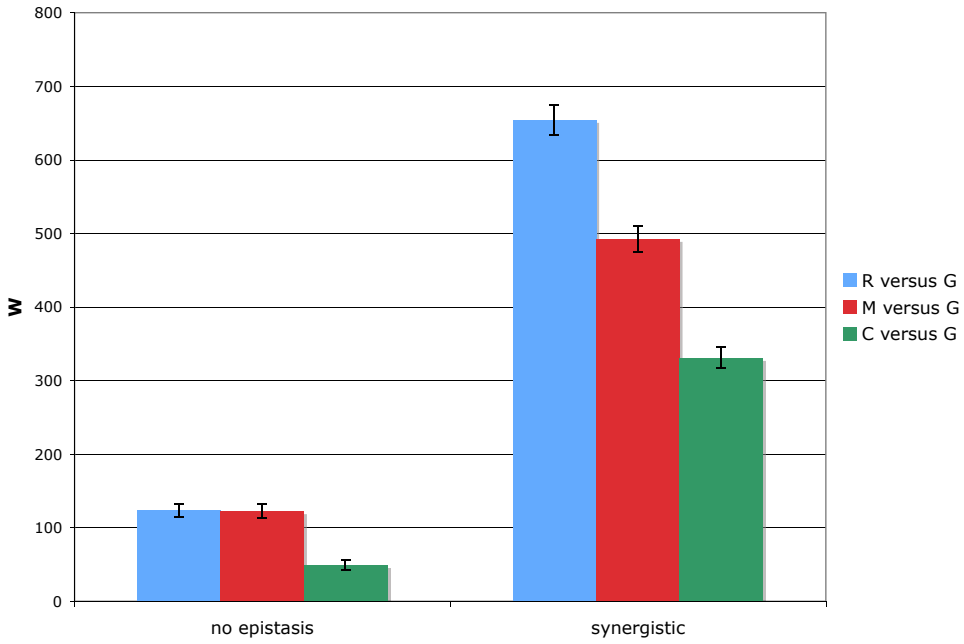

Figure 4.6: Competitions during adaptive evolution. Clonal populations were initialized at $b = 0.5$ and allowed to evolve to $b = 0.7$ before the invader was introduced. Recombination is generally favored, especially with synergistic epistasis. M is $50 - 100\%$ more successful than C at invading G. Parameters are the same as in Fig.4.4. Error bars represent one standard error.

- *Vegetative (growing) (G)*: grows and dies quickly, and cannot perform recombination ($\rho = 0$).
- *Slow (S)*: grows and dies slowly, and cannot perform recombination ($\rho = 0$).
- *Recombining (R)*: grows and dies quickly, and performs recombination ($\rho > 0$).
- *Competent (C)*: grows and dies slowly, and performs recombination ($\rho > 0$).
- *Mixed (M)*: stochastically switches between competent and vegetative phenotypes. The switching rates $\sigma_{in} = \sigma_{out}$, resulting in 50-50 mixed strategy.

To avoid confusion between the concepts of strains and phenotypes, strains will be denoted by their capital letter abbreviation. One can abstractly imagine the different strains being coded by a pair of modifier loci that code for recombination ability and the persister effect of competence (decreased birth and death rate). However, in order to keep the situation as simple as possible, we forbid members of one strain from transitioning to another strain. Thus, these modifier loci cannot be mutated or transferred by recombination.

4.4.1 Competition experiments

We first simulated competition experiments between strains in which a single "invader" cell was placed among $N_{eq} - 1$ "residents." Since transitions between strains are forbidden, after a long time the only possible outcomes are the fixation or loss of the invader. The probability of fixation P_{fix} of the invader in the context of of the resident was estimated by performing many independent competitions. The invader's success is quantified by $W \equiv P_{fix} \cdot N(t_{init})$ which equals the expected number of progeny left by the invader. Because the effect of recombination depends on the degree of genomic diversity, populations were prepared in a natural state prior to competition. This was done in two regimes:

Resident population near the fitness peak

Resident populations were founded by a clone having the maximum possible birth rate ($b = 1$) and allowed to evolve for $\sim 10^4$ generations (Fig.4.4). With none or

synergistic epistasis, mean birth rate decreased until mutation selection equilibrium was reached. However, with antagonistic epistasis the mean birth rate continually decreased under the influence of Muller's ratchet. The effects of finite N are less drastic, but still apparent, with synergistic or no epistasis. C strain populations had a much larger equilibrium fitness near the predicted value for $N \to \infty$. See Fig.4.4 caption for further discussion.

In each case, after $\sim 10^4$ generations a randomly chosen cell was manually switched to be of the invading strain, and competition commenced. Competitions with G strain resident are shown in Fig.4.5. R,M, and C strains were all able to successfully invade ($W \geqslant 35$), indicating a significant advantage to recombination, irrespective of the form of epistasis. R and M strains performed comparably to one another, indicating that there is little cost to the reduced level of recombination that results from cells switching into the vegetative *phenotype*. Slow (S) strains were unable to invade in $\approx 10^5$ trials, implying that they are either disfavored or nearly neutral. Most interestingly, the M strain was approximately twice as likely as the C strain to succeed at invasion.

However, M strains were unable to invade C strains in $\sim 10^5$ trials. Thus, the only definitive conclusion that can presently be drawn about this competition is that strain M is not clearly favored over strain C in the competition. In order to resolve the difference between a nearly neutral and a disfavored strain in populations of this size, several κ trials must be run (perhaps 10^7 to achieve the same resolution as the data plotted in Fig.4.5).

Resident population far from fitness peak

When a population's environment changes (e.g. by significantly reducing the glucose concentration available to *E. coli*), the fitness peak "moves" elsewhere in sequence space. The population may then adaptively evolve up the new peak. From Fig.4.4 it is clear that adaptive evolution not possible on our antagonistic birth rate function, so we limit our attention to the synergistic and no epistasis cases.

Resident populations were founded by a clone with $b = 0.5$ and allowed to evolve to $b = 0.7$, at which point the invader was placed in the population as before. Fig.4.6 shows a similar qualitative picture as we obtained when the population was near the fit-

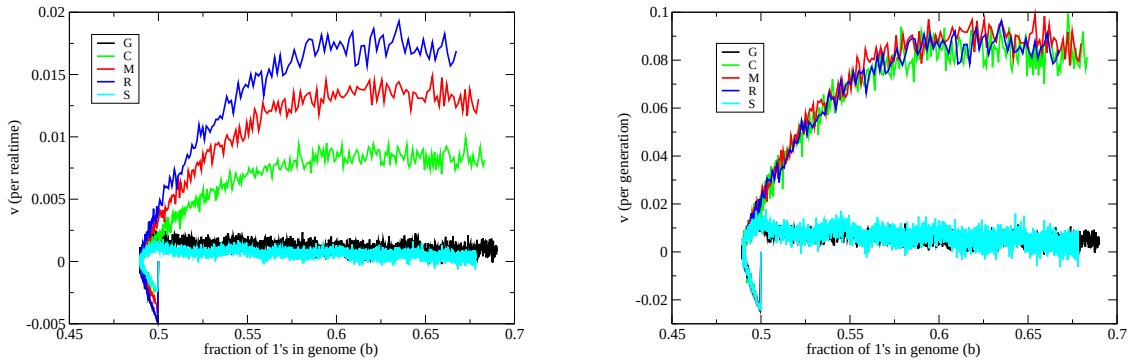

Figure 4.7: Strains that perform recombination (R,C,M) evolve faster than asexual strains (G,S). The horizontal axis *b* serves to parameterize the population's placement on the fitness function. When velocity is measured in dimensions realtime^{-1} (left), M evolves faster than C, which is consistent with the outcome of competition experiments. Insight into the advantage of M over C is gained by considering *v* measured in dimensions of generation^{-1} (right). By this measure, the R,C, and M strategies are equally successful. Once this fact is understood, the real time velocity ordering follows naturally. Parameters are the same as in Fig.4.4. The linear fitness function was used here.

ness peak. Values of W are larger in Fig.4.6 than in Fig.4.5, showing that recombination is more strongly favored when populations are acquiring beneficial mutations and not merely purging themselves of deleterious mutations. Synergistic epistasis provides an especially strong advantage, probably because of the (additional) LD generated by the fitness function. M strains are $50-100\%$ more successful than C strains at invading G strains.

If M invades C during adaptive evolution, the invader is either quickly lost or else persists for a long time without sweeping to fixation. Since M and C can both perform recombination, their gene pools are shared. Consequently a beneficial mutation acquired by one strain is soon picked up by its competitor in a recombination event. We were unable to complete enough trials to conclude whether $W > 1$ for M invading C. These slow dynamics also likely describe the evolutionary adjustment of recombination rates.

4.4.2 Speed of evolution

Simulation data

The previous section concerned the fixation probability of a rare invader, which is the most direct way to quantify the evolutionary pressure acting on a strain. Unfortunately, we are unaware of any method to approximate P_{fix} for the recombining strains. By contrast, the mathematical techniques developed for front propagation can help to approximate the speed of evolution v.

We first examine the speed of evolution achieved by pure populations of each strain. When v is measured in dimensions of realtime^{-1}, the ranking of strains according to v agrees with the ranking according to P_{fix} (Fig.4.7, left). This is consistent with the idea that successful invaders win by increasing their fitness before their opponents. This rapid fitness increase, in turn, is the result of two distinct factors: (i) rapid execution of events (birth, death, mutation, recombination) and (ii) the efficient genetic structuring of the population. The C,S, and M strains all suffer a penalty with respect to effect (i) because (some) members of their population undergo birth, death, and mutation slowly (by a factor γ). On the other hand C, R, and M strains evolve faster because recombination increases the efficiency of their genetic structure by, for example, bringing different beneficial mutations into the same genome (Fig.4.1).

To a large extent factor (ii) can be isolated by examining v measured in dimensions of generations^{-1}, i.e. (birth events)$^{-1}$. Fig.4.7 (right) shows that once this is done, the strains that undergo recombination (R,C,M) perform equally well, and are far superior to the asexual strains (G,S, which perform equally to one another). The fact that there is sufficient recombination in the M population to fully reap the rewards of recombination is not at all obvious. However, once this fact is accepted, it is clear that M will evolve faster than C in real time since half ($=\frac{\sigma_{in}}{\sigma_{in}+\sigma_{out}}$) of the M population "acts" $1/\gamma$ (two) times faster than cells in C.

Semi-deterministic equations

We would like to derive equations that describe the number of cells having a certain value of b (i.e. fraction of ones in their genomes). Presently, we will only treat the

linear birth rate function (Eq.4.4). Adapting this method to the other fitness functions is straightforward. For the vegetative strain (G), the basic approach is discussed in section 1.4. Once the replication and death terms are modified so as to represent the logistic scheme used here,

$$\frac{d}{dt}G_b = (\mathscr{L}b-\delta)G_b\cdot\theta(G_b-1)+\lambda\mathscr{L}\,\mathscr{M}[G_b] \tag{4.5}$$

where $\mathscr{M}$ is the mutation operator:

$$\begin{aligned}\mathscr{M}[G_b] &= \mu_{\leftarrow}\left(b+\frac{1}{\lambda}\right)\left(b+\frac{1}{\lambda}\right)G_{b+\frac{1}{\lambda}}\\ &+ \mu_{\rightarrow}\left(b-\frac{1}{\lambda}\right)\left(1-(b-\frac{1}{\lambda})\right)G_{b-\frac{1}{\lambda}}\\ &- (\mu_{\rightarrow}+\mu_{\leftarrow})bG_b\end{aligned} \tag{4.6}$$

Here we have used a value of unity inside the cutoff. There is no loss of generality since G_b is scaled by κ via $\mathscr{L}$.

Much of the simplicity of Eq.4.5 stems from the fact that genomes were binned according to their value of b. This act precludes a full treatment of recombination, which sees the diversity within a bin. However, recombination can be introduced in a tractable way by making the strong assumption that, within a bin, all genomes compatible with that birth rate are uniformly populated [CKL05c]. This overstates the genetic diversity in the population and the effect of recombination. Nevertheless, it yields reasonable results, especially at large N. In particular, we assume that the incoming foreign allele is a one with probability $\bar{b}$, irrespective of the value of its homologue in the receptor cell. Given this assumption, one can introduce the recombination operator:

$$\begin{aligned}\mathscr{R}[C_b] = &- \rho C_b\left((1-\bar{b})b+\bar{b}(1-b)\right)\\ &+ \rho C_{b-\frac{1}{\lambda}}\bar{b}\left[1-(b-\frac{1}{\lambda})\right]\\ &+ \rho C_{b+\frac{1}{\lambda}}(1-\bar{b})\left(b+\frac{1}{\lambda}\right)\end{aligned} \tag{4.7}$$

where we have chosen for $\mathscr{R}$ to operate on the competent population C. If we include phenotypic switching between the C and G population, we arrive at the following set of

coupled equations:

$$\begin{aligned}\frac{d}{dt}G_b &= (\mathscr{L}b-\delta)G_b\cdot\theta(G_b-1)+\lambda\mathscr{L}\ \mathscr{M}[G_b] \\ &+ \sigma_{out}C_b-\sigma_{in}G_b \qquad (4.8)\\ \frac{d}{dt}C_b &= \gamma(\mathscr{L}b-\delta)C_b\cdot\theta(C_b-1)+\gamma\lambda\mathscr{L}\ \mathscr{M}[C_b]+\mathscr{R}[C_b] \\ &- \sigma_{out}C_b+\sigma_{in}G_b \qquad (4.9)\end{aligned}$$

These equations are easily integrated numerically. Their results are compared to simulations in Fig.4.8. The agreement is rather poor when the simulated populations are founded with a clone. This is because it takes a long time to build up the level of diversity that the semi-deterministic equations assume to exist. The agreement improves through time as this diversity builds. On the other hand, if simulations are founded with randomized genomes of a given fitness, the agreement is excellent. When the environment of wild bacteria also predict that there is an optimum fraction of competent cells in a mixed population (Fig.4.9). For reasonable values of κ, this optimal fraction is $\sim 40\%$, somewhat larger than the $\sim 10\%$ witnessed in the laboratory. The optimal fraction is found to decrease with κ and vanish in the limit $\kappa\to\infty$.

4.5 Discussion

Recent work by Elowitz and colleagues [SGOLE06, SKD$^+$07] vividly shows that cells of *B. subtilis* stochastically enter and exit the competent state. This leads to a dynamic, mixed population of competent and vegetatively growing (i.e. normal) cells. If recombination has adaptive value, why does only a finite fraction of cells become competent? This work reports a novel population genetic effect that rationalizes the experimental observation.

Recently, there has been much interest in the possibility that stochastic phenotype-switching mechanisms may function to cope with uncertain environments [KL05], [AMvO08]. In these studies, there are several phenotypes, each of which is adapted to one of several possible environments. One elegant strategy (stochastic switching) for coping with uncertainty exploits phenotypic noise to produce a distribution of phenotypes that hedge against the various environments that may be encountered. Members

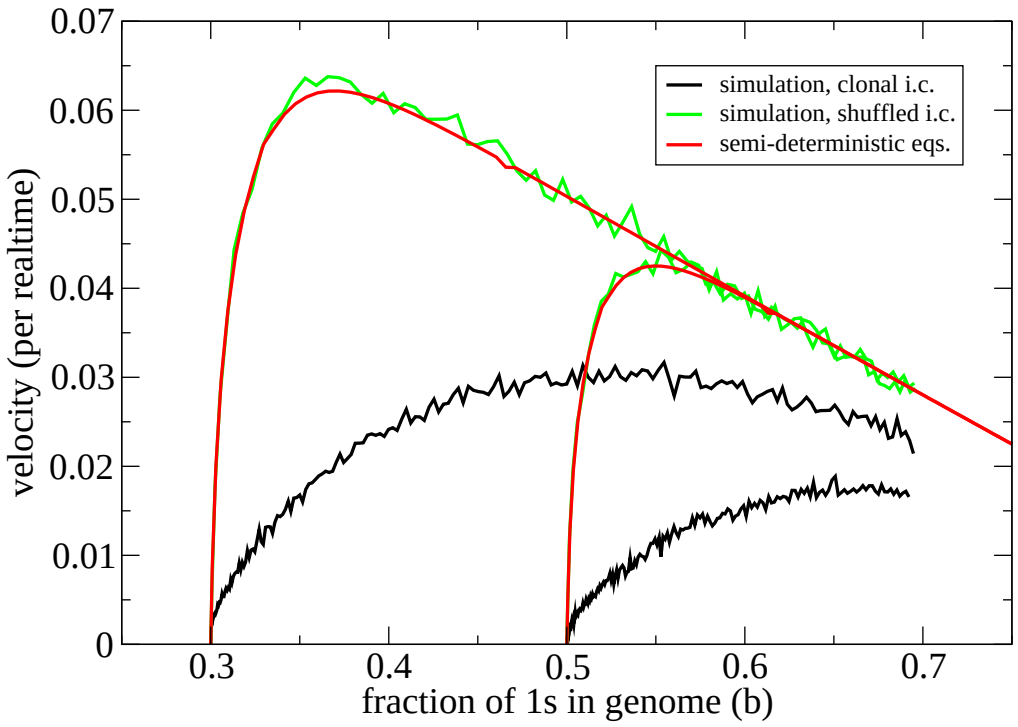

Figure 4.8: Comparison of semi-determinstic equations to simulation data. Agreement is good only if there is ample genetic diversity in the founding populations. Parameters are the same as those in Fig.4.4.

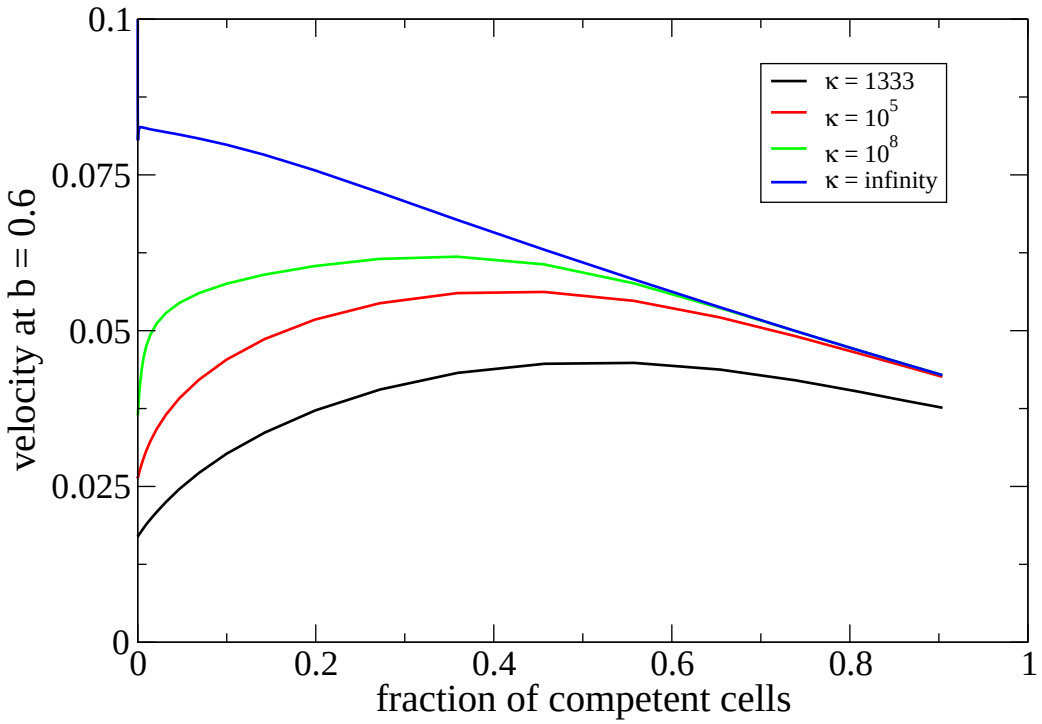

Figure 4.9: Optimal mixed strategy. In qualitative agreement with simulations, the semi-deterministic equations predict that populations can achieve the fastest evolution if only a finite fraction of cells enter competence. Parameters are the same as those in Fig.4.4, but σ_{in} is varied to adjust the fraction of competent cells $\frac{\sigma_{in}}{\sigma_{in}+\sigma_{out}}$

of the population in the inappropriate phenotype represent the fitness cost to stochastic switching. The experimentally observed subpopulation of persister cells in *E. coli* is thought to arise by stochastic switching [BMC$^+$04, KKBL05]. An alternative strategy (responsive switching) is to measure the environment and respond with the appropriate phenotype, but this comes with the cost of maintaing the sensor and the switch.

Competence in *B. subtilis* employs a puzzling combination of these two switching strategies. On the one hand, the competence system employs responsive switching since it is regulated by a quorum sensing module that is activated in early stationary phase as population density increases [SHA00]. On the other hand, competence seems to employ stochastic switching because it commits only a finite fraction to each phenotype.

This suggests the intriguing hypothesis that competence switching in *B. Subtilis* is in fact responsive switching and that the noisy phenotype is best. This chapter argues for this viewpoint and suggests a population genetic function for phenotypic noise with respect to competence.

4.6 Acknowledgements

Text and data in chapter four is being prepared for publication. The dissertation author is the primary investigator and author of the prepared manuscript. Aaron Trout, David Kessler, and Herbert Levine are co-authors of the prepared manuscript.

A Numerical integration in chapter 2

In order to determine the spectrum $\Omega_0(v)$ we numerically integrated Eq. 2.7, and this required numerically integrating Eq. 2.5. Integration of Eq. 2.5 was initialized in the bulk state, from the left, where we defined $z \equiv 0$. We set v arbitrarily, took $\phi_0(0) = .99$, and calculated $\phi_0'(0)$ from the solution to the version of Eq. 2.5 linearized around $\phi_0 \approx 1$

$$\phi_0'(0) = -\frac{.01v}{2D}\left(-1+\sqrt{1+\frac{4Dr_{init}}{v^2}}\right)$$

r_{init}, which we set to one, differs from the previously defined r_0 in that it fixed the rate at a definite location in the bulk state rather than the location where $\phi_0 = 1/2$. Integration terminated in the neighborhood of the cutoff, half way between timesteps where ϕ_0'/ϕ_0 crosses $-v/D$. N was then read off from the relation $N = -\frac{vk}{D\phi_0(z_{cut})}$ and the value of the cutoff was recorded for subsequent numerics. This value is measured relative to the bulk position where $\phi_0 = .99$, not relative to $\bar{z}$, where $\phi_0 = 1/2$. All of this was done using ode45 from MATLAB, with a maximum stepsize of .001.

The solution for ϕ_0 appears as a coefficient in Eq. 2.7, and was incorporated into the ODE integration scheme with a cubic spline. Numerical integration of Eq. 2.7 was initialized at $z = 0$ with some trial Ω_0, $\eta(0) = 1$ and

$$\eta'(0) = \frac{v}{2D}\left(-1+\sqrt{1+\frac{4D(r_{init}+\Omega_0)}{v^2}}\right)$$

which follows from Eq. 2.7 if we plug in $\phi_0 \approx 1$. Integration terminated at the z_{cut} obtained from integration of Eq. 2.5, where we checked if Eq. 2.14 was satisfied with the trial Ω. This procedure was iterated with a root solver while varying Ω until Eq. 2.14 was satisfied. Each integration of Eq. 2.7 was done over 1000 timesteps with a fourth order Runge-Kutta ODE solver with fixed step size, meant to facilitate incorporation of the spline.

This yielded the exact numeric solution presented in Fig. 2.3. Our “exact analytic approximation" presented in Fig. 2.3 is just the solution to Eq. 2.15 obtained with a root solver. The required values for N and z_{cut} were obtained from the previous integration of Eq. 2.5, and we took $r_0 = 1$. Since we dropped the term involving ϕ_0 in Eq. 2.10, this equation is insensitive to the precise definition of $\bar{z}$, e.g. it could be defined naturally as the coordinate where $\phi_0 = 1/2$ or it could be defined out of numerical convenience as the coordinate where $\phi_0 = .99$. This insensitivity explains why the results agree so well despite the fact that r_0 and r_{init} are not defined in the same way.

B Asymptotic solutions to Eq.3.12, when $\mu_- = 0$

As in the main text, we define $B \equiv \mu_+ [1 - \alpha_e(1-s)]$ and $C \equiv \mu_+ \alpha_e s$. If $N\alpha_e s \gg 1$ but μ_+ is sufficiently small, NS_μ is no longer much larger than 1, and the approximations in the main text are not valid. This occurs when $\mu_+ \sim O(1/N^2\alpha_e s)$. In this case, the B term, and hence deleterious mutations, in Eq.3.12 is irrelevant, and $G_\infty(x_o)$ can be expressed in terms of a modified Bessel function:

$$G_\infty(x_o) = \frac{\sqrt{1-x_o} I_1(2N\sqrt{C(1-x_o)})}{I_1(2N\sqrt{C})} \tag{B.1}$$

When $N\sqrt{C}$ is not large, this does not have the exponential dependence on Nx_o required to interpret the fixation probability as resulting from a true effective selection coefficient. We can nevertheless calculate the fixation probability for small x_o:

$$P_{fix}(x_o) \approx N\sqrt{C}x_o \frac{I_0(2N\sqrt{C})}{I_1(2N\sqrt{C})} = N\sqrt{\mu_+\alpha_e s}x_o \frac{I_0(2N\sqrt{\mu_+\alpha_e s})}{I_1(2N\sqrt{\mu_+\alpha_e s})} \tag{B.2}$$

For $\mu_+ \gg 1/(N^2\alpha_e s)$, the argument of the Bessel function is large, and we recover our previous result: $P_{fix} \approx Nx_o\sqrt{\mu_+\alpha_e s}$. For small argument, we get $P_{fix} \approx x_o(1+N^2C/2) = x_0(1+N^2\mu_+\alpha_e s/2)$. Thus the fixation probability approaches the neutral result x_o as $\mu_+ \to 0$ and starts out rising linearly in μ_+. If we wanted to translate this into an effective selection coefficient, since for small Ns, $P_{fix}(x_o) \approx x_o(1+Ns/2)$, the effective selection coefficient would be $S_\mu = N\mu_+\alpha_e s$, whose explicit N dependence again points to the inability to define an effective selection coefficient in this regime.

When $N\mu_+ \sim O(1)$ and $N^2\mu_+\alpha_e s \sim O(1)$, all the terms in the equation are of the same order, and no approximation can be made. However, for smaller μ_+, one can

use perturbation theory to find an approximate solution by writing $G_\infty = 1 - x_o + \eta(x_o)$, where $\eta(x_o) \ll 1 - x_o$. After dropping terms $\sim NB\eta'$ and $\sim N^2C\eta$, we obtain

$$G_\infty(x_o) \approx 1 - x_o - \frac{CN - B}{2} N x_o(1 - x_o) \tag{B.3}$$

with a fixation probability $P_{fix}(x_o) \approx x_o(1 + N(CN - B)/2) = x_o[1 + \mu_+ N(\alpha_e(Ns + 1) - 1)]$, which linearly approaches the neutral value x_o as $\mu_+ \to 0$. As above, in this very small μ_+ regime, no mapping to an N-independent effective selection coefficient can be made. Note that we again recover our threshold criterion for mutators to be favored (Eq.3.13).

C N_e for a population of periodically changing size

Whereas our model describes a population of constant size, experiments by [SGL97] were done according to a serial dilution protocol in which a population of size $N_o \approx 5 \times 10^6$ was grown to size $N_f \approx 5 \times 10^8$, diluted 100 fold, then repeated. Under these dynamics, all lineages grow essentially deterministically from N_o to N_f, at which point binomial sampling abruptly reduces the population size back to N_o. In this case, the fixation probability π of an advantageous mutant depends not only on s, but also on *when* it is generated during the dilution cycle. Mutants that are generated during the early part of the cycle are allowed more time to grow exponentially faster than the wild-type and thus have an advantage over late occurring mutants. It can be shown [WG01, WGSV02] that the stochastic effects of these population bottlenecks are in many ways equivalent to those of a population with constant size N_e. More precisely, if we let $m \equiv$ the number of newly generated mutants that will achieve fixation, then we require that the average value of $\frac{dm}{dt}$ to be the same in the two populations. In the bottleneck population, the total number of newly generated individuals $\equiv v(t) = N_o(e^{t\ln 2} - 1)$, and $dm = \mu\pi(s,t)dv = N_o\mu\pi(s,t)\ln(2)e^{t\ln 2}dt$. In the constant size population, $\frac{dm}{dt} = N_e\mu s$. Equating these two expressions for $\frac{dm}{dt}$ and averaging over one dilution cycle, we obtain

$$N_e s = \frac{N_o \ln 2}{g} \int_0^g e^{t\ln 2}\pi(s,t)dt \tag{C.1}$$

where $g = \frac{1}{\ln 2}\ln(\frac{N_f}{N_o}) \approx 6.6$ is the number of growth generations separating N_o and N_f. For $gs\ln 2 \ll 1$ it can be shown [WG01] that $\pi(s,t) \approx 2s\ln(2)ge^{-t\ln 2}$, and therefore Eq.C.1 implies that $N_e = 2N_o g\ln^2 2 \approx 6.3 \times 10^7$.

D Approximate solution to equation 3.10 when $\mu_- = 0$

Eq.3.10 can be approximately solved if we take $\mu_- = 0$. As in the main text, we define $B \equiv \mu_+ [1 - \alpha_e(1-s)]$ and $C \equiv \mu_+ \alpha_e s$. The equation then reads

$$\frac{\partial P}{\partial t} = \frac{1}{N}\frac{\partial^2}{\partial x^2}[x(1-x)P] + B\frac{\partial}{\partial x}[x(1-x)P] - NCx\mu_+ P \tag{D.1}$$

The biological problem we are interested in solving is the fixation probability for a small initial fraction of mutators. This corresponds to solving for $\int_{1-\varepsilon}^{1+\varepsilon} P(x, t \to \infty)dx$ as $\varepsilon \to 0$, subject to the initial condition $P(x,0) = \delta(x - x_o)$, where $x_o \ll 1$ and $\delta(x-x_o)$ is a Dirac delta function. Furthermore analytic progress can be made if we note that x is in some sense small. The idea is that the probability cloud $P(x,t)$ is initially localized around $x_o \ll 1$, and that the only process that moves probability solidly into the interior of $x \in (0,1)$ is random genetic drift. We anticipate this effect to be small when the mutator is significantly favored, i.e. $NS_\mu \gg 1$, and hence $P(x,t) \approx 0$ for x not $\ll 1$. Thus, we can approximately neglect the $O(x^2)$ terms in Eq.D.1 and obtain

$$\frac{\partial P}{\partial t} = \frac{1}{N}\frac{\partial^2}{\partial x^2}[xP] + B\frac{\partial}{\partial x}[xP] - NCx\mu_+ P \tag{D.2}$$

This second order PDE in (x,t) can be converted to a first order PDE in (k,t) by taking the spatial Fourier transform, which yields

$$\begin{aligned} N\frac{\partial \tilde{P}}{\partial t} &= -i(k^2 - iBk + C)\frac{\partial \tilde{P}}{\partial k} \\ \tilde{P}(k, t=0) &= \exp(-ikx_o) \end{aligned} \tag{D.3}$$

This equation can be solved by the "method of characteristics", in which we seek curves in the kt plane along which $\tilde{P}(k,t)$ is constant. We find $\frac{d\tilde{P}}{dt} = \frac{\partial \tilde{P}}{\partial t} + \frac{\partial \tilde{P}}{\partial k}\frac{dk}{dt} = 0$ along the

family of curves defined by

$$\frac{t}{N} + \frac{i}{z_+ - z_-}\left[\ln\frac{k-z_+}{k-z_-} - \ln\frac{\kappa - z_+}{\kappa - z_-}\right] = 0 \tag{D.4}$$

$$z_\pm \equiv \frac{iNB}{2}\left[1 \pm \sqrt{1+\frac{4C}{B^2}}\right]$$

κ serves to label different characteristic curves and is chosen to appear in this manner so that $\kappa = k$ when $t = 0$. Then, $\tilde{P}(k,t) = \tilde{P}(k,0) = \tilde{P}(\kappa,0) = \exp(-i\kappa x_o)$ along the characteristic curves, and we obtain the formal solution

$$P(x,t) = \frac{1}{2\pi}\int_{-\infty}^{\infty} e^{-i\kappa(k,t)x_o} e^{ikx} dk \tag{D.5}$$

where $\kappa(k,t)$ is obtained from Eq.D.4.

This formidable inversion integral gives the full solution for all x and t, but fortunately we do not need to evaluate the integral in order to obtain the fixation probability of the mutator. A moment's reflection convinces us that the $t \to \infty$ behavior of Eq.D.2 is the build-up of a delta function at the absorbing state $x = 0$ and a "decay" of the remaining probability to the fixation state. We note that the probability which corresponds to the delta function is the $k \to \infty$ component of $\tilde{P}(k,t)$. Taking the $k \to \infty$ limit of Eq.D.4, we obtain

$$P(x=0,t) = e^{-i\kappa_\infty x_o}$$

$$\kappa_\infty = z_- \frac{\frac{z_+}{z_-} - e^{-i(z_+ - z_-)t/N}}{1 - e^{-i(z_+ - z_-)t/N}}$$

Finally, taking the $t \to \infty$ limit and setting $P(1,t\to\infty) = 1 - P(0,t\to\infty)$, we obtain the familiar expression

$$P(1,t\to\infty) = 1 - e^{x_o|z_-|} \equiv 1 - e^{-Nx_o z} \tag{D.6}$$

$$S_\mu = z = \frac{\sqrt{B^2+4C} - B}{2} \approx \frac{\mu_+}{2}\left[\sqrt{(1-\alpha_e)^2 + 4\alpha_e s/\mu_+} - (1-\alpha_e)\right] \qquad NS_\mu \gg 1 \tag{D.7}$$

which is the same as Eq. 3.16 obtained from the backward equation (3.12).

E Perturbative correction to Eq.3.12 for finite μ_-

The small effect of mutations in wild-type backgrounds observed in simulations motivates a perturbative solution to Eq.3.12. In terms of the parameters $B_\pm \equiv \mu_\pm[1-\alpha_e(1-s)]$ and $C_\pm \equiv \mu_\pm \alpha_e s$,

$$\frac{d^2}{dx_o^2}G_\infty - N(B_+ - B_-)\frac{d}{dx_o}G_\infty - N^2 C_+ \frac{G_\infty}{1-x_o} = -N^2 C_- \frac{1-G_\infty}{x_o}$$

In order to make analytic progress, we make the following assumptions. (i) The mutator is strongly favored, and therefore $\frac{G_\infty}{1-x_o} \to G_\infty$. (ii) $G_\infty \approx G_o + G_1$, where G_o is given by the solution to the case $\mu_- = 0$ and $G_o \gg G_1$. Then we have

$$G_1''(x_o) - NB_+ G_1'(x_o) - N^2 C_+ G_1(x_o) = -N^2 C_- \frac{1 - e^{N(B_+ - \sqrt{B_+^2 + 4C_+})x_o/2}}{x_o} \qquad \text{(E.1)}$$

where we have also dropped the small term $B_- G_1(x_o)$. This equation can be solved using the theory of non-homogeneous linear differential equations. A convenient way to write the two independent solutions to the homogeneous version of Eq.E.1 is

$$\begin{aligned} g_<(x_o) &= e^{B_+ N x_o/2} \sinh\left(\frac{N}{2}\sqrt{B_+^2 + 4C_+}\, x_o\right) \\ g_>(x_o) &= e^{B_+ N x_o/2} \sinh\left(\frac{N}{2}\sqrt{B_+^2 + 4C_+}\,(1-x_o)\right) \end{aligned}$$

If we denote the inhomogeneity $m(x_o)$, our solution for $G_1(x_o)$ can be written in terms of the integrals

$$G_1(x_o) = \int_0^{x_o} m(x)\frac{g_<(x)g_>(x_o)}{Wr(x)}dx + \int_{x_o}^1 m(x)\frac{g_>(x)g_<(x_o)}{Wr(x)}dx$$

where the Wronskian $Wr(x) = g'_>(x)g_<(x) - g_>(x)g'_<(x)$. The first-order contribution to the fixation probability for small x_o is then

$$F_1(x_o) \approx -x_o \left.\frac{d}{dx_o}G_1(x_o)\right|_{x_o=0} = -x_o \int_0^1 m(x)\frac{g_>(x)g'_<(0)}{Wr(x)}dx$$

The Wronskian is evaluated as

$$Wr(x) = -\frac{1}{2}e^{B_+ Nx}\frac{N}{2}\sqrt{B_+^2+4C_+}\sinh\left(\frac{N}{2}\sqrt{B_+^2+4C_+}\right)$$

Thus, $f_>(x)/Wr(x)$ decays rapidly for large x as $e^{-N(B+\sqrt{B_+^2+4C_+})x/2}$. This allows us to simplify the integral by extending the range of integration to infinity, which yields

$$F_1(x_o) \approx -\mu_-\alpha_e s N^2 x_o \int_0^\infty dx \frac{1-e^{N(B_+-\sqrt{B_+^2+4C_+})x/2}}{x} e^{-N(B_++\sqrt{B_+^2+4C_+})x/2}$$

Using the identity

$$\int_0^\infty dx \frac{e^{-ax}-e^{-bx}}{x} = \ln(b/a)$$

we finally arrive at

$$F_1(x_o) \approx -\mu_-\alpha_e s N^2 x_0 \ln\left(\frac{2\sqrt{1+4\frac{\alpha_e s}{\mu_+(1-\alpha_e)}}}{1+\sqrt{1+4\frac{\alpha_e s}{\mu_+(1+\alpha_e)}}}\right) \tag{E.2}$$

The logarithmic factor varies between zero in the limit $\mu_+ \gg 4\alpha_e s$ and $\ln(2)$ in the opposite limit. This method breaks down when$F_1 \gtrsim F_o$. Now, F_o is bounded from above by $Nx_oS^*_\mu < Nx_o\alpha_e s$, as given in Eq(11, main text). Therefore, Eq.E.2 will typically fail when $\mu_-\alpha_e s N^2 \sim N\alpha_e s$, or, $N\mu_- \sim 1$, which is, unfortunately, usually the case.

F Alternative formulation is ISLA in section 3.5

As mentioned in the main text, A2 is somewhat awkward. An alternative, which we call A2*, it immediately kill advantageous mutations which are destined to eventually succumb to drift. This approximation merely modifies a coefficient in Eq.3.12. The effect is simply the transposition $\frac{\alpha_e}{1-\alpha_e} \to \alpha_e$. In fact, we occasionally made this substitution in the text, when we anticipated that $\alpha_e \ll 1$. Typical behavior of A2 relative to A2* is illustrated in Fig.F.1. Even though A2* yields results that are arguably more accurate than those of A2, we preferred A2 in the main text because it nicely serves as an upper bound on mutator success.

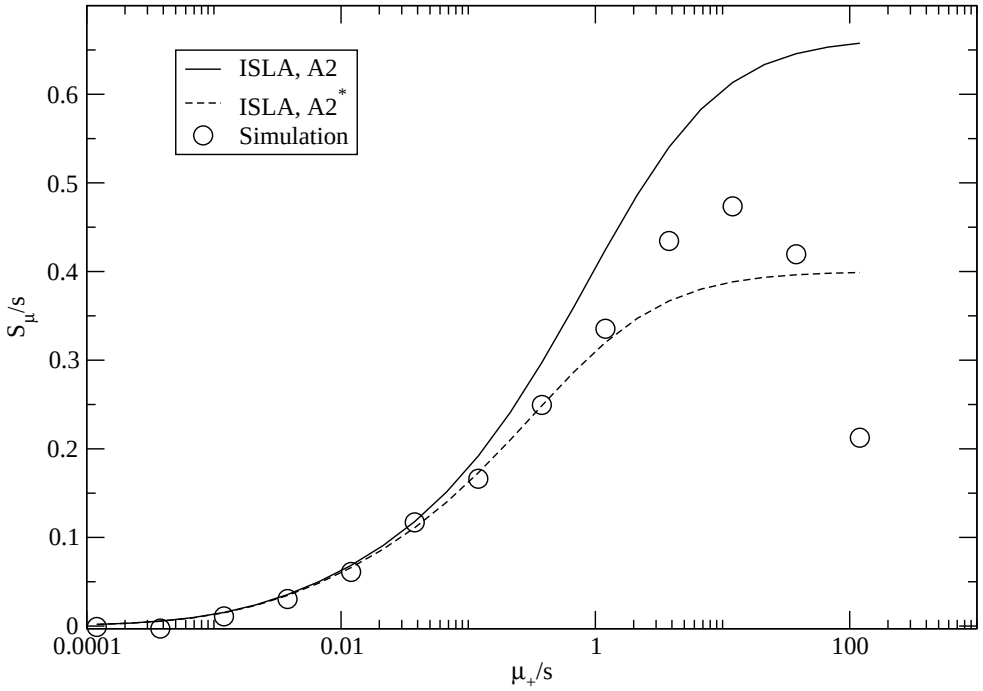

Figure F.1: The effect of using A2* instead of A2. When $\mu_+/s \lesssim 1$, ISLA overestimates the results of simulations when it uses A2. The opposite effect is observed if we instead make the assumption A2*, which immediately kills the fraction (1-s) of advantageous mutants that are eventually lost to random drift. This suggests that the error accumulated for $\mu_+/s \lesssim 1$ is due to the approximate manner in which ISLA treats these advantageous mutants. Parameters are $N = 5000$, $\mu_- = 0$, $\alpha = .4$, $s = 1/120$, $\delta = 0$.

G Ensemble averaging in chapter 3

The point-like symbols in the figures in the main text result from values of $P_{fix}(N, x_o, s, \alpha, \mu_{\pm})$ obtained by simulating numerous competition experiments. The averaging procedure varied somewhat, depending on parameters used, though this had no effect on our results. Here, we explicitly report the averaging details for each case.

- All data from populations of size $N = 5000$ result from $10,000$ trials run for each $x_o \in \{.003, .009, .015, .021\}$. The P_{fix} obtained from each value of x_o was then translated into a value for S_μ via Eq.(2, main text). These four values were averaged to obtain the values presented in the figures.

- For data from populations of size $N = 1000$, the procedure was identical to the case where $N = 5000$, but with $100,000$ trials for each x_o.

- For data from populations of size $N = 100,000$, the procedure varied slightly between different parameter choices. In Fig(2, main text) (left) and Fig(5, main text) we used $20,000$ trials each from $x_o \in \{10^{-4}, 5 \times 10^{-4}\}$. In Fig(6, main text), we used $20,000$ trials from $x_o = 2 \times 10^{-4}$. In Fig(2, main text)(right) we used $10,000$ trials from $x_o \in \{10^{-4}, 10^{-3}\}$

H Numerical integration in chapter 3

In order to produce the solid curves in Figs.(4, 5, 7, 8) from the main text, we first had to numerically integrate Eq.3.12, subject to the boundary conditions $G_\infty(0) = 1$ and $G_\infty(1) = 0$. The procedure for the case $\mu_- = 0$ is relatively simple. We initiate integration near the singular point at $x_o = 1$, taking $G'_\infty(1-\varepsilon) = -1$ and $G_\infty(1-\varepsilon) = \varepsilon$. Here, ε is a very small positive number and the initial slope -1 is arbitrary. The integration is then performed from $x_o = 1-\varepsilon$ to $x_o = 0$ using a fourth order Runge-Kutta algorithm. The resulting trial solution to Eq.3.12 does not obey the boundary condition at $x_o = 0$. However, because the equation is linear, the correct solution is obtained simply by re-scaling the trial solution so that the boundary condition is satisfied. We then evaluate $G_\infty(.001)$ using a cubic spline and obtain S_μ by inverting Eq(2, main text) using a root solver.

For $\mu_- > 0$, the procedure is slightly more involved. Eq.3.12 now has singular points at both $x_o = 0$ and $x_o = 1$. Therefore, we must integrate from both the right and the left, then match these two solutions and their derivatives in the middle. Specifically, we first integrate Eq.3.12 from the right, as before, but now stopping at $x_o = .5$. Call this un-scaled solution solution $G_r(x_o)$. We then generate a trial solution $G_l(x_o)$ initialized near $x_o = 0$, taking $G'_l(\varepsilon) = -NS_o$ and $G_l(x_o) = 1 - NS_o\varepsilon$. Here, S_o is given by Eq(10, main text) and merely serves as an initial guess as to the behavior of the solution near $x_o = 0$. We can ensure that $G_r(.5) = G_l(.5)$ simply by re-scaling $G_r(x_o)$. However, the slopes will, in general, not match at $x_o = .5$. In order to accomplish this matching, we link the above procedure to a root solver which repeatedly adjusts $G'_l(\varepsilon)$ and generates trial solutions until one is found for which $G'_l(.5) = G'_r(.5)$. We then proceed to calculate S_μ as before, using the correct solution $G_l(x_o)$.

I Multiplicative vs. additive fitness function

Let k equal the number of deleterious mutations (0's) carried by a genome of length λ and let time be measure in generations. Then, using our linear birth rate function (Eq.4.4) and setting the death rate equal to the mean birth rate $\equiv 1-\bar{r}$,

$$\begin{aligned}\langle n_k(t+1)\rangle &= n_k(t)e^{(1-k/\lambda)-(1-\bar{k}/\lambda)} \\ &= n_k(t)e^{-(k-\bar{k})/\lambda}, \end{aligned} \tag{I.1}$$

where the bar refers to the population average (as opposed to the ensemble average). The canonical multiplicative fitness function used in discrete Wright-Fisher models is (see, for example, [Ewe04]) $W_k = (1-s)^k$, where W_k denotes the expected number of offspring left in a generation. The corresponding equation for a typical discrete model is

$$\begin{aligned}\langle n_k(t+1)\rangle &= n_k(t)\frac{(1-s)^k}{\overline{(1-s)^k}} \\ &\approx n_k(t)\frac{e^{-sk}}{\overline{e^{-sk}}}. \end{aligned} \tag{I.2}$$

Eqs.I.1,I.2 are approximately the same if $s = 1/\lambda$ and $\overline{e^{-sk}} \approx e^{-s\bar{k}}$. Therefore, up to a deterministic approximation, the continuous model in which the exponential growth rate decreases *linearly* with k corresponds to a discrete model in which the "fitness" decreases *multiplicatively* with k.

Bibliography

[AG06] J.B. Andre and B. Godelle. The evolution of mutation rate in finite asexual populations. *Genetics*, 172(1):611–626, 2006.

[AMvO08] M. Acar, J.T. Mettetal, and A. van Oudenaarden. Stochastic switching as a survival strategy in fluctuating environments. *Nature Genetics*, 40(4):471–475, 2008.

[AS65] Abramowitz and Stegun. *Handbook of Mathematical Functions*. Dover, 1965.

[Bar95] NH Barton. A general model for the evolution of recombination. *Genetics Research*, 65(02):123–144, 1995.

[BD97] E. Brunet and B. Derrida. Shift in the velocity of a front due to a cutoff. *Physical Review E*, 56(3):2597–2604, 1997.

[BDK+00] L. Boe, M. Danielsen, S. Knudsen, J.B. Petersen, J. Maymann, and P.R. Jensen. The frequency of mutators in populations of escherichia coli. *Mutation Research*, 448:47–55, 2000.

[Big44] W.B. Bigger. Treatment of staphylococcal infections with penicillin by intermittent sterilisation. *The Lancet*, 244(6320):497– 500, 1944.

[BLT91] E. Brener, H. Levine, and Y. Tu. Mean-field theory for diffusion-limited aggregation in low dimensions. *Physical review letters*, 66(15):1978–1981, 1991.

[BMC+04] N.Q. Balaban, J. Merrin, R. Chait, L. Kowalik, and S. Leibler. Bacterial persistence as a phenotypic switch. *Science*, 305(5690):1622–1625, 2004.

[BO05] NH Barton and S.P. Otto. Evolution of recombination due to random drift. *Genetics*, 169(4):2353–2370, 2005.

[BSF+04] B. Björkholm, M. Sjölund, P.G. Falk, O.G. Berg, L. Engstrand, and D.I. Andersson. Mutation frequency and biological cost of antibiotic resistance in Helicobacter pylori. *Proceedings of the National Academy of Sciences*, 168(3):1119–1130, 2004.

[CC83] L. Chao and E.C. Cox. Competition between high and low mutating strains of Escherichia coli. *Evolution*, 37(1):125–134, 1983.

[Cha90] B. Charlesworth. Mutation-selection balance and the evolutionary advantage of sex and recombination. *Genetics Research*, 55(03):199–221, 1990.

[CK06] E. Cohen and D.A. Kessler. Front Propagation Dynamics with Exponentially-Distributed Hopping. *Journal of Statistical Physics*, 122(5):925–948, 2006.

[CKL05a] E. Cohen, D.A. Kessler, and H. Levine. Fluctuation-regularized front propagation dynamics in reaction-diffusion systems. *Physical review letters*, 94(15):158302, 2005.

[CKL05b] E. Cohen, D.A. Kessler, and H. Levine. Front propagation up a reaction rate gradient. *Physical Review E*, 72(6):66126, 2005.

[CKL05c] E. Cohen, D.A. Kessler, and H. Levine. Recombination Dramatically Speeds Up Evolution of Finite Populations. *Physical Review Letters*, 94(9):98102, 2005.

[CKL06] E. Cohen, D.A. Kessler, and H. Levine. Analytic approach to the evolutionary effects of genetic exchange. *Physical Review E*, 73(1):16113, 2006.

[Cro70a] J.L. Crosby. The evolution of genetic discontinuity: computer models of the selection of barriers to interbreeding between subspecies. *Heredity*, 25(2):253–297, 1970.

[Cro70b] Crow, J.F. and Kimura, M. *An Introduction to Population Genetics Theory*. Harper and Row Publishers, 1970.

[DCCC98] J.W. Drake, B. Charlesworth, D. Charlesworth, and J.F. Crow. Rates of spontaneous mutation. *Genetics*, 148(4):1667–1686, 1998.

[dCMdlP+04] R. del Campo, M.I. Morosini, E.G.G. de la Pedrosa, A. Fenoll, C. Munoz-Almagro, L. Maiz, F. Baquero, and R. Canton. Population structure, antimicrobial resistance, and mutation frequencies of Streptococcus pneumoniae isolates from cystic fibrosis patients. *Journal of Clinical Microbiology*, 43(5):2207–2214, 2004.

[DF07] Michael Desai and Daniel Fisher. Beneficial mutation-selection balance and the effect of linkage on positive selection. *Genetics*, 176(3):1759, 2007.

[DFM07] Michael Desai, Daniel Fisher, and Andrew Murray. The speed of evolution and maintenance of variation in asexual populations. *Current Biology*, 17(5):385–394, March 2007.

[DM06] E. Denamur and I. Matic. Evolution of mutation rates in bacteria. *Molecular Microbiology*, 60(4):820–827, 2006.

[Dub99] D. Dubnau. DNA uptake in bacteria. *Annu. Rev. Microbiol*, 53:217–244, 1999.

[Eig71] M. Eigen. Selforganization of matter and the evolution of biological macromolecules. *Naturwissenschaften*, 58(10):465–523, 1971.

[Ewe04] W.J. Ewens. *Mathematical Population Genetics*. Springer, 2004.

[EWK07] A. Eyre-Walker and PD Keightley. The distribution of fitness effects of new mutations. *Nature Reviews: Genetics*, 8(8):610, 2007.

[Fel74] J. Felsenstein. The evolutionary advantage of recombination. *Genetics*, 78(2):737–756, 1974.

[Fis30] RA Fisher. The genetical theory of natural selection. Clarendon, 1930.

[GC08] I. Gordo and P.R.A. Campos. Sex and deleterious mutations. *Genetics*, 179(1):621, 2008.

[GCPS07] P.J. Gerrish, A. Colato, A.S. Perelson, and P.D. Sniegowski. Complete genetic linkage can subvert natural selection. *Proceedings of the National Academy of Sciences*, 104(15):6266, 2007.

[GL98] P.J. Gerrish and R.E. Lenski. The fate of competing beneficial mutations in an asexual population. *Genetica*, 102:127–144, 1998.

[GMT+01] A. Giraud, I. Matic, O. Tenaillon, A. Clara, M. Radman, M. Fons, and F. Taddei. Costs and benefits of high mutation rates: adaptive evolution of bacteria in the mouse gut. *Science*, 291(5531):2606–2608, March 2001.

[GT05] J.P. Gogarten and J.P. Townsend. Horizontal gene transfer, genome innovation and evolution. *Nature Reviews Microbiology*, 3(9):679–687, 2005.

[HHHD01] B.J. Haijema, J. Hahn, J. Haynes, and D. Dubnau. A ComGA-dependent checkpoint limits growth during the escape from competence. *Molecular Microbiology*, 40(1):52–64, 2001.

[HSHK06] M. Hegreness, N. Shoresh, D. Hartl, and R. Kishony. An equivalence principle for the incorporation of favorable mutations in asexual populations. *Science*, 311(5767):1615–1617, March 2006.

[IMIS89] K. Ishii, H. Matsuda, Y. Iwasa, and A. Sasaki. Evolutionarily stable mutation rate in a periodically changing environment. *Genetics*, 121(1):163–174, 1989.

[IS01] M. Imhof and C. Schlotterer. Fitness effects of advantageous mutations in evolving escherichia coli populations. *Proceedings of the National Academy of Sciences*, 98(3):1113, 2001.

[JDL09] P.J. Johnsen, D. Dubnau, and B.R. Levin. Episodic Selection and the Maintenance of Competence and Natural Transformation in Bacillus subtilis. *Genetics*, 181:1521–1533, April 2009.

[Joh99a] T. Johnson. Beneficial mutations, hitchhiking and the evolution of mutation rates in sexual populations. *Genetics*, 151(4):1621–1631, 1999.

[Joh99b] T. Johnson. The approach to mutation-selection balance in an infinite asexual population, and the evolution of mutation rates. *Proc. R. Soc. Lond. B*, 266:2389–2397, 1999.

[Kas02] R. Kassen. The experimental evolution of specialists, generalists, and the maintenance of diversity. *Journal of Evolutionary Biology*, 15(2):173, 2002.

[Kau93] S.A. Kauffman. *The Origins of Order: Self-organization and Selection in Evolution (1993)*. New York: Oxford University Press, 1993.

[KEW99] P.D. Keightley and A. Eyre-Walker. Terumi Mukai and the riddle of deleterious mutation rates. *Genetics*, 153(2):515–523, 1999.

[Kim67] M. Kimura. On the evolutionary adjustment of spontaneous mutation rates. *Genet. Res*, 9(1):23, 1967.

[KKBL05] E. Kussell, R. Kishony, N.Q. Balaban, and S. Leibler. Bacterial Persistence A Model of Survival in Changing Environments. *Genetics*, 169(4):1807–1814, 2005.

[KL96] T.T. Kibota and M. Lynch. Estimate of the genomic mutation rate deleterious to overall fitness in E. coli. *Nature*, 381(6584):694–696, 1996.

[KL98a] D.A. Kessler and H. Levine. Fluctuation-induced diffusive instabilities. *Nature*, 394(6):556–558, 1998.

[KL98b] D.A. Kessler and H. Levine. Mutator Dynamics on a Smooth Evolutionary Landscape. *Physical Review Letters*, 80(9):2012–2015, 1998.

[KL05] E. Kussell and S. Leibler. Phenotypic Diversity, Population Growth, and Information in Fluctuating Environments. *Science*, 309(5743):2075–2078, 2005.

[KNS98] D.A. Kessler, Z. Ner, and L.M. Sander. Front propagation: Precursors, cutoffs, and structural stability. *Physical Review E*, 58(1):107–114, 1998.

[KO06] P.D. Keightley and S.P. Otto. Interference among deleterious mutations favours sex and recombination in finite populations. *Nature*, 443(7107):89–92, 2006.

[Kon84] A.S. Kondrashov. Deleterious mutations as an evolutionary factor: 1. The advantage of recombination. *Genetics Research*, 44(02):199–217, 1984.

[KPZ86] M. Kardar, G. Parisi, and Y.C. Zhang. Dynamic scaling of growing interfaces. *Physical Review Letters*, 56(9):889–892, 1986.

[LCB$^+$00] J.E. LeClerc, T.A. Cebula, J. Blazquez, A. Oliver, and F. Baquero. Pseudomonas survival strategies in cystic fibrosis. *Science*, 289(5478):391–392, July 2000.

[LCFT06] L. Le Chat, M. Fons, and F. Taddei. Escherichia coli mutators: selection criteria and migration effect. *Microbiology*, 152(1):67–73, 2006.

[Len04] R.E. Lenski. Phenotypic and genomic evolution during a 20,000-generation experiment with the bacterium Escherichia coli. *Plant Breeding Reviews*, 24:225–265, 2004.

[LJ70] E.G. Leigh Jr. Natural selection and mutability. *American Naturalist*, 104(937):301, 1970.

[LLPC96] JE LeClerc, B. Li, WL Payne, and TA Cebula. High mutation frequencies among Escherichia coli and Salmonella pathogens. *Science*, 274(5290):1208–11, 1996.

[Loe91] L.A. Loeb. Mutator phenotype may be required for multistage carcinogenesis. *Cancer Research*, 51(12):3075, 1991.

[LPG+05] F. Labat, O. Pradillon, L. Garry, M. Peuchmaur, B. Fantin, and E. Denamur. Mutator phenotype confers advantage in Escherichia coli chronic urinary tract infection pathogenesis. *FEMS Immunology and Medical Microbiology*, 44(3):317–321, 2005.

[LRST91] R.E. Lenski, M.R. Rose, S.C. Simpson, and S.C. Tadler. Long-term experimental evolution in Escherichia coli. I. Adaptation and divergence during 2,000 generations. *The American Naturalist*, 138(6):1315–1341, 1991.

[Miy60] T. Miyake. Mutator factor in Salmonella typhimurium. *Genetics*, 45(1):11–14, 1960.

[MLLM97] EF Mao, L. Lane, J. Lee, and JH Miller. Proliferation of mutators in A cell population. *Journal of Bacteriology*, 179(2):417–422, 1997.

[Mor92] P. Moran. *The Statistical Processes of Evolutionary Theory*. Oxford University Press, 1992.

[MRT+97] I. Matic, M. Radman, F. Taddei, B. Picard, C. Doit, E. Bingen, E. Denamur, and J. Elion. Highly variable mutation rates in commensal and pathogenic Escherichia coli. *Science*, 277(5333):1833–1834, 1997.

[MSH74] J Maynard-Smith and J. Haigh. The hitch-hiking effect of a favourable gene. *Genet Res*, 23(1):23–35, 1974.

[Mul32] HJ Muller. Some genetic aspects of sex. *American Naturalist*, 66(703):118–138, 1932.

[Nes64] EW Nester. Penicillin resistance of competent cells in deoxyribonucleic acid transformation of Bacillus subtilis. *Journal of Bacteriology*, 87(4):867–875, 1964.

[NS63] EW Nester and BAD Stocker. Biosynthetic Latency in Early Stages of Deoxyribonucleic Acid Transformation in Bacillus Subtilis 1. *Journal of Bacteriology*, 86(4):785–796, 1963.

[OCC+00] A. Oliver, R. Cantón, P. Campo, F. Baquero, and J. Blázquez. High frequency of hypermutable Pseudomonas aeruginosa in cystic fibrosis lung infection. *Science*, 288(5469):1251, 2000.

[OF97] S.P. Otto and M.W. Feldman. Deleterious mutations, variable epistatic interactions, and the evolution of recombination. *Theoretical Population Biology*, 51(2):134–147, 1997.

[Orr03] H.A. Orr. The distribution of fitness effects among beneficial mutations. *Genetics*, 163(4):1519–1526, 2003.

[PFMG07] L. Perfeito, L. Fernandes, C. Mota, and I. Gordo. Adaptive mutations in bacteria: High rate and small effects. *Science*, 317(5839):813, 2007.

[PL06] M.E. Palmer and M. Lipsitch. The influence of hitchhiking and deleterious mutation upon asexual mutation rates. *Genetics*, 173(1):461–472, 2006.

[PML+03] A.L. Prunier, B. Malbruny, M. Laurans, J. Brouard, J.F. Duhamel, and R. Leclercq. High rate of macrolide resistance in Staphylococcus aureus strains from patients with cystic fibrosis reveals high proportions of hypermutable strains. *Journal of Infectious Diseases*, 187(11):1709–1716, 2003.

[PQ07a] T.L. Parsons and C. Quince. Fixation in haploid populations exhibiting density dependence I: The non-neutral case. *Theoretical Population Biology*, 72(1):121–135, 2007.

[PQ07b] T.L. Parsons and C. Quince. Fixation in haploid populations exhibiting density dependence II: The quasi-neutral case. *Theoretical Population Biology*, 72(4):468–479, 2007.

[PQP08] T.L. Parsons, C. Quince, and J.B. Plotkin. Absorption and fixation times for neutral and quasi-neutral populations with density dependence. *Theoretical Population Biology*, 74(4):302–310, 2008.

[RdVG02] D.E. Rozen, J.A.G.M. de Visser, and P.J. Gerrish. Fitness effects of fixed beneficial mutations in microbial populations. *Current Biology*, 12(12):1040–1045, 2002.

[Red01] R.J. Redfield. Opinion: Do bacteria have sex? *Nature Reviews Genetics*, 2(8):634–639, 2001.

[Ric02] W.R. Rice. Experimental tests of the adaptive significance of sexual recombination. *Nature Reviews Genetics*, 3(4):241–251, 2002.

[RWC03] I.M. Rouzine, J. Wakeley, and J.M. Coffin. The solitary wave of asexual evolution. *Proceedings of the National Academy of Sciences*, 100(2):587–592, 2003.

[RYPS02] A.R. Richardson, Z. Yu, T. Popovic, and I. Stojiljkovic. Mutator clones of Neisseria meningitidis in epidemic serogroup A disease. *Proceedings of the National Academy of Sciences*, 99(9):6103, 2002.

[SDS+02] A.C. Shaver, P.G. Dombrowski, J.Y. Sweeney, T. Treis, R.M. Zappala, and P.D. Sniegowski. Fitness evolution and the rise of mutator alleles in experimental Escherichia coli populations. *Genetics*, 162(2):557–566, 2002.

[SGJS00] P.D. Sniegowski, P.J. Gerrish, T. Johnson, and A. Shaver. The evolution of mutation rates: separating causes from consequences. *BioEssays*, 22(12):1057–1066, 2000.

[SGL97] PD Sniegowski, PJ Gerrish, and RE Lenski. Evolution of high mutation rates in experimental populations of E. coli. *Nature*, 387(6634):659–661, 1997.

[SGOLE06] G.M. Süel, J. Garcia-Ojalvo, L.M. Liberman, and M.B. Elowitz. An excitable gene regulatory circuit induces transient cellular differentiation. *Nature*, 440(7083):545–550, 2006.

[SHA00] G. Storz and R. Hengge-Aronis. *Bacterial stress responses*. Amer Society for Microbiology, 2000.

[SKD+07] G.M. Süel, R.P. Kulkarni, J. Dworkin, J. Garcia-Ojalvo, and M.B. Elowitz. Tunability and noise dependence in differentiation dynamics. *Science*, 315(5819):1716, 2007.

[Smi68] J.M. Smith. Evolution in sexual and asexual populations. *American Naturalist*, 102(927):469, 1968.

[SPA06] M.S. Samoilov, G. Price, and A.P. Arkin. From fluctuations to phenotypes: the physiology of noise. *Science's STKE*, 2006(366), 2006.

[Stu37] AH Sturtevant. Essays on evolution. I. On the effects of selection on mutation rate. *Quarterly Review of Biology*, 12(4):464, 1937.

[TBL03] M.M. Tanaka, C.T. Bergstrom, and B.R. Levin. The evolution of mutator genes in bacterial populations: the roles of environmental change and timing. *Genetics*, 164(3):843–854, 2003.

[TLK96a] L.S. Tsimring, H. Levine, and D.A. Kessler. RNA Virus Evolution via a Fitness-Space Model. *Physical Review Letters*, 76(23):4440–4443, 1996.

[TLK96b] L.S. Tsimring, H. Levine, and D.A. Kessler. RNA virus evolution via a fitness-space model. *Physical Review Letters*, 76(23):4440–4443, 1996.

[TMGR97] F. Taddei, I. Matic, B. Godelle, and M. Radman. To be a mutator, or how pathogenic and commensal bacteria can evolve rapidly. *Trends in Microbiology*, 5(11):427–428, 1997.

[TRMS+97] F. Taddei, M. Radman, J. Maynard-Smith, B. Toupance, PH Gouyon, and B. Godelle. Role of mutator alleles in adaptive evolution. *Nature*, 387:701, 1997.

[TSB54] H.P. Treffers, V. Spinelli, and N.O. Belser. A factor (or mutator gene) influencing mutation rates in Escherichia coli. *Proceedings of the National Academy of Sciences*, 40(11):1064–1071, 1954.

[TT02] JM Travis and ER Travis. Mutator dynamics in fluctuating environments. *Proc. R. Soc.*, 269:591–597, 2002.

[TTLN+99] O. Tenaillon, B. Toupance, H. Le Nagard, F. Taddei, and B. Godelle. Mutators, population size, adaptive landscape and the adaptation of asexual populations of bacteria. *Genetics*, 152(2):485–493, 1999.

[WBS04] M.E. Watson, J.L. Burns, and A.L. Smith. Hypermutable Haemophilus influenzae with mutations in mutS are found in cystic fibrosis sputum. *Microbiology*, 150(9):2947–2958, 2004.

[WG01] L.M. Wahl and P.J. Gerrish. The probability that beneficial mutations are lost in populations with periodic bottlenecks. *Evolution*, 55(12):2606–2610, 2001.

[WGSV02] L.M. Wahl, P.J. Gerrish, and I. Saika-Voivod. Evaluating the impact of population bottlenecks in experimental evolution. *Genetics*, 162(2):961–971, 2002.

[WH96] G. Woodcock and P.G. Higgs. Population Evolution on a Multiplicative Single-Peak Fitness Landscape. *Journal of Theoretical Biology*, 179(1):61–73, 1996.